UNIVERSITA' POLITECNICA DELLE MARCHE

FACOLTA' DI INGEGNERIA

Master's Degree in Biomedical Engineering

CHEMICAL AND RHEOLOGICAL CHARACTERIZATION OF VISCO-MODULATED POLYMERIC HYDROGEL FOR BIOMEDICAL APPLICATIONS

Advisor:

Prof. LORENZO SCALISE

Co-Advisor:

Dr. PAOLO FATTORI

Candidate:

VERONICA CROGNALETTI

ACADEMIC YEAR: 2018/2019

Index

Abstract

The growing interest in the regeneration of pathologically altered tissues has involved a multitude of researches in the use of 3D scaffolds. In this scenario, hydrogels have received significant attention.

A biodegradable scaffold can be infected by microorganisms; the consequent risk of disease transmission has been reduced through sterilization. However, PVA-, PVP- and PEO-based hydrogel formulations can be subjected to crosslinking reactions during irradiation processes; as a consequence, these hydrogels undergo to undesirable effects such as viscosity increase.

Thanks to its antioxidant, anti-inflammatory and antimicrobial properties, hydroxytyrosol could be selected as a valid anti-crosslinking agent: the hypothesis is that radiation-induced crosslinking of hydrogels could be either prevented or limited by tailoring the concentration of hydroxytyrosol. In addition, this work aims to evaluate how the use of a specific kind of buffer saline solution can affect the final characteristics of the optimized hydrogel.

The study has been performed by producing gels with PEO, HT and two different buffer (Phosphate and Citrate) solutions. The samples characterization has been carried out – in addition to a visual observation and pH measurement of the prepared hydrogels – on two analytical levels: the rheological and the chemical one (through Fourier-Transform Infrared Spectroscopy and High Performance Liquid Chromatography).

The results obtained demonstrate that crosslinking of PEO-based hydrogels could be prevented by tailoring the concentration of hydroxytyrosol introduced as an anti-crosslinking agent. The different salinity of the buffers influences both the viscoelasticity of the gel and the formation of bonds after gamma radiation sterilization. In addition, since hydroxytyrosol results to be more preserved when formulated in Citrate Buffer Solution, the choice of the use of CBS is the most convenient in order to increase the biocompatibility of the final Sterile Hydrogels.

1. Introduction

1.1 Regenerative Medicine and Tissue Engineering

Millions of patients annually suffer the loss of or experience damage to organs, tissues, or body parts [1]. The desire to improve the human condition and to provide for the loss of organs and tissues has made possible the development of therapies that can regenerate tissues and decrease reliance on transplantations [2]. Regenerative Medicine, thus, represents the field of medicine which aims to the replacement or regeneration of human cells, tissues and organs, in order to re-establish normal functionality [3].

Tissue Engineering (TE) is a multidisciplinary field that involves the application of the principles and methods of engineering and life sciences towards [4]:

- the fundamental understanding of structure-function relationships in normal and pathologic mammalian tissues;
- the development of biological substitutes to restore, maintain or improve tissue function.

The first clinical application of human cells in tissue engineering, started around 1980, has been applied to skin tissue using fibroblasts, and keratinocytes. During the past two decades, Tissue Engineering and Regenerative Medicine (TERM) field have invested in the regeneration and reconstruction of pathologically altered tissues, such as cartilage, bone, skin, heart valves, nerves, tendons, and many others [4]. Their advances have involved a multitude of research, including biomaterials design and processing, surface characterization, and functionalization for improved cell-material interactions and imaging [5].

The most frequent TERM approach involves the combination of harvested cells from donor tissue, supportive biomaterial construct (scaffold) and micro-environmental factors [4]. The first phase is the *in vitro* formation of a tissue construct by placing the chosen cells and scaffold in a metabolically and mechanically supportive environment with growth media (e.g., in a bioreactor), in which the cells proliferate and elaborate extracellular matrix. In the second phase, the construct is implanted in the appropriate anatomic location, where remodelling *in vivo* is intended to recapitulate the normal functional architecture of an organ or tissue [6]. The process is carried out in order to [4]:

- promote cell attachment and restrict their distribution in the tissue;
- direct cell distribution and differentiation;
- sustain large tissue losses while new tissue is formed;
- lead to new tissue formation.

Thus, the central challenge for TERM is to develop cell-based substitutes in order to promote tissue repair and/or functional restoration [7].

The addition of another dimension, the mechanical environment, to the basic three point or triangular diagram used to illustrate the concept of tissue engineering (cells, biomaterials and signaling molecules) leads to the formation of a 4 point diamond shaped structure (Figure 1). This diamond structure has two V's, which emphasize the importance of vascularization, and thus the need for a functional blood supply in tissue engineering. The diamond concept also indicates the importance of the host response for successful tissue regeneration [8].

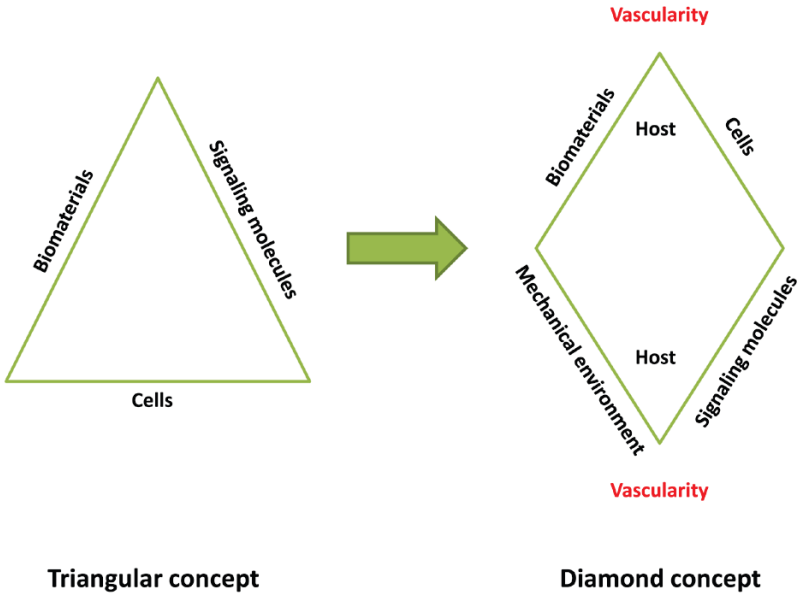

Figure 1. *Evolution of the diamond concept from the basic triangular concept [8].*

The Tissue Engineering approach involves the development of functional substitutes to replace missing or malfunctioning human tissues and organs: the general strategies adopted by tissue engineering can be classified into three groups [9]:

- direct implantation of isolated cells or cell substitutes into the organism;
- delivering of tissue inducing substances (such as growth factors);
- placing cells on or within different matrices.

1.2 Scaffolds

The field of TERM – that has significantly increased over the past decades – relies on the use of porous, three-dimensional (3D) scaffolds to provide the appropriate environment for the regeneration of tissues [10]. In fact, a tissue engineering process generally begins with the fabrication of a biologically compatible scaffold that will support living cells for their attachment, proliferation and differentiation, and thus promote tissue regeneration both *in vitro* and *in vivo* [4].

On the 3D scaffold, cells grow and organize to form an extracellular matrix (ECM), used in the regenerative process. In natural tissues, in fact, cells are immersed in an ECM, a relatively structurally stable material, composed of a complex mixture of proteins and polysaccharides; the polymeric network that constitutes the support structure affects both the behaviour of cells and the biochemical and biomechanical properties of different tissues and organs [11]. In fact, the principal functions of the ECM are mechanical support for cell anchorage, determination of cell orientation, control of cell growth and maintenance of cell differentiation, establishment of tissue microenvironment and scaffolding for orderly tissue renewal [6]. Native ECM, thus, is the ideal biological scaffold, since it contains all the components of the tissue from which it has been derived except for the living cells [11].

1.2.1 Choice of Biomaterial

Current strategies for TERM involve the use – in the scaffold synthesis – of a wide variety of materials that imitate the ECM, when native ECM is pathologically altered [11].

A complete understanding of the chemistry and physicochemical properties of the tissue to be engineered and the materials used in this process is necessary, in order to achieve this goal. Several characterizations are performed for the fabrication of successful 3D scaffolds [12]:

- external geometry (e.g., macro- and micro- structure, interconnectivity);
- surface properties (e.g., surface energy, chemistry, charge, surface area);
- porosity and pore size;
- interface adherence and biocompatibility;
- degradation characterization (e.g., biodegradation);
- mechanical competence (e.g., compressive and tensile strength).

Criteria of an ideal scaffold for bone regeneration and tissue engineering are summarized in Table I [13, 14, 15].

Table I. *Criteria of an ideal scaffold for bone and tissue engineering*

CRITERIA OF AN IDEAL SCAFFOLD	
Criteria	**Requirement**
Biocompatibility	Support and foster cells' attachment proliferation and differentiation, and initiate tissue regeneration both *in vitro* and *in vivo*.
Osteoconductivity	Encourage host bone adherence and growth into the scaffold.
Biodegradability	Be able to degrade at a physiologically relevant rate.
Mechanical properties	Maintain proper mechanical stability for tissue regeneration.
Porous structure	Be highly porous (> 90%) and interconnected, with pore diameters between 300 and 500 μm, to allow cells to penetrate into a pore structure and promote new bone formation, as well as vascularization. It must be able to deliver nutrients into the scaffold and transport undesiderable metabolites outside scaffold.
Fabrication	Possess desired fabrication capabilities (e.g., being readily produced into irregular shapes of scaffolds that match the defects in the bone of individual patients).
Commercialization	Be fabricated at an acceptable cost for commercialization.

1.2.1.1 External Geometry

Physical characteristics are certainly one of the important factors to consider when scaffolds are applied for tissue reconstruction [12]. The scaffold should be easily fabricated into a variety of shapes and sizes, in order to geometrically and topologically mimics the natural ECM in living tissues [4].

One of the most important requests is to maintain highly interconnected porous fabrics of high surface density, in order to provide an extremely high surface-to-volume ratio, favoring cell attachment and proliferation [12].

1.2.1.2 Surface Properties

Surface properties include both chemical and topographical characteristics, which can control and affect cellular adhesion, differentiation and proliferation. Since most cells utilized in tissue engineering are anchorage dependent, it has been reasoned that the scaffold should facilitate their attachment; thus, scaffolds with a large and accessible surface area are favorable [1].

Surface properties can be selectively customized in order to enhance the performance of the biomaterials: the optimal surface, chemical and physical properties can be obtained modifying the surface functionality using thin film deposition [12].

1.2.1.3 Porosity and Pore Size

An ideal scaffold should possess inter-connecting pores of appropriate scale for providing a large surface area that favours cell ingrowth, uniform cell distribution and facilitates tissue integration and vascularization [5]. For this reason, average pore size, pore size distribution, pore volume, pore interconnectivity and pore shape are important parameters to consider while designing a scaffold, because they hold a direct influence over its functionality [12].

1.2.1.4 Interface Adherence and Biocompatibility

Biocompatibility is the ability of a biomaterial to achieve its desired function with respect to a medical therapy, without arousing undesirable local or systemic effects in the beneficiary of that therapy. It should generate the most appropriate beneficial cellular or tissue response in that specific situation and optimize the clinically relevant performance of that therapy [12].

Biocompatibility of a scaffold for a tissue engineering product refers to the ability to perform as a substrate that will support the appropriate cellular activity, including the facilitation of molecular and mechanical signalling systems; so an ideal scaffold should adhere and integrate easily into the surrounding native tissue [11].

Important factors that determine scaffolds' biocompatibility are their chemistry, structure and morphology, which in turn are affected by the polymer synthesis, scaffold processing and sterilization conditions. A lot of surface treatments are possible in order to enhance the biocompatibility of surfaces in contact with living tissue, to seal in undesirable residues or additives and to regulate excretion and/or absorption [12].

1.2.1.5 Degradation Rates

Biodegradable polymers have revolutionized the applications of biomaterials in the field of drug delivery and implants for tissue engineering applications. Scaffold degradation can occur through mechanisms that involve physical or chemical processes and/or biological processes that are mediated by biological agents, such as enzymes in tissue remodelling [12].

Degradation results in scaffold dismantling and material dissolution/reabsorption through the scaffolds bulk and/or surface types of degradation. In addition, the released by-products during materials degradation should be non-toxic and the degradation rate should be controllable and congruent with the tissue regeneration [5].

1.2.1.6 Mechanical Properties

An ideal scaffold should possess adequate mechanical properties to match the intended site of implantation and handling: the proper mechanical properties for a biomaterial are, in fact, critical to the success of the implant [4].

The biostability of many scaffolds depends on factors such as strength, elasticity, and absorption at the material interface and its chemical degradation. It is important, therefore, to evaluate one or more of the following rheological parameters [12]:

- elastic modulus: measured strain in response to a given tensile or compressive stress along the force;
- flexural modulus: measured the relationship between a bending stress and the resulting strain in response to a given tensile or compressive stress perpendicular under load;
- tensile strength: maximum stress that the material can withstand before it breaks;
- maximum strain: ductility of a material or total strain exhibited prior to fracture.

1.2.2 Biomaterials for Scaffolds

To achieve clinical tissue success, functional biomaterials research has been directed toward the development of improved scaffolds for regenerative medicine. The three main material types which have been successfully investigated to be applied in developing scaffolds include natural polymers, synthetic polymers, and ceramics [1].

Polymers represent the largest class of biomaterials; many types of them are widely used in biomedical devices that include orthopaedic, dental, soft tissue and cardiovascular implants [6]. Polymeric materials are popular for regenerating hard and soft tissues, thanks to their biodegradation, mechanical properties, high porosity and small pore size. Different materials could be used depending on the tissue to be engineered and its specific applications, in order to obtain similar properties to the native tissue. Thus, the selected manufacturing process should guarantee control over

macro-structural (geometry, mechanical strength, density, porosity) and micro-structural aspects (pores size, distribution and interconnection) [5].

1.2.2.1 Natural Polymers

Natural polymers (or biopolymers) obtained from renewable resources, such as algae, plant, animal, and micro-organisms, have shown the biological properties that better fit to the regular microenvironment of tissues (Figure 2) [5].

Natural polymers offer the advantage of being almost identical to macromolecular substances which the biological environment is prepared to recognize and to deal metabolically with [6]. Thanks to their similarity with the ECM, in fact, they promote desirable cellular responses, biocompatibility, degradability and may also elude chronic inflammation toxicity or immunological reactions, frequently noticed with synthetic polymers. Thus, these types of polymers are crucial for designing therapeutic systems to be used as bioactive compounds and drug delivery systems for disease treatment, or even to bioengineer functional tissues [5]. Furthermore, their low mechanical strength and high deterioration have conditioned their use in the production of scaffolds [11].

Natural polymers can be classified as proteins (e.g., silk fibroin, collagen, gelatine, keratin, fibrinogen, elastin, actin and myosin), polysaccharides (e.g., cellulose, chitosan, chitin, alginate and glycosaminoglycans) or polynucleotides (DNA, RNA) [1].

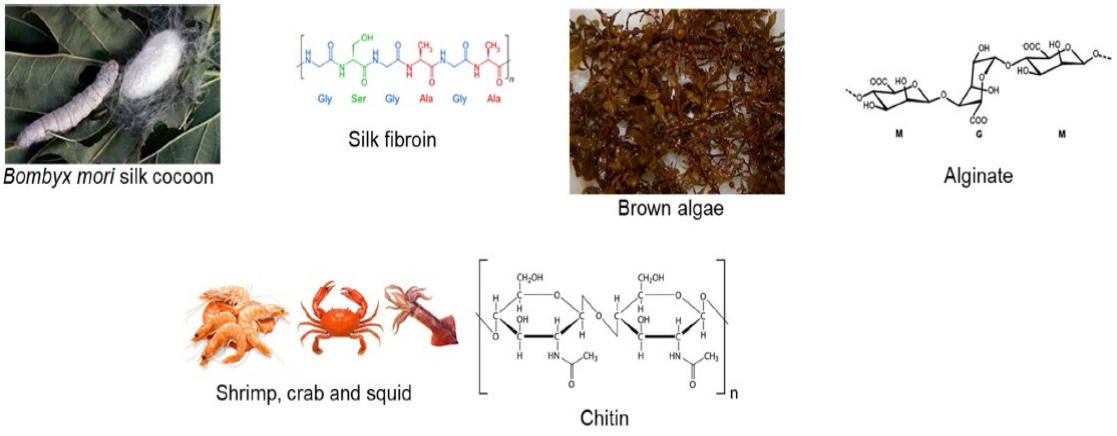

Figure 2. *Some biopolymers derived from renewable resources and respective chemical structures: silk, fibroin, alginate and chitin [5].*

The most used natural polymers for scaffolding applications are:

- Collagen: it is the most abundant protein found in mammalian ECM, constituting about 30% of the whole-body protein content [1] and therefore it is considered by many scientists as an ideal scaffold or matrix for tissue engineering [4]. Collagen fibers are self-aggregating triple-stranded helical structures that are held together by both hydrogen and covalent bonds [11]; collagen is defined by high mechanical strength and good biocompatibility may also be processed into a variety of formats [4]. Collagen can be reinforced by the method of crosslinking, which increases its mechanical strength and prevents structural alterations [1]; however, for medical applications, the implantation of foreign cells - derived from human or animal sources - can lead to disease transmission and other immunological problems [4]. Collagen has been used for creating synthetic tissues such as heart valves, cartilage, skin , spinal cord, vocal cord and breast reconstruction [11];
- Chitosan: it is a cationic polymer obtained by the full or partial deacetylation of chitin, by alkaline hydrolysis at high temperature, to yield the primary amino groups of the polymer backbone [1]. It is a natural polysaccharide found particularly in the shell of crustacean, cuticles of insects and cell walls of fungi and is the second most abundant polymerized carbon found in nature [4]. Chitosan is a biologically renewable source material that is also biodegradable, biocompatible, non-antigenic, non-toxic, and biofunctional [1]. It can be used for wound dressing, drug delivery, and tissue engineering (cartilage, nerve and liver tissue) applications; current difficulties applying chitosan as a polymer scaffold in tissue engineering include low strength and inconsistent behaviour with seeded cells [4];
- Hyaluronic Acid: it is a relatively simple glycosaminoglycan (GAG) found in most connective tissues of the body, including skin, cartilage, and the vitreous humor [1] and it is essential for cell growth, embryonic development, wound healing, and tumor development [11]. Hyaluronic Acid (HA) is commonly extracted from rooster combs and human umbilical cords or easily and controllably produced from strains of bacteria, through microbial fermentation [1]. High molecular weight HA is water soluble, biodegradable and non-immunogenic, but low molecular weight HA is seen as inflammatory, immunostimulatory and angiogenic; thus, crosslinking is introduced in order to reduce the rapid in vivo degradation [11].

1.2.2.2 Synthetic Polymers

In contrast to natural biomaterials, synthetic biomaterials are produced by controlled processes that yield consistent properties without batch-to-batch variation, even on a large scale [1].

Thanks to their properties, synthetic polymers are highly useful in biomedical field [12]: they are, in fact, highly versatile materials with physical and chemical properties that can be easily controlled and altered to produce a wide range of mechanical properties and degradation rates [11]. Synthetic polymers, in addition, offer excellent characteristics in term of porosity and molecular weight [5] and are often cheaper than natural polymers [12]; however, they are less biocompatible than naturally derived polymers and not as bioactive [11].

The main synthetic polymers (Figure 3) used in tissue engineering are:

- Polyethylene Oxide (PEO) / Polyethylene Glycol (PEG): they are some of the most commonly used materials for biomedical applications, especially as an ingredient for scaffolds [1]. PEO is an hydrophilic polymer, generally inert and with limited immunogenicity, antigenicity, protein binding and cell adhesion; PEG, instead, is the shorter version of PEO (oligomer) with lower molecular weight [11]. Both PEO and PEG are nonionic and biocompatible materials with extraordinary physicochemical and biological properties [1]. In fact, they are capable of photo-polymerization, have adjustable mechanical properties and an easy control of scaffold architecture and chemical composition: all of these characteristics make them attractive materials to produce 3D templates for tissue regeneration [11]. PEG has mainly been employed in the form of hydrogels, which have been extensively used as matrices for scaffold applications [1];
- Polyvinyl Alcohol (PVA): it is a water-soluble synthetic polymer that forms a stable and crystallizing hydrogel at low temperatures. PVA hydrogels offer a number of advantages, such as reduced protein-binding tendency, higher water content and higher elasticity; thus, it has been evaluated as scaffold for tissue engineering [1] and used in many biomedical and pharmaceutical applications [16];

- Polyvinylpyrrolidone (PVP): it is physiologically compatible, non-toxic, chemically inert, temperature-resistant and pH-stable polymer; for these reasons has been used to fabricate scaffolds for TERM applications [16];
- Poly Lactic Acid (PLA): it is a biodegradable synthetic polyester, extensively investigated for tissue engineering and mostly used for bone or cartilage engineering [11], thanks to its biodegradability, biocompatibility and mechanical strength [4];
- Polyglycolic Acid (PGA): it is a thermoplastic aliphatic polyester, extensively used or tested on a wide range of medical applications [12], in particular for the fabrication of scaffolds, thanks to its good biocompatibility [1].

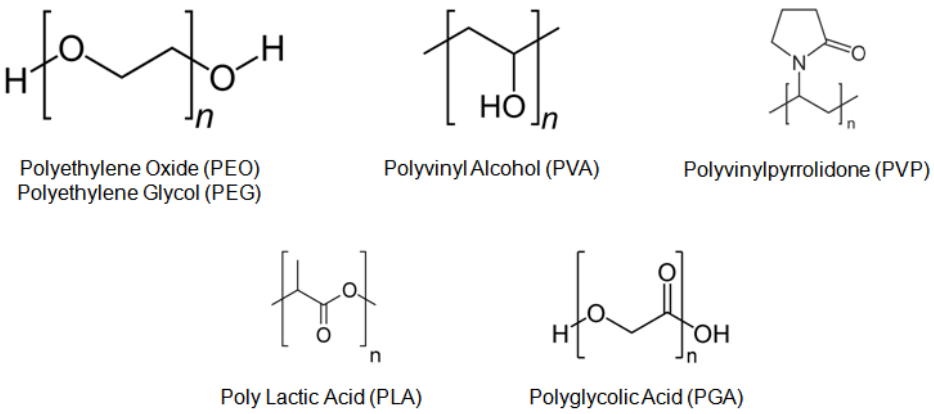

Figure 3. *Main Synthetic Polymers [4].*

1.2.2.3 Ceramics

Bioactive ceramics (e.g., bioglasses and glass-ceramics) react with physiological fluids and through cellular activity form tenacious bonds to hard and, in some cases, soft tissue engineering [12]; for this reason, they have been applied to fill small bone defects and periodontal irregularities [5]. However, their biocompatibility and biodegradability are often insufficient, limiting their potential use in the clinical side [12].

1.3 Hydrogel-based Scaffolds

1.3.1 Introduction to Hydrogels and Applications

Hydrogels are a class of crosslinked polymeric materials that, thanks to their hydrophilic properties, have the capacity to hold water within its porous structure; the water holding capacity of the hydrogels arise mainly due to the presence of hydrophilic

groups (e.g., amino, carboxyl and hydroxyl groups) in the polymer chains [17]. Generally, an hydrogel has an high water content up to 90% by weight [11].

Hydrogel can be formed from natural or synthetic polymer backbones. Hydrogels comprised of naturally derived macromolecules have potential advantages of biocompatibility, cell-controlled degradability and intrinsic cellular interaction [12]; characteristic disadvantages of these natural products include inconsistent hydration and limited range of mechanical properties [18]. In contrast, synthetic polymers can be prepared with precisely controlled structures and functions [12]. The multitude of hydrogels available leaves numerous choices for polymeric formulations: the best approach for developing an hydrogel with the desired characteristics for biomedical application is to correlate the macromolecular structures of the polymers available with the swelling and mechanical characteristics desired [6].

Hydrogels have received significant attention because of their exceptional promise in biomedical applications [6]; hydrogel-based systems offer moderate-to-high physical, chemical and mechanical stability: the elastic behaviour and swelling capability resemble the natural ECM of many tissues, making hydrogels particularly suitable to scaffold production [5].

Thanks to their properties, hydrogels have been used since the 1960s in diverse areas of application, such as contact lenses and intraocular lenses. Today, hydrogels are being employed for clinical applications, such as wound healing and more recently, they are being used as scaffolds to provide a biomimetic 3D microenvironment for the growth of cells [11].

1.3.2 Hydrogel Synthesis

The structural integrity of the hydrogels depends on the crosslinking formed by covalent polymer chains and non-covalent physical interactions. The polymer crosslinking process, if not spontaneous, can be triggered by external agents [1].

In general, the three integral parts of hydrogels synthesis are monomer, initiator, and crosslinker. Some diluents – such as water or other aqueous solutions – can be used in order to control the heat of polymerization and the final hydrogels properties. After the synthesis, the hydrogels mass needs to be washed to remove impurities left from the synthesis process (Figure 4). Hydrogels properties can be modulated by varying the synthetic factors, such as reaction vessel, reaction time, reaction temperature,

monomer type, type of crosslinker, crosslinker-to-monomer ratio, monomer concentration, and type and amount of initiator [19].

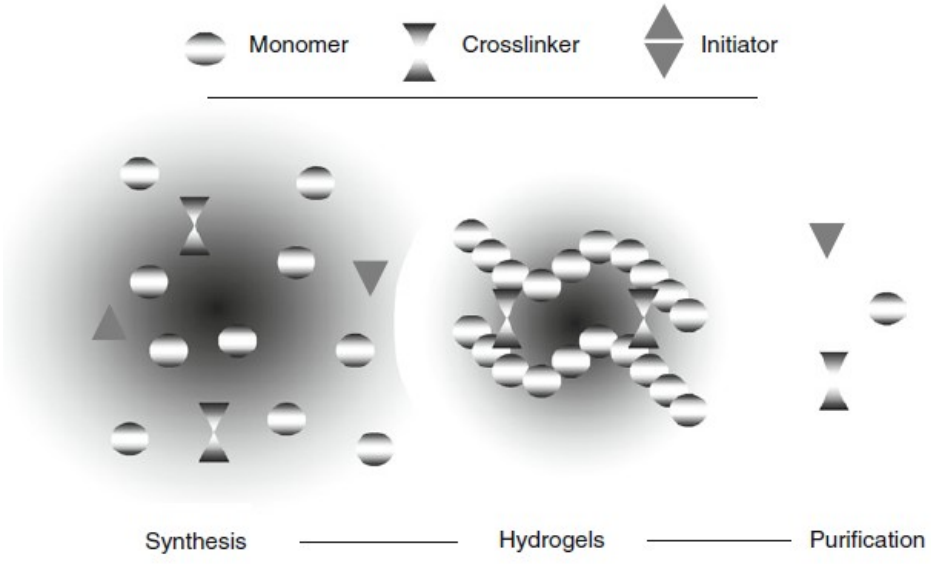

Figure 4. *Hydrogels Synthesis [19].*

The main polymerization methods are (Figure 5):

- physical crosslinking: this method consists in the formation of a network without adding chemical agents, by adjusting parameters such as pressure, temperature and volume; by far the most studied types of physical interactions useful for the formation of hydrogels are hydrophobic interactions [19]. The main advantages of these types of hydrogels are that they can be easily administered and their physical properties can be tailored in response to particular physiological stimuli; conversely, a significant disadvantage is the formation of internal inhomogeneities due to the creation of domains, determined by hydrophobic or ionic interactions [1];
- chemical crosslinking: this method calls for direct reaction of a linear or branched polymer with at least one difunctional, small molecular weight, cross-linking agent [6]. Thanks to the formation of covalent bonds between the polymer chains through the use of chemical reagents (crosslinkers) or the irradiation – gamma, beta and ultraviolet irradiation – short crosslinking times and excellent mechanical properties are guaranteed [19].

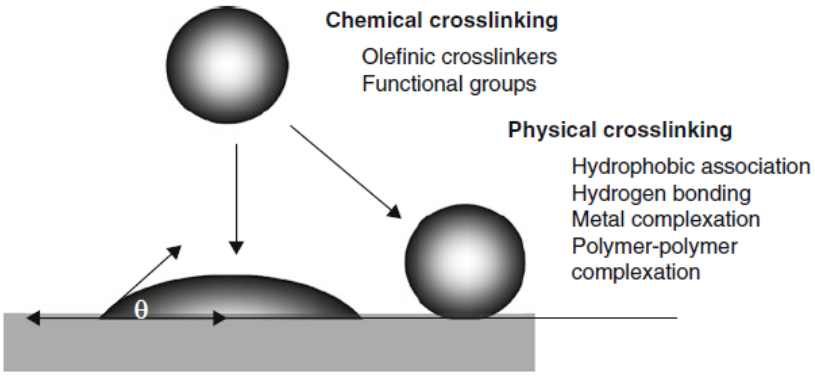

Figure 5. *Physical and Chemical Crosslinking* [19].

1.3.3 Swelling Forces in Hydrogels

The physical behaviour of hydrogels is dependent on their equilibrium and dynamic swelling behaviour in water, since upon preparation they must be brought in contact with water to yield the final, swollen network structure [6]. Thus, hydrogels are usually defined by their degree of swelling. Hydrogels swelling, by definition, is the restricted solubility: infinite solubility of an hydrogel is prevented by elastic forces, which originate from the network crosslinking; the balance of these two different forces determines the equilibrium hydrogels swelling (Figure 6) [19].

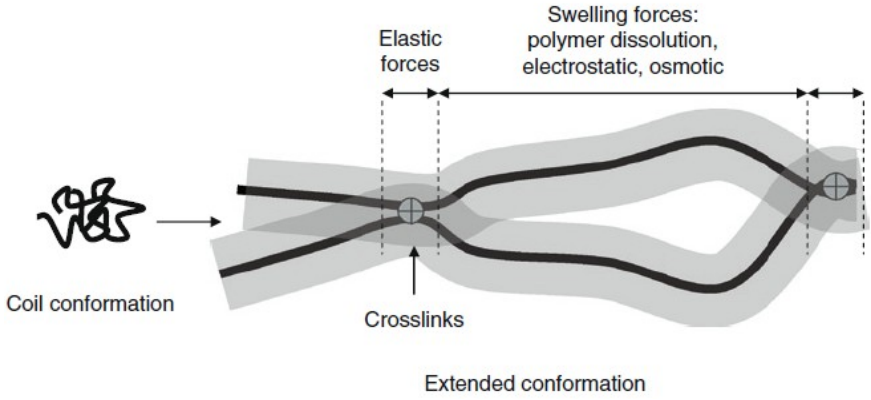

Figure 6. *Swelling Forces in Hydrogels* [19].

The swelling capacity of a hydrogels can be determined by the amount of space inside the hydrogels network available to accommodate water. The water absorption in hydrogels is dependent on many factors, such as network parameters, nature of the solution, hydrogels structure (porous or pore-less), and drying techniques [19].

Since an hydrogel is a composite of a solid (a polymer) and a liquid (water), the final properties of the hydrogel are also determined by the composition of the composite (the polymer-to-water ratio): a low- or a high-swelling hydrogel is characterized by a high or low-polymer/water ratio, respectively (Figure 7) [19].

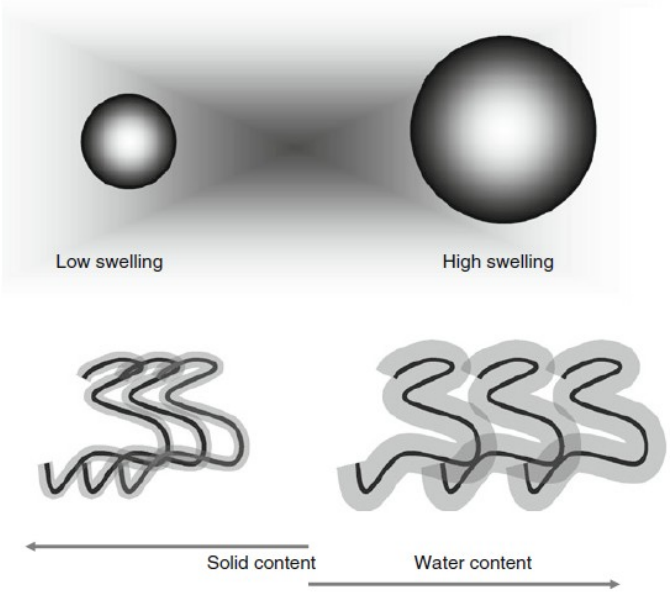

Figure 7. *Composite Properties of Hydrogels [19].*

1.4 Main Scaffolds Sterilization Techniques

A biodegradable scaffold has a potential to be infected by a wide range of microorganism, such as virus, bacteria, and fungi; infections associated with *in vivo* use of biomaterials scaffolds by different microbiological contaminants remain to be a significant challenge [20].

Sterilization is a process by which a product can be made free of contamination from living microorganisms, and it is a compulsory production step for any scaffold or biomaterial to be used in clinical setting: sterilization of hydrogels may alter the characteristics of the biodegradable scaffold; hence, in order to ensure that the scaffold will fulfil the intended purposes post-sterilization, a consideration on the sterilization method should be given before [17].

Various sterilization techniques have been attempted on biodegradable scaffolds; due to the lack of techniques designed specifically for such scaffolds, conventional sterilization techniques have been used [20]. The most important sterilization techniques

include steam, ethylene oxide and irradiation (gamma and beta); characteristics of most used sterilization techniques are summarized in Table II [12].

Table II. *Characteristics of Sterilization Techniques*

STERILIZATION TECHNIQUES		
Technique	**Unique Factors**	**Applications**
Steam	Removal of all contamination and scaffold can be reused	Porous scaffold for living cell immobilization
Gamma radiation	Proven process is safe, reliable and highly effective at treating single-use medical devices	Surgical disposables: surgical sutures, bandages, dressings, gauge pads, implants
Electron beam (Beta radiation)	Compatibility, low penetration, in line sterilization of thin product	Commercially successful technology for sterilizing a variety of disposable medical devices with a wide range of densities
Ethylene Oxide	For degradable polymers and porous scaffolds, high penetration ability, and compatibility	Absolute freedom from biological contamination in scaffolds

Based on the ability to kill different types of microorganism at given conditions, the inactivation level of these sterilization techniques has been calculated and classified as high, medium or low. The inactivation level, also called D-value, is the exposure time required to achieve the killing of 90% of the living population [21]. If N is the number of micro-organism after the exposure time t and N_0 is initial number of micro-organism:

$$\frac{N}{N_0} = 10^{-kt}$$

where t is the elapsed exposure (sterilization) time and k is the reaction rate constant (which depends on the species and conditions of the micro-organism). Thus, D-value is the reciprocal of the reaction rate k [21]:

$$D = \frac{t}{\log N_0 - \log N}$$

1.4.1 Steam

Steam sterilization (ISO 11134, 1994) – performed thanks to a steam sterilizer, also known as autoclave (Figure 8) – is realized by treating the product with saturated steam at 121 °C to 132 °C for around 15 to 30 minutes, under a pressure of 106 kPa (1 atm) once all surfaces have reached a temperature of 121 °C [22]. High-vacuum pumps are used in order to remove as much as possible air before the steam is admitted, so

the required temperature is reached very rapidly. The most common steam sterilization cycles used are gravity-displacement and dynamic air removal: in a gravity-displacement system, steam enters the sterilization chamber and expels the residual air through an open vent (hot air rises). Dynamic air removal has been shown to be more efficient because the machine can pump in conditioning air and then forcefully discharge this environment (humid and warm) and replace with subsequent cycles [23].

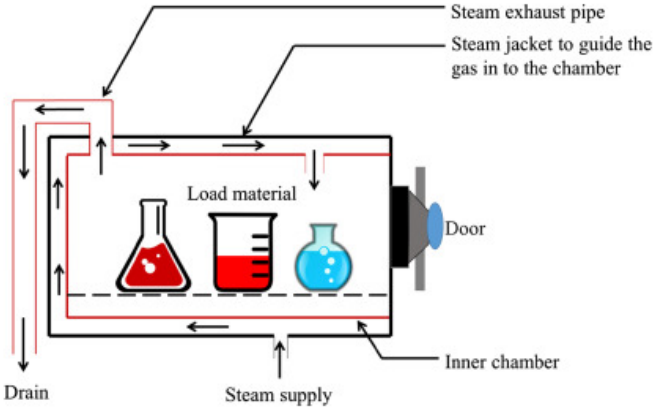

Figure 8. *Steam Sterilization Technique [24].*

The main advantage of this treatment is that it is a simple, effective, fast, safe, environment-friendly and low-cost sterilization method [22]; in addition the penetration ability of steam treatment is one of the best among all of the sterilization techniques and it can completely eliminate all microorganisms (high D-value) [20].

The main limitation of steam sterilization is that it is incompatible with many materials; in fact this technique damages most polymers [22]. Thus, the use of steam treatment as a sterilization technique for biodegradable polymeric scaffolds is problematic: the presence of water vapor has been shown to cause hydrolytic degradation of the material to be sterilized [20]. To minimize this side effect, Rozema et al. [25] modified the steam sterilization process for PLA scaffolds; nevertheless, a substantial loss in molecular weight and an increase in mechanical strength has been registered. Thus, before choosing steam treatment sterilization approach to sterilize degradable scaffolds, a careful evaluation of side effects on material mechanical strength and molecular weight must be carried out [20].

Limitations of steam sterilization have led to the development and use of ionizing radiation and ethylene oxide to sterilize medical devices and scaffolds [6].

1.4.2 Radiation

In comparison with heat treatments, radiation methods offer features such as low temperatures, short process in time, and comparatively lower cost of operation, making the radiation techniques promising candidates to sterilize biodegradable scaffolds [20].

There are two general types of radiation used for sterilization [20]:

- ionizing radiation: it is the use of short wavelength, high-intensity radiation to destroy microorganisms;
- non-ionizing radiation: it uses longer wavelength and lower energy; as a result, non-ionizing radiation loses the ability to penetrate substances and can only be used for sterilizing surfaces.

Gamma (γ) and Beta (β, electron beam) irradiation are both categorized as ionizing radiation techniques and are often compared [20].

1.4.2.1 Gamma Rays

Gamma irradiation (ISO 11137, 1995) (Figure 9), being electromagnetic in nature, is usually obtained from a source of ^{60}Co and is produced within a dose range of 10–30 kGy/h.

The treatment works by transferring energy to valence electrons, causing electrons to be ejected from materials to be sterilized through which gamma rays pass [20].

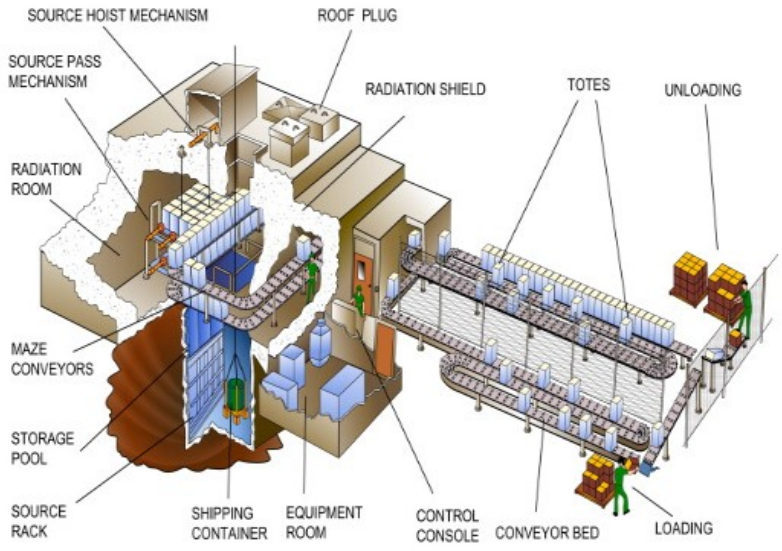

Figure 9. *Gamma Irradiation Sterilization Technique [26].*

It is important to note four key variables that allow to accurately evaluate the method used for applying gamma irradiation and the potential impact on clinical outcomes. These four key variables include [27]:

- target dose, that refers to the intended dose delivered to the tissue;
- dose range, that is a more precise description, because it conveys both the minimum and maximum amount of radiation exposure a graft has received (a narrow dose range indicates a higher degree of control);
- temperature at irradiation;
- tissue treatment before irradiation.

Gamma radiation sterilization technique is simple, rapid and effective; in addition, γ irradiation has the ability to inactivate both gram-negative and gram-positive bacteria, molds, yeasts, most viruses and some bacterial spores (high D-value). Unfortunately, γ radiation may induce some changes in scaffold material chemical properties, reduces compressive mechanical properties and molecular weights and increases rates of degradation post-sterilization [20].

1.4.2.2 Electron Beam (e-beam)

Differently from gamma irradiation, e-beam irradiation (Figure 10) is produced by an accelerating stream of electrons: materials to be sterilized move through a conveyor belt and under an electron beam gun that releases electrons that are accelerated through a gradient of charge [28]. Its dosage depends on the power of the source emitting it; generally, materials are irradiated and sterilized by electrons at energies between 5-10 MeV [20].

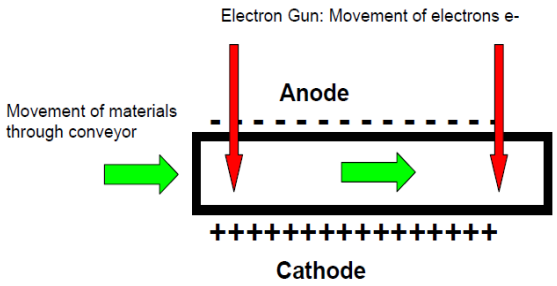

Figure 10. *Schematic Electron Beam Irradiation Sterilization Technique [28].*

There are several differences between e-beam and gamma sterilization: the first process uses no radioactive source and applies lower energy radiation than gamma

sterilization. In addition, e-beam sterilization is commonly shorter and it causes less degradation to materials [29].

The penetration depth of e-beam is dependent on the kinetic energy of electrons and on the density of the biomaterial being sterilized: in fact, increasing the intensity of the e-beam irradiation could be damaging to the scaffold structure; decreasing the intensity, instead, could limit the penetration depth of the e-beam irradiation, decreasing, in turn, the effectiveness of the e-beam sterilization. For these reasons, thick scaffolds generally cannot be sterilized by e-beam sterilization technique; moreover, e-beam sterilization results vary significantly from materials to materials and D-value is generally high, also with this technique [20].

While both radiation sterilization techniques have shortcomings, they are still considered promising candidates for sterilizing degradable scaffolds among all currently available techniques; however, key operating conditions such as radiation dosage and scaffold material moisture must be sufficiently studied and carefully controlled [20].

1.4.3 Ethylene Oxide

Ethylene oxide (EtO) is a well-known sterilizing agent (ISO 11135, 1994), but only recently its use has significantly emerged, thanks to its range of applications in the field of new medical device development and sterilization [30].

The preconditioning of the products in a chamber to specified temperatures and relative humidity constitutes the first step in EtO sterilization. After conditioning, the products are introduced into the sterilization chamber which is first evacuated and then heated to a temperature of 50-60 °C; moisture and EtO gas are then introduced for a specified amount of time (gas concentrations are typically 200-800 mg/l). After the specified exposure time, the EtO is removed and the chamber is flooded with filtered sterile air to aerate the products and remove any residual EtO to reach the acceptable levels. Thus the products are tested for sterility and residual ethylene oxide content [31]. The effectiveness of sterilization by EtO is dependent on operation parameters such as concentration, temperature, duration, and relative humidity [20]. .

EtO sterilization has some disadvantages: in fact, it is known to affect structural and biochemical properties of biodegradable scaffolds. In addition, residual toxicity of EtO is the major concern for EtO sterilization: the American Health Industry Manufacturers

Association (HIMA) and the American National Institute for Occupational Safety and Health (NIOSH) have set guideline of 25–250 ppm as the maximum EtO residual concentration in medical devices post-EtO sterilization, with recommended range of 10–25 ppm. Thus, aeration of scaffolds after EtO sterilization is mandatory in order to remove residual EtO [20].

1.4.4 Advantages and Disadvantages of Sterilization Techniques

Sterilization is a very important and crucial aspect in order to reduce the risk of microbial contaminations for the ultimate promotion or preservation of health [32]. However, incomplete microorganism inactivation, toxic residues and changes in scaffold structural and biochemical properties can be problematic to safety and efficacy, creating obvious problems for scaffolds applications [1].

The main sterilization techniques' advantages, disadvantages and post-sterilization effects on structural and biochemical properties of biodegradable scaffolds are summarized in Table III [20].

Table III. *Advantages, Disadvantages and Post-sterilization Effects of Sterilization Techniques*

STERILIZATION TECHNIQUES			
Technique	**Advantages**	**Disadvantages**	**Post-Sterilization Effects**
Steam	Simple, fast, effective, high penetration ability, no toxic residues	High temperature, affect the structural properties of biodegradable polymers	Increase in mechanical strength; decrease in molecular weight
Gamma radiation	High penetration ability, low temperature, effective, easy to control, no residue	Induce structural properties changes, dose rate is lower than electron beams, long time	Decrease in molecular weight and mechanical strength; increase in degradation rate; crosslinking
Electron beam	Low temperature, easy to control, no residue, fast	Induce structural properties changes, electron accelerator needed, low penetration ability	Crosslinking, chain scission; increase in the modulus of elasticity; decrease in inherent viscosity; faster mechanical degradation
Ethylene Oxide	Effective, low temperature	Induce structural property change, leave toxic residue, flammable, explosive, carcinogenic	Decrease in yield strength and stiffness

Unfortunately, as it is possible to see from Table III, irradiation is known to cause chain scission and crosslink degradation, leading to weakened mechanical properties, reduction of biocompatibility and increased degradation [28].

PVA, PVP and PEO based hydrogel formulations can be subjected to crosslinking reactions during irradiation processes [33]: because of their chemical composition, in fact, the irradiation introduces crosslinking among polymer chains and, consequently, leads to the formation of a three-dimensional polymer network complexity [34]. As a consequence, these hydrogels undergo to undesirable effects such as embrittlement, solidification, plasticization or viscosity increase [35].

1.5 Biomolecules limiting Sterilization Disadvantages

As already said, radiation crosslinking, caused by sterilization or high dose irradiation of PEO, PVA or PVP-based hydrogels, could compromise their chemical-physical and bio-mechanical properties. Therefore, there is a need for development of a method for preventing or limiting crosslinking phenomena of hydrogels and for designing of crosslink-resistant hydrogel formulations [33].

A lot of studies have been conducted using Vitamin C as an anti-crosslinking molecule. It is known that Vitamin C is an antioxidant and acts as a regenerating agent for oxidized and free radical species in the body; in the studies of Pucic et al. [34] and of Oral et al. [35] Vitamin C has been used as an anti-crosslinking agent for irradiated PEO and PVA, respectively. Both studies have highlighted that the addition of Vitamin C prevents radiation crosslinking and that the strategy is valid in order to enhance stability, injectability and high temperature processability of PEO- and PVA- based medical formulations after irradiation.

1.5.1 Hydroxytyrosol as Anti-crosslinking Molecule

Polyphenols are a broad family of compounds that can be found in fruits and vegetables, wine, tea, cocoa and extra-virgin olive oil and which exhibit strong antioxidant activity by scavenging different families of Reactive Oxygen Species (ROS) [36].The major phenolic compounds in olive oil (Figure 11) are oleuropein, hydroxytyrosol (2-(3,4-dihydroxyphenyl)ethanol) and tyrosol (2-(4-hydroxyphenyl)ethanol) [37]. The chemical structures of these phenolic compounds can protect the organism against the oxidative damage caused by oxidant agents (active

oxygen, free radicals, etc.); they also prevent the food deterioration by prevention of lipid oxidation [37].

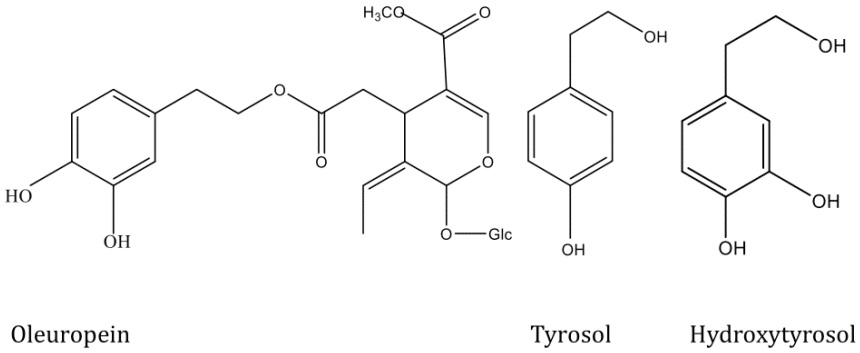

Figure 11. *Major Phenolic Compounds in Olive Oil [37].*

Hydroxytyrosol (HT) is an amphipathic phenol with a molecular weight of 154.16 g/mol and a phenylethyl-alcohol structure [38]. HT is obtained through hydrolysis of oleuropein which originates during the maturation of the olives, storage of the oil, and preparation of table olives [39]; on the other hand, the content of HT in olive oil depends on the kind of olive tree and olive, the location of the plantation, the oil quality and the olive oil elaboration process [38]. HT can be considered as a superior antioxidant and radical scavenger to oleuropein and tyrosol [37].

Historically, olive tree leaves have been used for traditional therapy by ancient civilizations; since the middle of last century, the benefits of minor olive components have been extensively investigated [36]. Hydroxytyrosol has a great bioactive power: its structural affinity to some compounds, its simple molecular structure and its presence in organism make it easy to assimilate by the human body, reaching blood plasma in 15 or 20 minutes until its elimination 6–8 h later by the renal or digestive system, so it does not present accumulation or toxicity problems. In addition, because it is a water-soluble and fat-soluble molecule, it is a good transporter of substances through the human body; therefore, it can penetrate the cellular membrane easier [40]. HT shows a broad spectrum of biological properties; it exerts:

- an antioxidant activity: it is the most studied property of olive phenolic compounds. The high antioxidant efficiency of HT – attributed to the presence of the o-dihydroxyphenyl moiety – is due to its high capacity for free radical scavenging during the oxidation process and to its reducing power on Fe^{3+}. Therefore, HT reduces oxidation of the low-density lipoproteins carrying

cholesterol (LDL-C), which is a critical step in the development of atherosclerosis and other cardiovascular diseases; it has also a potential protective effect against oxidative stress induced by tertbutyl hydroperoxide [36];

- an anticancer activity: the antitumor effect of HT has been studied as a result of its capacity to inhibit proliferation and promote apoptosis in several tumor-cell lines by diverse mechanisms, in addition to its ability to be chemo-preventive with its high antioxidant activity [39];
- an antimicrobial activity: olive oil and extracts from olive leaves were identified as antimicrobial agents with activity against Escherichia coli, Candida albicans, Streptococcus mutans, Salmonella enterica, and others. In addition, it has been demonstrated in vitro that HT also possesses antimicrobial properties against infectious agents of the respiratory and gastrointestinal tracts such as Vibrio parahaemolyticus, Vibrio cholerae, Salmonella typhi, Haemophilus influenzae, Staphylococcus aureus [39];
- an effect on the formation and maintenance of bone: like cancer incidence, lower osteoporosis incidence was observed in countries where the Mediterranean diet is predominant; thus, it is possible to say that Mediterranean diet has protective effect about bone health. According to the results of the conduced studies, particularly hydroxytyrosol may have critical effects on the formation and maintenance of bone and prevented bone loss; it can be used as potent remedies in the prevention and treatment of osteoporosis [37];
- an anti-inflammatory activity: inflammation and its consequences play a crucial role in the development of atherosclerosis and cardiovascular diseases; polyphenols have been shown to decrease the production of inflammatory markers in several systems. HT was proven to inhibit the chemically induced aggregation, the accumulation of the proaggregant agent thromboxane in human serum, the production of the pro-inflammatory molecules leukotrienes and the activity of arachidonate lipoxygenase [36];
- an antiviral activity: HT and oleuropein have been identified as a unique class of HIV-1 inhibitors that prevent HIV from entering into the host cell and binding the catalytic site of the HIV-1 integrase; thus, these agents provide an advantage over other antiviral therapies in which both, viral entry and integration, are inhibited [36];
- an antinitrosating effect: it has been shown that HT reacts with sodium nitrite at pH 3 to give 2-nitrohydroxytyrosol, supporting a protective role of HT as an

efficient scavenger of nitrosating species [36]. In addition, it is remarkable that HT presents a powerful capacity to scavenge radical species and to induce antioxidant enzymes that could improve some neurodegenerative disorders such as Parkinson's disease [38];

- an effect in metabolic syndrome: it has been demonstrated in middle-aged overweight men that a phenolic-enriched supplementation with oleuropein and HT for 12 weeks, improves the glucose regulation and β-cell secretion capacity of insulin [38];
- an effect in respiratory diseases: HT could decrease the levels of superoxide anion in in vitro and in vivo models it can scavenge hydrogen peroxide in a dose dependent manner during the respiratory burst when human neutrophils were stimulated. In addition, HT can inhibit the growth of several Gram-positive and Gram-negative bacteria related to respiratory tract infections [38].

Since HT properties are very similar to those of Vitamin C (antioxidant molecule, acting as a regenerating agent for oxidized and free radical species in the body), this study aims to use HT as a method for preventing crosslinking of injectable hydrogels and, thus, limiting related modifications in the mechanical behaviour (embrittlement, solidification, viscosity increase).

1.6 Analytical Methods

1.6.1 Viscosimetry

Rheology is the study of flow behaviour; it is normally applied to fluid materials (or materials that exhibit a time-dependent response to stress) [41], either simply in terms of viscosity or also relative to various viscoelastic properties [42].

Knowledge of rheological behaviour is essential: the extent to which a material deforms under a certain force depends strongly on its properties [43]. For this reason, there are obviously many areas where the rheology is very important, like foods, personal care products, pharmaceuticals, paints, medicine, agrochemicals [42].

Flow is typically measured using shear: shear parameters of stress (τ) and rate of strain ($\dot{\gamma}$) are calculated from measurements of torque and flow rate. Viscosity (η) is defined as [41]:

$$\eta = \frac{\tau}{\dot{\gamma}}$$

Several types of flow behaviour are generally recognized (Figure 12). The simplest is Newtonian behaviour, with a linear relationship between stress and strain rate and zero stress at zero strain rate: this is the ideal fluid behaviour (typical of water or plasma). Many fluids show plastic behaviour (also called Bingham-Green), in which flow only initiates above some level of stress (called yield stress τ_c), and once flow initiates the relationship between stress and strain rate is linear. Another common behaviour is pseudo-plastic (or shear thinning), in which viscosity decreases as strain rate increases; occasionally materials show shear thickening behaviour [41].

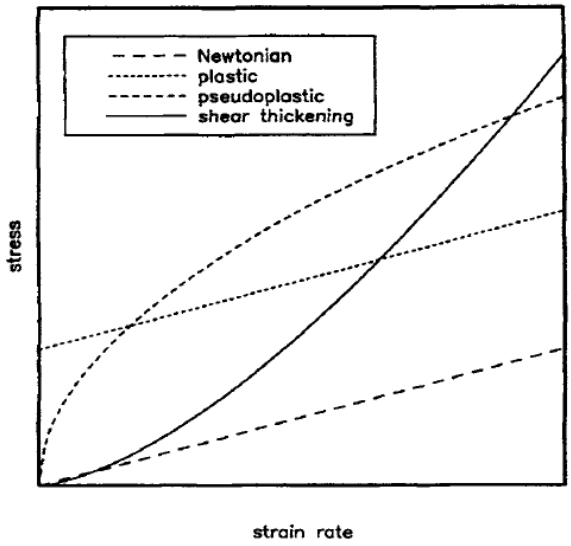

Figure 12. *Types of rheological behaviour [41].*

The flow can be measured in a static or in a dynamic way [41]:

- the static flow technique measures the stress to achieve a given strain rate (or vice versa): this is usually done at a series of strain rates to provide a flow curve, a plot of stress as a function of strain rate. The rheological behaviour can alternatively be presented as a plot of viscosity as a function of strain rate or stress;
- a key development in recent years in rheology has been the use of dynamic techniques for characterization of viscoelastic materials: such techniques measure the behaviour when there is a change in strain rate or shear stress. The key dynamic techniques used are low-amplitude oscillatory shear – that measures stress, when the materials are subjected to an oscillating (according

to a sine function) strain (or vice versa) from which is determined the modulus (G) or the viscosity (η) – and creep/recovery – that measures strain, when a stress is applied (creep) or removed (recovery); from this is determined the compliance (strain divided by stress).

Moreover, the dynamic techniques provide information for the full range of material behaviour (elastic solids, viscoelastic solids, viscoelastic liquids, and viscous liquids) while the static technique provides only limited information about elastic behaviour (i.e. the yield stress) and only for viscoelastic liquids [41].

Shear rheometers are instruments for measuring flow behaviour; they usually operate in rotation and measure torque and rotational speed. The rheological parameters of stress and strain rate are, then, computed from these measurements. The most used rheometers employ coaxial cylinders or parallel plates (Figure 13): sample sits between and one of the cylinders or plates rotates. In this geometry it is necessary that the gap be considerably wider than the diameter of the largest particles [41].

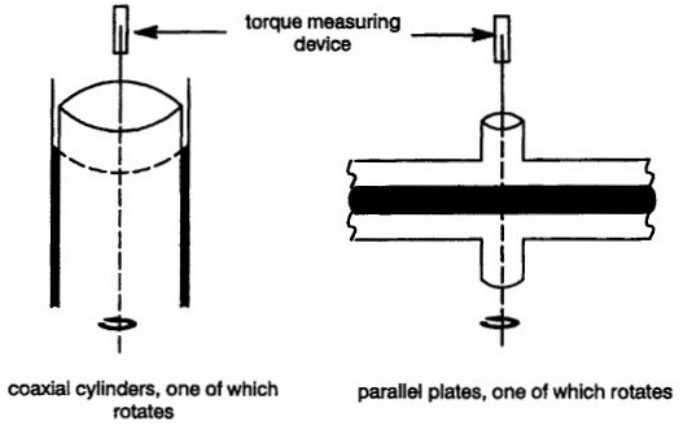

Figure 13. *Common Geometries for Rotational Rheometry [41].*

1.6.2 IR Spettroscopy

Spectroscopy and spectrography are terms used to refer to the measurement of radiation intensity as a function of wavelength [44]. In fact, if a molecule is placed in an electromagnetic field (e.g., light), a transfer of energy from the field to the molecule will occur only when Bohr's frequency condition is satisfied [41]:

$$E = h\nu$$

where h is the Plank's constant and ν is the frequency of light.

Infrared (IR) spectroscopy is a technique based on the vibrations of the atoms of a molecule [45], used in the areas of determination of molecular structure, identification of chemical species and quantitative/qualitative determination of chemical species [41]. It has been used in labs since the mid of 1980s [46] and now it is gaining much importance with the advent of user-friendly equipment and continuing research on identification and characterization of reaction products and new materials [41].

The analysis can be conducted in three ways, by measuring absorption, transmission or reflection (Figure 14). Generally, the most used method is the IR absorption spectroscopy, with which scientists determine the structures of molecules [52]: the infrared spectrum is commonly obtained by passing infrared radiation through a sample and determining what fraction of the incident radiation is absorbed at a particular energy [45].

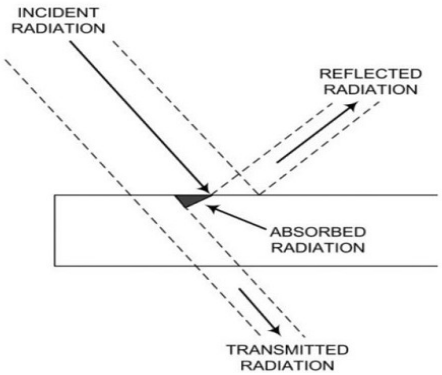

Figure 14. *Incident Radiation, Reflected Radiation, Absorbed Radiation and Transmitted Radiation in the ideal case of a super-smooth, homogeneous material [46].*

When exposed to infrared radiation – the range of IR region is from 10^4 nm to 10^6 nm – sample molecules selectively absorb radiation of specific wavelengths: this causes the change of dipole moment of sample molecules; consequently, the vibrational energy levels of sample molecules transfer from ground state to excited state [47].

Band positions in IR spectra are presented here as wave numbers whose unit is the reciprocal centimeter (cm^{-1}), proportional to the energy of vibration. Band intensities can be expressed either as [45]:

- transmittance ($T = \frac{\phi^t}{\phi^i}$), that is the ratio of the radiant flux transmitted by a sample (ϕ^t) to the radiant flux incident on the sample (ϕ^i); so, T is the effectiveness of the surface of a material in transmitting radiant energy;

- absorbance ($A = \log_{10}(1/T)$), that is the logarithm, to the base 10, of the reciprocal of the transmittance.

From the point of view of the qualitative analysis of organic compounds, complexes and inorganic compounds, the most interesting region of the infrared spectrum is that one ranging from 4000 cm^{-1} to 600 cm^{-1} (Figure 15). The area of fundamental vibrations can be divided into two parts [48]:

- the region of functional groups, from 4100 cm^{-1} to 1500 cm^{-1};
- the fingerprints region, from 1500 cm^{-1} to 600 cm^{-1}.

None of the IR bands is a pure vibration, but it is the set of vibrations of the entire molecule. However, if the weight of the individual vibrations for a given absorption is very high, it is justified to attribute the absorption in a certain range of frequencies to a particular group [48]. Through the correlation papers, a specific group can be identified based on the position in the spectrum and the intensity of some absorption maxima. The bands, in fact, are classified according to the frequencies and intensities of their maximum; the intensity symbols are vs (very strong), m (medium), w (weak) and vw (very weak) [48].

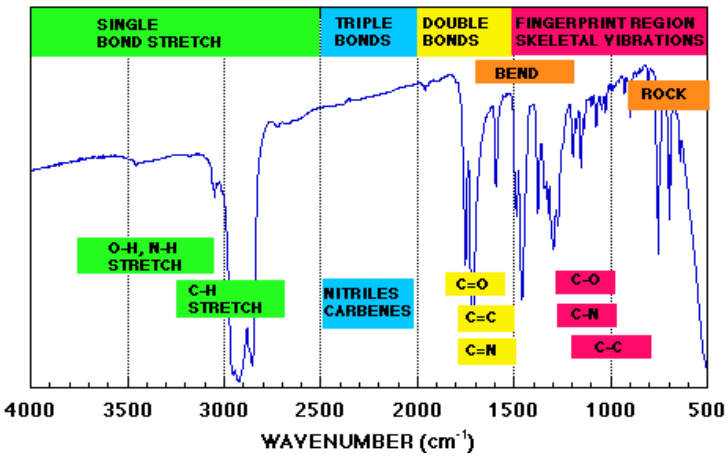

Figure 15. *Different areas of IR spectra [48].*

In addition, there are two different types of molecular vibrations [48]:

- stretching, that is a rhythmical symmetric or asymmetric movement along the bond axis such that the inter-atomic distance is increasing or decreasing;
- bending, that is a change in bond angle between bonds. There are several types of bending, like rocking (a change in angle between a group of atoms),

wagging (a change in angle between the plane of a group of atoms), twisting (a change in the angle between the planes of two groups of atoms) and scissoring (when two atoms move away and toward each other).

By analyzing the infrared spectrum, one can readily obtain abundant structure information of a molecule, because [47]:

- the frequency of the absorption peak is determined by the vibrational energy gap;
- the number of absorption peaks is related to the number of vibrational freedom of the molecule;
- the intensity of absorption peaks is related to the change of dipole moment and the possibility of the transition of energy levels.

Fourier Transform Infrared (FT-IR) Spectroscopy employs an interferometer and exploit the well-established mathematical process of Fourier transformation [45]; FT-IR is a rapid, economical, easy and non-destructive technique. The progress in FT-IR spectrometer designs has greatly enhanced the field of their applications: modern instruments offer several prominent advantages [49]:

- the signal-to-noise ratio of spectrum is significantly higher than the previous generation IR spectrometers;
- the accuracy of wave-number is high (the error is in the range of ± 0.01 cm^{-1});
- the scan time of all frequencies is short (approximately 1 s);
- the resolution is extremely high (0.1 - 0.005 cm^{-1});
- the scan range is wide (1000 - 10 cm^{-1});
- the interference from stray light is reduced.

Thanks to its multiple advantages, FT-IR spectrometers have replaced dispersive IR spectrometers [47].

A common FT-IR spectrometer (Figure 16) consists of a source, interferometer, sample compartment, detector, amplifier, A/D convertor, and a computer. The source generates radiation which passes through the interferometer to the sample before reaching a detector; upon amplification of the signal, in which a filter has eliminated high frequency contributions, the data are converted to a digital form by an analog-to-digital converter and transferred to the computer for Fourier transformation [45].

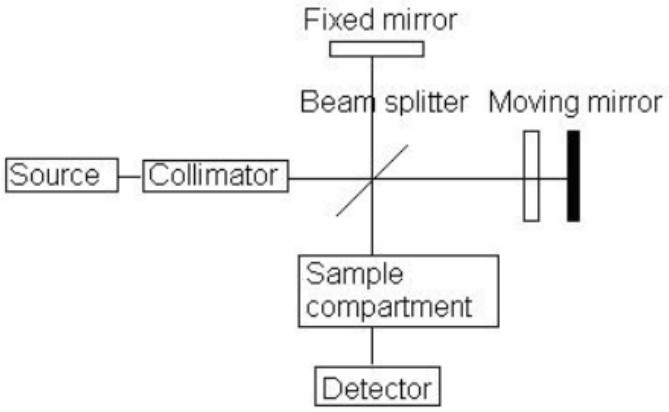

Figure 16. *Block Diagram of a FT-IR Spectrometer* [45].

The major difference between an FT-IR spectrometer and a dispersive IR spectrometer is the Michelson interferometer (Figure 17): this is the core of the FT-IR spectrometer and it is used to split one beam of light into two, so that the paths of the two beams are different. The Michelson interferometer is, generally, composed by two perpendicular mirrors – one stationary and one movable – and a beamsplitter, designed to transmit half the light (strike the stationary mirror) and reflect half of the light (strike the movable mirror). When a collimated beam of monochromatic radiation of wavelength λ is passed into an ideal beamsplitter, 50% of the incident radiation will be reflected to one of the mirrors and 50% will be transmitted to the other mirror. Then, the Michelson interferometer recombines the two beams and conducts them into the detector where the difference of the intensity of these two beams are measured as a function of the difference of the paths [45].

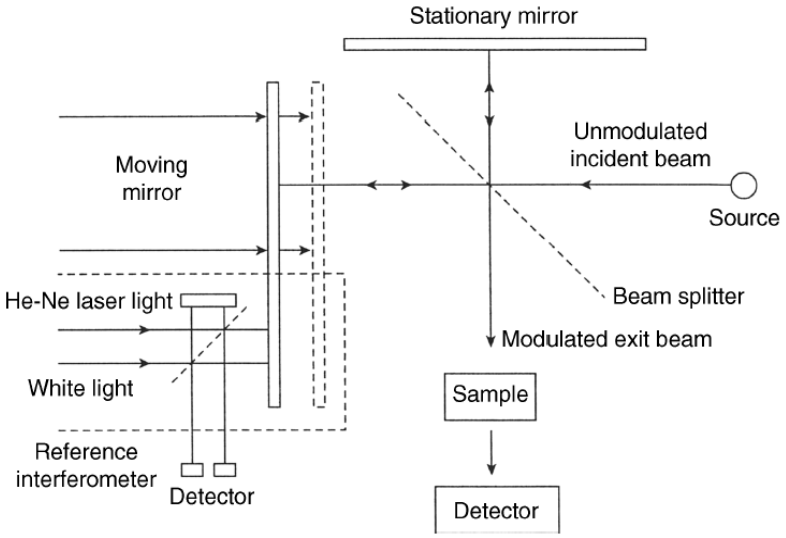

Figure 17. *Schematic Representation of the Michelson Interferometer* [45].

Since the mirror moves back and forth, the intensity of the signal increases and decreases: in this way a cosine wave is created. The plot is defined as an interferogram: it is a signal produced as a function of the change of path length between the two beams. The two domains of distance and frequency are inter-convertible by the mathematical method of Fourier transformation [45].

Fast Fourier Transform (FFT) method on which the modern FT-IR spectrometer based was introduced to the world by Cooley and Turkey in 1965. Fourier transform is a mathematical method to transform a function into a new function; it relates the intensity falling on the detector, $I(\delta)$, to the spectral power density at a particular wave number $\bar{\nu}$, given by $B(\bar{\nu})$, as follows [45]:

$$I(\delta) = \int_0^{+\infty} B(\bar{\nu}) cos 2\pi\bar{\nu}\delta d\bar{\nu}$$

$$B(\bar{\nu}) = \int_{-\infty}^{+\infty} B(\delta) cos 2\pi\bar{\nu}\delta d\delta$$

These two equations are known as a Fourier transform pair: the first equation shows the variation in power density as a function of the difference in path length, which is an interference pattern; the second equation shows the variation in intensity as a function of wave number [45].

1.6.3 High Performance Liquid Chromatography (HPLC)

High-performance liquid chromatography (or high pressure liquid chromatography, HPLC) is a particular type of column chromatography and it is generally used in biochemistry and analysis to separate, identify and quantify the active compounds. HPLC methods are advantageous compared to direct measurement techniques, especially in what regards to specificity, sensitivity, or easiness of operation [50].

During separation the sample components are distributed between a solid stationary phase - normally packed inside a stainless steel column - and a liquid mobile phase [51] (Figure 18): retention time varies depending on the interactions between the stationary phase, the molecules being analyzed, and the solvent(s) used [50].

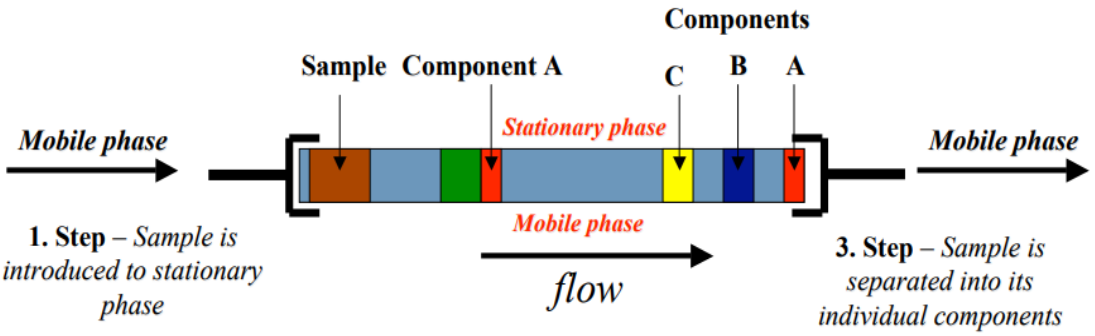

Figure 18. *Separation of the Sample Components* [51].

There are some parameters which are used as a standard for a particular compound; the most commonly used parameters are [50]:

- internal diameter (ID): t is a critical aspect that determines the quantity of analyte that can be loaded onto the column and also influences sensitivity (low ID columns have improved sensitivity and lower solvent consumption);
- particle size: most traditional HPLC is performed with the stationary phase attached to the outside of small spherical silica particles (very small beads); smaller particles generally provide more surface area and better separations;
- pore size: it defines the ability of the analyte molecules to penetrate inside the particle and interact with its inner surface; small pores provide greater surface area while larger pore size has better kinetics especially for larger analyte;
- pump pressure: modern HPLC systems have been improved to work at much higher pressures, and therefore be able to use much smaller particle sizes in the columns.

The apparatus (Figure 19) consists of [51]:

- a pumping system: HPLC pumping systems are required to deliver metered amounts of mobile phase at a constant flow rate; computer- or microprocessor-controlled pumping systems are capable of accurately delivering a mobile phase of either constant (isocratic elution) or varying (gradient elution) composition, according to a defined program. Depending on a lot of factors like column dimensions, particle size of the stationary phase, the flow rate and composition of the mobile phase, operating pressures of up to 42000 kPa can be generated;

- an injector: the sample solution is usually introduced into the flowing mobile phase at or near the head of the column using an injection system based on an injection valve design which can operate at high pressure;
- a chromatographic column: columns are usually made of polished stainless steel, are between 50 and 300 mm long and have an internal diameter of between 2 and 5 mm (columns with internal diameter of less than 2 mm are referred to as microbore column); they are commonly filled with a stationary phase with a particle size of 3–10 μm;
- stationary phases: there are many types of stationary phases used in HPLC including unmodified silica, alumina or porous graphite – used in normal-phase chromatography, where separation is based on differences in adsorption) – or a variety of chemically-modified supports prepared from polymers, silica or porous graphite – used in reversed-phase HPLC, where separation is based principally on partition of the molecules between the mobile phase and the stationary phase;
- mobile phases: the choice of mobile phases is based on the desired retention behaviour and the physicochemical properties of the analyte as well as the type of detector chosen. For normal-phase HPLC using unmodified stationary phases lipophilic solvents should be employed; in reversed-phase HPLC aqueous mobile phases, with and without organic modifiers, are used;
- connecting tubing and fittings: connections between injector/column, column/detector and/or detector/detector may compromise the overall efficiency of the system; any fittings should be of the "zero dead volume" (ZDV) type;
- detectors: there are several ways of detecting when a substance has passed through the column; UV absorption spectrophotometers are commonly used detectors in pharmaceutical analysis. Many organic compounds absorb UV light of various wavelengths: the amount of light absorbed will depend on the amount of a particular compound that is passing through the beam at the time [55];
- data collection devices: signals from the detector may be collected on chart recorders or electronic integrators that vary in complexity and in their ability to process, store and reprocess chromatographic data.

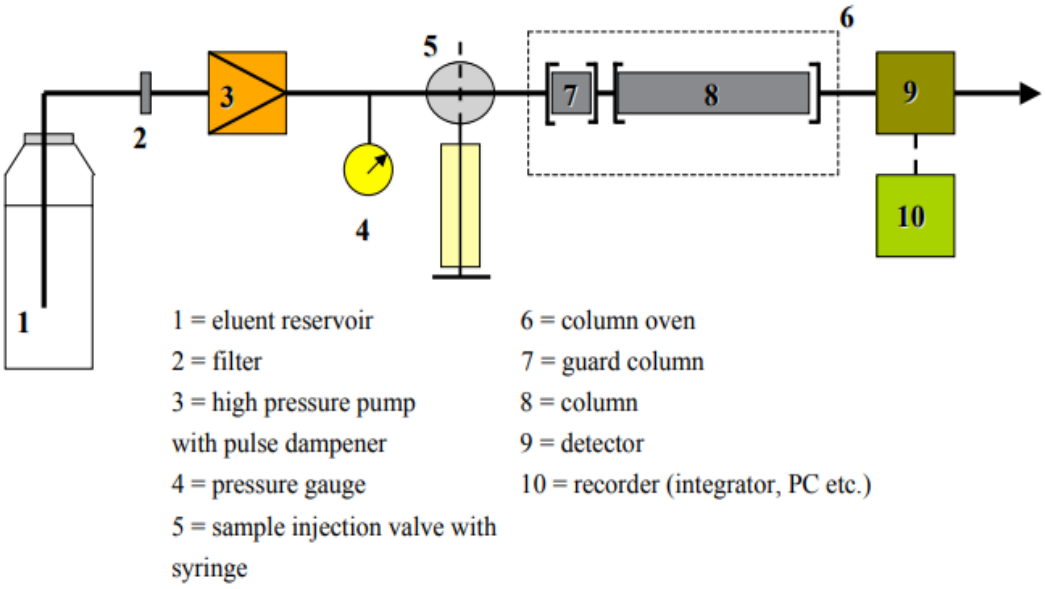

Figure 19. *Block Scheme HPLC System for Isocratic Operation* [51].

After separation the components can be quantified and even identified: the chromatogram shows the separation [50]. Chromatographic peaks should possess Gaussian profiles in the optimal case and are characterized by the following parameters [51] (Figure 20):

- retention time t_R: it is the time measured from the point of injection to the maximum point of the retained peak;
- peak height h: it is the distance measured from the base of the peak to the peak maximum;
- efficiency of a chromatographic column N: it is defined in terms of the number of theoretical plates N and can be calculated as $N = 5.54 \frac{t_R^2}{W_h^2}$ where t_R is the retention time and W_h is the width of the peak of interest determined at half peak height;
- capacity factor or mass distribution ratio D_m: it is defined as the ratio between the amount of solute in stationary phase and the amount of solute in mobile phase or using the formula $D_m = \frac{(t_R - t_M)}{t_M}$ where t_R is the retention time of the solute and t_M is the retention time of an unretained component;
- peak-to-valley ratio p/v: it is calculated as $\frac{p}{v} = \frac{H_p}{H_v}$ where H_p is the height above the extrapolated baseline of the minor peak and H_v is the height above the

extrapolated baseline at the lowest point of the curve separating the minor and the major peaks;

- the resolution factor R_S: it is calculated using the formula $R_S = \frac{1.18\,(t_{R2}-t_{R1})}{(W_{b1}+W_{b2})}$ with $t_{R2} > t_{R1}$ where t_{R1} and t_{R2} are retention times or baseline distances between the point of injection and the perpendicular dropped from the maximum of each of the two peaks and W_{b1} and W_{b2} are the respective peak widths determined at half peak height;
- peak symmetry factor or tailing factor A_S: it is calculated as $A_S = \frac{W_x}{2d}$, where W_x is peak width at 5% of peak height, measured from the baseline and d is the baseline distance between the perpendicular dropped from the peak maximum and the leading edge of the peak at 5% of the peak height;
- dead time: it is the time the mobile phase front or an unretained peak travel through the column, measured from the point of injection until the time the peak maximum appears in the chromatogram.

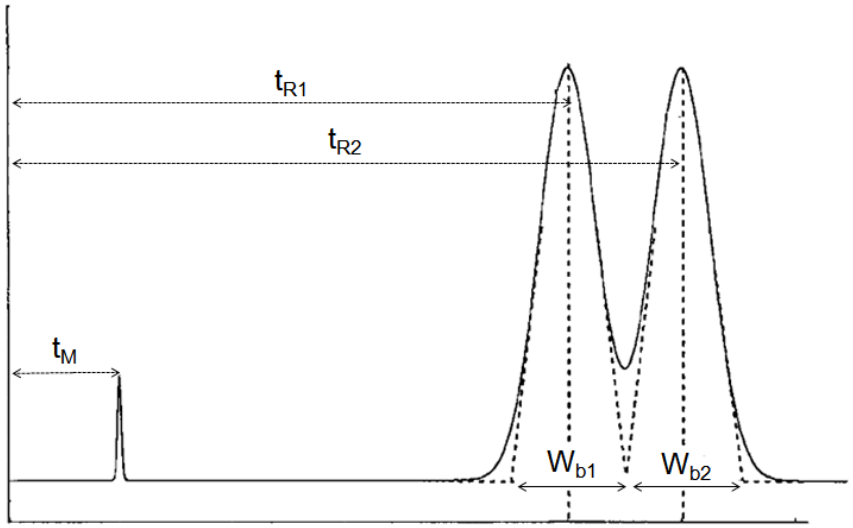

Figure 20. *Parameters describing Chromatographic Peaks* [51].

1.7 Previous Studies and Aim

The growing interest in the regeneration and reconstruction of pathologically altered tissues has involved a multitude of researches in the use of 3D scaffolds [1]. In this scenario, hydrogels have received significant attention thanks to their properties and their exceptional promise in biomedical applications [6].

A biodegradable scaffold has a potential to be infected by a wide range of microorganism; the consequent risk of disease transmission has been reduced through terminal sterilization, which has shown high efficiency for neutralizing pathogens [20].

Sterilization of hydrogels, however, may alter the characteristics of the biodegradable scaffolds, inducing some changes either in chemical or physical properties and increasing rates of post-sterilization degradation [17]. Specifically, PVA-, PVP- and PEO-based hydrogel formulations can be subjected to crosslinking reactions during irradiation processes; as a consequence, these hydrogels undergo to undesirable effects such as embrittlement, solidification, plasticization or viscosity increase [33].

These data underline that there is the need for development of a method for preventing or limiting crosslinking phenomena of hydrogels; the use of at least one anti-crosslinking agent is, in fact, an effective way in preventing crosslinking of the hydrogel during irradiation. Anti-crosslinking agents may include compounds with antioxidant and/or free-radical scavenger properties; the anti-crosslinking agent, thus, can be selected among ascorbic acid (including ester and acetate forms of Vitamin C), vitamins (such as Vitamin E, D and B), quinones, amino acids (such as arginine, cysteine, tryptophan), citric acid or phenolic derivatives [33].

Since it has been known that antioxidants as Vitamin C and Vitamin E act as regenerating agents for oxidized and free radical species in the body [33], a lot of studies have been conducted using them as anti-crosslinking molecules.

In a 2007 study, Oral et al. [35] has discovered that radiation-induced cross-linking of PVA solutions could be prevented by using Vitamin C; in addition this study has demonstrated that Vitamin C can also be used to decrease the viscosity of irradiated hydrogels and, thus, to enhance the stability and injectability of PVA-based medical formulations.

In another study of 2010, Oral et al. [52] has demonstrated that Vitamin E reduces crosslinking efficiency in ultrahigh molecular weight polyethylene (UHMWPE) during irradiation and that is possible to spatially control the crosslink density distribution by tailoring the Vitamin E concentration profile.

Thanks to its antioxidant, anti-inflammatory and antimicrobial properties, hydroxytyrosol (HT) could be selected as a good alternative to Vitamin C and Vitamin E. In fact, HT has an oxygen radical absorption capacity of 40,000 μmolTE/g, ten times higher than

green tea and two times higher than that of coenzyme Q-10, a molecule that is naturally present inside human cells [53]. According to the study of Fruhwirth et al. [54] hydroxytyrosol has an antioxidant capacity significantly higher than ascorbic acid; in fact, expressing capacities of samples containing pure antioxidants as Trolox equivalent antioxidant capacities (TEAC) – defined as the concentration of the Trolox solution (mM) that produces an antioxidant effect equivalent to the effect of a 1.0 mM solution of the substance of interest – HT and ascorbic acid shows a TEAC of 1.17±0.04 and only 0.53±0.08, respectively.

On the basis of these considerations, the hypothesis is that radiation-induced cross-linking of PEO-based hydrogels could be either prevented or limited by tailoring the concentration of hydroxytyrosol introduced as an anti-crosslinking agent. In addition, this work aims to evaluate how the use of a specific kind of buffer saline solution can affect the final characteristics of the optimized hydrogel.

In order to verify the above mentioned assumptions, the study has been performed by producing gels with PEO, HT and two different buffer solutions (such as, Phosphate Buffer Solution, PBS and Citrate Buffer Solution, CBS). The samples characterization has been then carried out on two analytical levels: the rheological and the chemical one.

The rheological analysis has been conducted in order to evaluate the hydrogel viscoelasticity changes depending on a variation of HT concentration (both in Not-Sterile and Sterile condition).

The chemical characterization has been conducted through both Fourier-Transform Infrared Spectroscopy (FTIR) – a powerful tool to study chemical changes and to provide informations on species crystallinity – and High Performance Liquid Chromatography (HPLC) – used to separate, identify and quantify the active compounds (e.g., hydroxytyrosol) detectable inside hydrogels.

2. Materials and Methods

In order to understand the various methods that have been applied, a summary block diagram has been created (Figure 21): as it is possible to see, light blue rectangles represent methods and light green circles represent the respective results. The first phase is the Production of HT-based Hydrogels, in particular, the Not-Sterile samples; consequently, some samples are sent to sterilizing facility (Gamma rays Sterilization). Then, both Not-Sterile and Sterile samples undergo the analysis process: after the Rheological Analysis in laboratory, samples are evaluated through FT-IR Analysis, HT Extraction and HPLC Analysis.

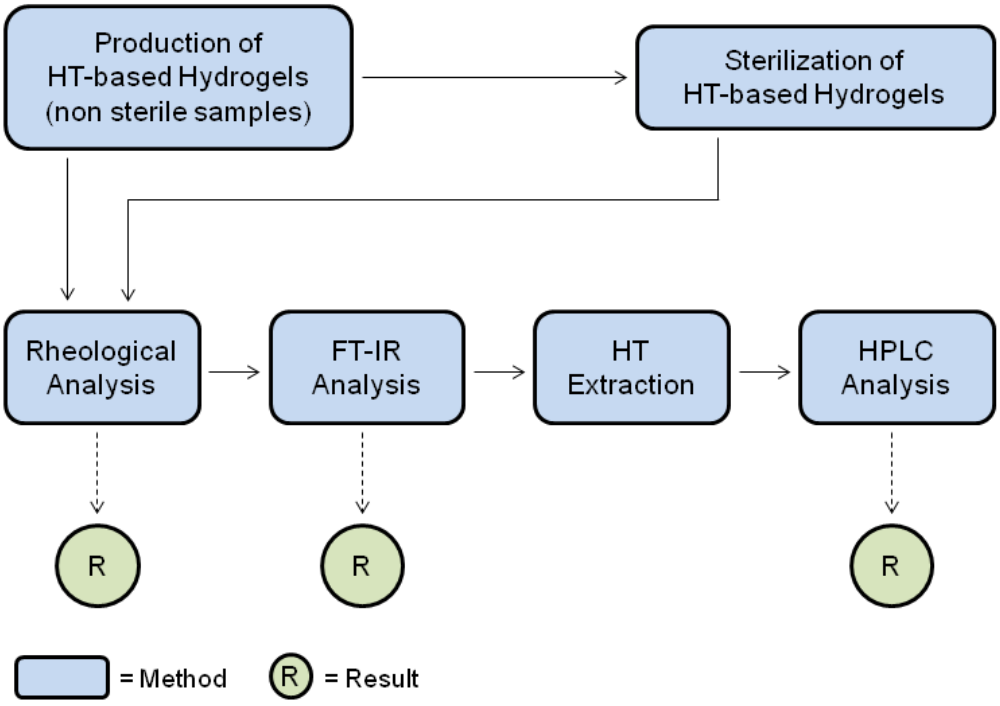

Figure 21. *Methods Block Diagram.*

2.1 Production

The Production of HT-based Hydrogels follows three main steps:

- Preparation of Solvent and Solutes with consequent weighting of different components;
- Mixture Preparation with stirrers in order to create HT-based Hydrogels;
- pH Measurement, in order to do a comparison between pre- and post-sterilization samples.

The following block scheme (Figure 22) represents the whole Production Process.

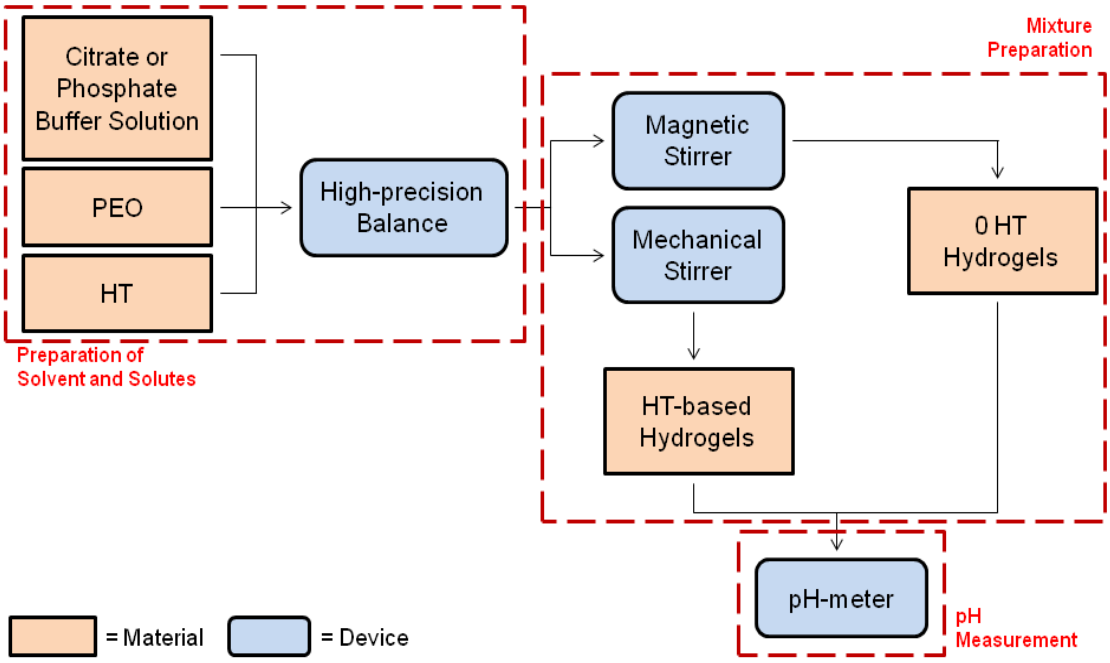

Figure 22. *Production Process Block Diagram.*

2.1.1 Preparation of Solvent and Solutes

The aim of this initial phase is to prepare n. 7 Phosphate Buffer-based Hydrogels and n. 9 Citrate Buffer-based Hydrogels, with different HT concentrations; in order to fulfil the aim, four components (Figure 23) have been involved:

- Potassium Phosphate Buffer (PBS; pH 6.00 1X; TL1102, HiMedia), that has been used only for n. 7 Phosphate Buffer-based Hydrogels;
- Citrate Buffer Solution, pH 5.00, that has been used only for n. 9 Citrate Buffer-based Hydrogels; 1 L of 10 mM solution has been prepared by mixing 0.86 g of Citric Acid (PM = 210.14 g/mol, C0759 Sigma-Aldrich), 1.74 g of Sodium Citrate Dihydrate (PM = 294.12 g/mol, W302600 Sigma-Aldrich) and 997.4 g of bi-distilled water with an high degree of purity, produced with ELGA system (UK);
- Polyethylene Oxide (PEO), 600 kDa, 4% w/w (182028, Sigma-Aldrich);
- Hydroxytyrosol (HT), PM = 154.16 g/mol (10597-60-1, Seprox Biotech).

Figure 23. *Hydrogels' Components. From left to right Potassium Phosphate Buffer, Citric Acid, Sodium Citrate Dihydrate, Citrate Buffer Solution, Polyethylene Oxide and Hydroxytyrosol.*

Samples of 100 g of Phosphate Buffer-based Hydrogels have been prepared with HT concentrations equal to 0 mM (0.0000 g HT), 1 mM (0.0154 g HT), 2 mM (0.0308 g HT), 5 mM (0.0771 g HT), 10 mM (0.1542 g HT), 50 mM (0.7708 g HT) and 100 mM (1.5416 g HT). Citrate Buffer-based Hydrogels have been prepared also with HT concentrations equal to 20 mM (0.3083 g HT), 40 mM (0.6173 g HT). Since PEO has been kept constant (4% w/w), the grams of Phosphate Buffer Solution or Citrate Buffer Solution to be added in each different solution have been calculated. The different HT-based Hydrogel formulations are shown in Table IV.

Table IV. *HT Hydrogel-based Formulations*

HT-BASED HYDROGEL-BASED FORMULATIONS				
HT [mM]	**BUFFER [g]**	**PEO (4%) [g]**	**HT [g]**	**Tot. (100 g)**
0	96.00	4.00	0.0000	100
1	95.98	4.00	0.0154	100
2	95.97	4.00	0.0308	100
5	95.92	4.00	0.0771	100
10	95.85	4.00	0.1542	100
20 *	95.69	4.00	0.3083	100
40 *	95.38	4.00	0.6166	100
50	95.23	4.00	0.7708	100
100	94.46	4.00	1.5416	100

* Hydrogels prepared only with Citrate Buffer Solution.

Components have been weighed with two types of high-precision balances:

- HT has been weighed using Adventurer AX124 by Ohaus (Figure 24) [55]; technical data of the balance are reported in Table V;
- other components have been weighed using Scout STX1202 by Ohaus (Figure 25) [56]; technical data of the balance are reported in Table V.

Table V. *Technical Data Adventurer AX124* [55] and *Scout STX1202* [56]

TECHNICAL DATA ADVENTURER AX124	
Max. Capacity	120 g
Resolution	0.1 mg
Pan Size	90 mm
Display	Display Touch-screen
Linearity	± 0.2 mg
Repeatability	0.1 mg
Stabilization Time	3 s
TECHNICAL DATA SCOUT STX1202	
Max. Capacity	1200 g
Resolution	0.01 g
Plate Dimension	140 x 170 mm
Display	Display Touch-screen
Linearity	± 0.03 g
Repeatability	0.02 g
Stabilization Time	1.5 s

Figure 24. *High-precision Balance Adventurer AX124 (Ohaus)* [55].

Figure 25. *High-precision Balance Scout STX1202 (Ohaus)* [56].

All measurements were performed 5 times for each component, in order to calculate the minimum and maximum values, the median, the mean value and the standard deviation (STD). Weight values of different hydrogels' components are reported in Tables VI and VII.

Table VI. *Weight values of Components of Phosphate Buffer-based Hydrogels*

WEIGHT VALUES OF COMPONENTS OF PHOSPHATE BUFFER-BASED HYDROGELS								
		HT 0	**HT 1**	**HT 2**	**HT 5**	**HT 10**	**HT 50**	**HT 100**
BUFFER [g]	**min** **max**	95.99 96.01	95.97 96.00	95.96 95.97	95.93 95.94	95.85 95.86	95.22 95.24	94.85 94.87
	median	96.00	95.99	95.96	95.93	95.86	95.24	94.86
	mean	96.00	95.99	95.96	95.93	95.86	95.23	94.86
	STD	0.0081	0.0125	0.0047	0.0047	0.0047	0.0094	0.0081
PEO 4% [g]	**min** **max**	3.98 4.01	4.00 4.02	4.00 4.02	3.99 4.01	3.98 4.00	4.00 4.01	4.00 4.01
	median	4.00	4.01	4.02	4.00	3.99	4.01	4.00
	mean	4.00	4.01	4.01	4.00	3.99	4.01	4.00
	STD	0.0125	0.0081	0.0094	0.0081	0.0081	0.0047	0.0047
HT [g]	**min** **max**	0.0000 0.0000	0.0151 0.0160	0.0305 0.0309	0.0782 0.0788	0.1549 0.1554	0.7738 0.7774	1.5442 1.5445
	median	0.0000	0.0154	0.0307	0.0782	0.1550	0.7740	1.5443
	mean	0.0000	0.0155	0.0307	0.0784	0.1551	0.7739	1.5443
	STD	0.0000	0.0004	0.0002	0.0003	0.0002	0.0001	0.0001

Table VII. *Weight values of Components of Citrate Buffer-based Hydrogels*

WEIGHT VALUES OF COMPONENTS OF CITRATE BUFFER-BASED HYDROGELS										
		HT 0	**HT 1**	**HT 2**	**HT 5**	**HT 10**	**HT 20**	**HT 40**	**HT 50**	**HT 100**
BUFFER [g]	**min**	95.99	95.97	95.96	95.93	95.84	95.69	95.36	95.22	94.45
	max	96.01	95.99	95.97	95.94	95.86	95.71	95.37	95.24	94.47
	median	96.01	95.99	95.97	95.93	95.85	95.70	95.37	95.22	94.46
	mean	96.00	95.98	95.97	95.93	95.85	95.70	95.37	95.23	94.46
	STD	0.0094	0.0094	0.0047	0.0047	0.0082	0.0082	0.0047	0.0094	0.0082
PEO 4% [g]	**min**	4.00	4.00	3.99	3.98	4.00	3.98	3.98	4.00	4.00
	max	4.02	4.02	4.01	4.00	4.01	4.00	4.01	4.02	4.02
	median	4.02	4.01	4.00	3.99	4.00	3.99	4.00	4.01	4.01
	mean	4.01	4.01	4.00	3.99	4.00	3.99	4.00	4.01	4.01
	STD	0.0094	0.0081	0.0081	0.0081	0.0047	0.0081	0.0125	0.0081	0.0081
HT [g]	**min**	0.0000	0.0152	0.0303	0.0787	0.1549	0.3073	0.6170	0.7740	1.5413
	max	0.0000	0.0159	0.0307	0.0791	0.1552	0.3078	0.6175	0.7749	1.5420
	median	0.0000	0.0154	0.0305	0.0788	0.1551	0.3073	0.6174	0.7745	1.5419
	mean	0.0000	0.0155	0.0305	0.0789	0.1551	0.3075	0.6173	0.7745	1.5417
	STD	0.0000	0.0003	0.0002	0.0002	0.0002	0.0002	0.0002	0.0004	0.0003

2.1.2 Mixture Preparation

Once all the components have been prepared, two different types of stirrer have been used to develop Hydrogels. A magnetic stirrer (Joan-SH-2, BIPEE; Figure 26) [57] has been used to prepare the 0 mM HT Hydrogels: the rotating magnetic field is used to cause the stir bar immersed in the liquid to spin. Technical data of the magnetic stirrer used are reported in Table VIII.

Table VIII. *Technical Data Joan-SH-2, BIPEE [57]*

TECHNICAL DATA JOAN-SH-2	
Speed	100 to 1600 rpm
Stirring Power	10 W
Heating Power	180 W
Max. Stir Volume	1 L (1000 mL)
Max. Temperature	380 °C
Continuous Operation	YES
Dimension of Panel	12 x 12 cm
Product Size	200 x 120 x 90 mm
Weight	2 kg
Material of Panel	Cast Aluminium, Surface Spraying

Figure 26. *Magnetic Stirrer Joan-SH-2 (BIPEE)* [57].

A mechanical stirrer (AM20-D, ArgoLab; Figure 27) [58] has been used for all the other Hydrogels' preparations.

Figure 27. *Mechanical Stirrer AM20-D (ArgoLab)* [58].

The mechanical stirrer has been used in combination with two types of stirring shafts, that generate an axial flow from top to the bottom:

- a stirring shaft with fixed blade (Figure 28), for Hydrogels with HT 1 mM, 5 mM and 40 mM;
- a stirring shaft with floating blades (Figure 28), for Hydrogels with HT 2 mM, 10 mM, 20 mM, 50 mM and 100 mM.

Figure 28. *Stirring Shaft with Fixed Blade (Type 1) and Stirring Shaft with Floating Blades (Type 2)* [58].

Technical data of the mechanical stirrer used are reported in Table IX.

Table IX. *Technical Data AM20-D, ArgoLab* [58]

TECHNICAL DATA AM20-D	
Speed	50 to 2200 rpm
Input Motor Power	60 W
Output Motor Power	50 W
Max. Stir Volume	20 L
Max. Torque	40 Ncm
Working Temperature	5 to 40 °C
Voltage - Frequency	220 V - 50/60 Hz
Shaft Dimensions	14 x 220 mm
Product Size	83 x 220 x 186 mm
Weight	2.4 kg

2.1.3 pH Measurement

In order to measure pH of Hydrogels, the probe HALO HI13302 by Hanna Instruments (Figure 29) [59] has been used: this pH-meter is characterized by a thin glass body and a spherical glass tip for low temperatures. It is an innovative pH electrode with Bluetooth technology (4.0); all readings are transmitted directly to an Apple or Android device, thanks to Hanna Lab App by Hanna Instruments (Figure 29). Technical data of the pH-meter used are reported in Table X.

Table X. *Technical Data HALO HI13302, Hanna Instruments* [59]

TECHNICAL DATA HALO HI13302	
pH Scale (Optimal)	From 0 to 12 pH
Resolution	0.1 pH, 0.01 pH, 0.001 pH
Accuracy	± 0.005 pH
Terms of Use	From – 5 to 50 °C
Length	175.5 mm
Weight	35 g

Figure 29. *Probe HALO HI13302 and Hanna Lab App (Hanna Instruments)* [59].

All measurements were performed 5 times for each Hydrogel sample, in order to calculate the minimum and maximum values, the median, the mean value and the standard deviation (STD).

2.2 Sterilization

The Sterilization of both 0 HT and HT-based Hydrogels has been carried out by an external company (Gammatom S.r.l.); the following block scheme (Figure 30) represents the Sterilization Process and the final pH measurement of the Sterile samples.

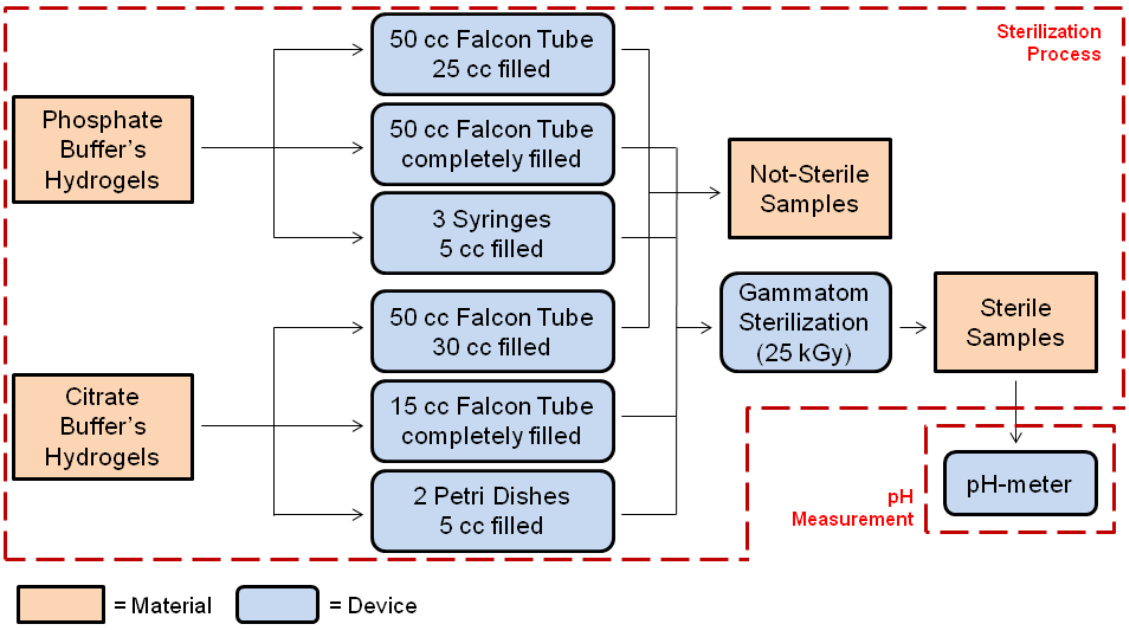

Figure 30. *Sterilization Process Block Diagram.*

Samples of Phosphate Buffer-based Hydrogels have been divided as follow (Figure 31):

- one 50 cc Falcon Tube filled up to 25 cc;
- one 50 cc Falcon Tube completely filled;
- three 5 cc Syringes filled up to 3 cc.

Samples of Citrate Buffer-based Hydrogels have been divided as follow (Figure 31):

- one 50 cc Falcon Tube filled up to 30 cc;
- one 15 cc Falcon Tube completely filled;
- two 35 x 10 mm Petri Dishes completely filled.

For Phosphate Buffer-based Hydrogels, the 50 cc Falcon Tubes filled to 25 cc have been placed in the refrigerator and have not been sterilized; the same treatment has been applied for 50 cc Falcon Tubes filled to 30 cc of Citrate Buffer-based Hydrogels. Conversely, the 50 cc Falcon Tubes completely filled, the Syringes 5 cc filled, the 15 cc Falcon Tubes completely filled and the Petri Dishes completely filled have been prepared to be sterilized: they have been inserted – according to their different HT concentration – in an envelope in coupled aluminium film, marked with color-changing indicators for sterilization process control.

Figure 31. *On the left, Containers used for Sterile Phosphate Buffer-based Hydrogels; on the right, Containers for Sterile Citrate Buffer-based Hydrogels.*

After the gamma ray sterilization process (25 kGy intensity, two weeks lead-time) the sterile samples returned to the laboratory to begin the Analysis Process.

Then, the probe HALO HI13302 by Hanna Instruments has been re-used in order to measure pH of Sterile Hydrogels; also in this case all measurements were performed 5 times for each Hydrogel prepared, in order to calculate the minimum and maximum values, the median, the mean value and the standard deviation (STD).

2.3 Rheological Analysis

2.3.1 Rheometer

In order to measure the viscosity of the prepared Hydrogels and to study their rheological properties, the rheometer RM 200 PLUS (Lamy Rheology) [60] has been used. The device (Figure 32) is composed by:

- a 7" colour touch screen;
- a luminous On/Off switch;
- an aluminium arm, equipped with the clamping knob – allows you to maintain the height of the measuring head – and an handle – for easy handling;
- a stainless steel rod, equipped with a ring with a clamping button – used as a stop for a repeatable positioning during the measurement – and a white Delrin ring – acting as a stop;
- a Pt100 probe to measure temperature.

Figure 32. *RM 200 PLUS (Lamy Rheology) [60].*

The rheometer used is equipped with a device for the temperature control, EVA MS-DIN PLUS (Lamy Rheology) [61]; the system (Figure 33) is able to measure temperatures from -20 to +150 °C, with an accuracy of ± 0.2 °C.

Figure 33. *EVA MS-DIN PLUS (Lamy Rheology) [61].*

Main technical data of RM 200 PLUS are summarized in Table XI.

Table XI. *Technical Data RM 200 PLUS, Lamy Rheology [60]*

TECHNICAL DATA RM 200 PLUS	
Rotation Speeds	0.3 ~ 1500 rpm
Torque range	0.05 to 30 mNm
Temperature	-50 to +300 °C
Accuracy	± 1% of full scale
Repeatability	± 0.2%
Supply Voltage	90-240 V AC, 50/60 Hz
Analog output	4 – 20 mA
Head Size	180 x 135 x 250 mm
Steel Stand Size	280 x 200 x 30 mm
Stainless Steel Rod Length	500 mm
Weight	6.7 kg

Different measuring systems are available with RM 200 PLUS device: choice of the measuring system must be done according to the product to be measured, favoring wide diameters for low viscosities (Figure 34).

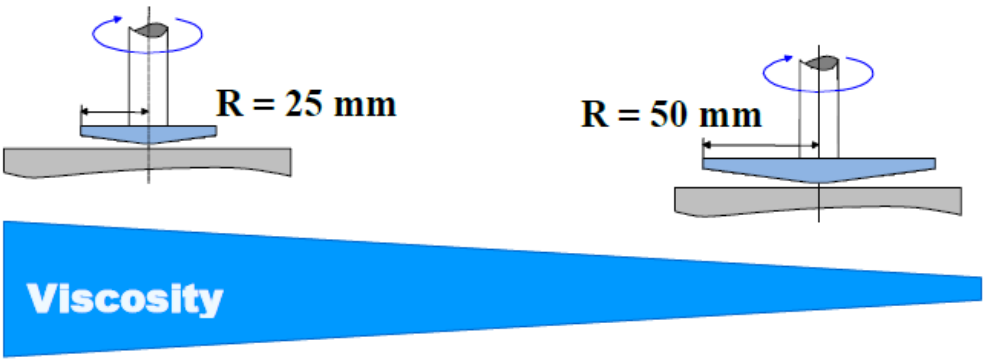

Figure 34. *Choice of the measuring system, according to the viscosity* [60].

We are particularly interested in coaxial cylinders measuring systems – DIN/ISO 3219 (316L stainless steel). In fact, these systems are suitable for the control of homogeneous products with liquid aspect and with or without particles (size < 200 µm). The measuring systems available are summarized in Table XII.

Table XII. *Measuring systems DIN/ISO 3219* [60]

MEASURING SYSTEM	
Name	**Part Number**
MK-DIN 1	112820
MK-DIN 2	112821
MK-DIN 3	112822
MK-DIN 9	111875
DIN 1 Tube	112932
DIN 2 Tube	112937
DIN 3 Tube	112938
DIN 1 Cap	112872
DIN 2 Cap	112877
DIN 3 Cap	112878
Mooney Cap	112874

Each tube is used with the matching cylinder: the cylinder MK-DIN 9 is used with the DIN 1 Tube; the Mooney plug is used exclusively with the DIN 1 Tube and the MK-DIN 1 and MK-DIN 9 cylinders.

The complete configurations of measuring systems (Figure 35) which we will refer to are MS DIN 19 (DIN 1 Tube and cylinder MK-DIN 9) and MS DIN 33 (DIN 3 Tube and

cylinder MK-DIN 3). The measuring ranges of the MS DIN measuring systems we are interested in are reported in Table XIII.

Table XIII. *Measuring ranges of MS DIN measuring systems* [60]

MEASURING RANGES OF MS DIN						
Measuring System	**Part Number** [a)]	**Inner Diameter (mm)**	**Outer Diameter (mm)**	**Sample volume (mm)** [b)]	**Shear Rate Range (s^{-1})**	**Viscosity Range (mPa·s)**
MS DIN 19	112806	31.5	32.5	25	1.0 to 4800	1 to 0.39M
MS DIN 33	112812	14	15	14	0.4 to 1900	34 to 10M

M for millions; a) Complete system (bob+cup+cap); b) Volume required for Pt100 immersion.

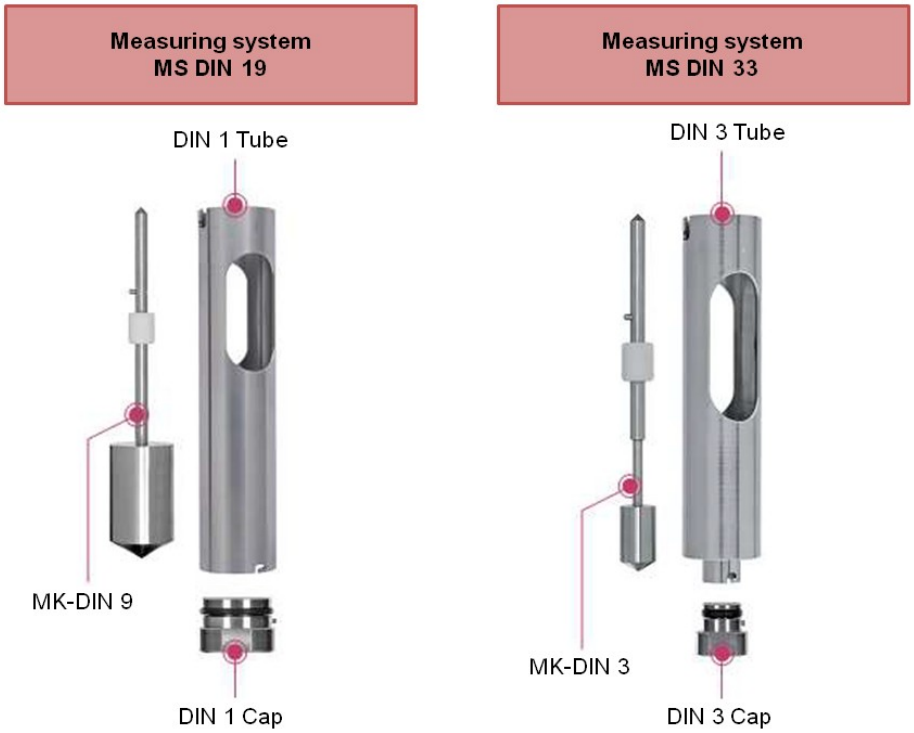

Figure 35. *Measuring systems: MS DIN 19 and MS DIN 33 (Lamy Rheology)* [60].

The rheometer RM 200 PLUS and the selected measuring system must be used coupled to the RheoTex software (Lamy Rheology) [60]: it allows programming of methods, measurement, recording, evaluation and presentation of measurement data.

On the software there are different programming methods available for the equipment (Figure 36); in each programming method it is possible to program a value or a temperature ramp:

- the method “Viscosity”, that allows programming of a constant shear rate to follow evolution of viscosity as a function of time;
- the method “Flow”, that allows programming of a ramp (shear rate) to obtain a flow curve (shear stress as function of shear rate) or a viscosity curve (viscosity as a function of shear rate);
- the method “Step by Step”, that is recommended to obtain a flow curve or a viscosity curve, having the possibility to create step by step the ramp, the plateau and the ramp decreasing;
- the method “Experience”, that allows to program a measurement and then start an automatic analysis after the measurement is done;
- the method “Free”, that offers the possibility to create a measurement method that allows to perform various steps.

For all, the window displays the type and name of method, as well as the measuring system used; you can also set a pre-shear by indicating the shear rate and time.

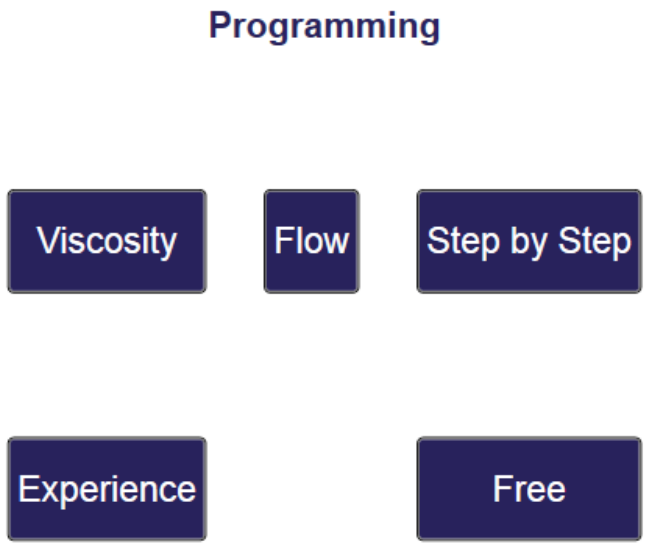

Figure 36. *Programming methods available for RM 200 PLUS* [60].

The launch of a measurement is done from the "Launch a measurement" view; during the measurement is possible to visualize:

- “Measurement Info”, resuming the essential information such as name of sample, program, date and time;
- “Info”, resuming the information displayed by instrument's screen;

- "Graph", displaying the measurement points on a diagram;
- "Data"; displaying the table of measured values.

When you have just finished a measurement, display or analysis view of measuring file is accessible; if you want to be able to compare measurements, the "Compilation" mode is done for that.

2.3.2 Protocol of Analysis

In order to graphically display the main steps of Rheological Analysis Protocol, a summary block diagram has been created (Figure 37).

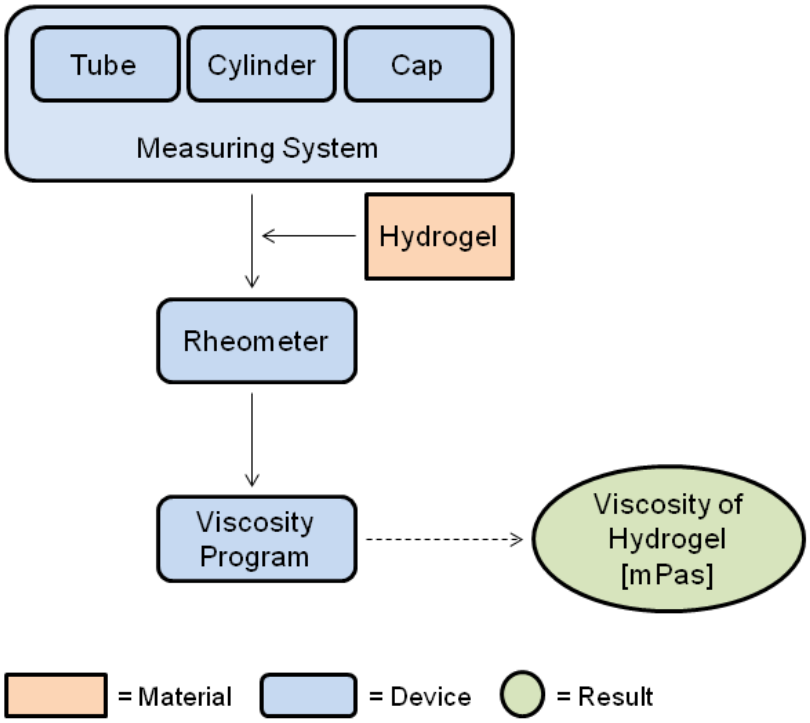

Figure 37. *Rheological Analysis Block Diagram.*

Before using the rheometer, it is important to clean the selected measuring system (MS DIN 19 or MS DIN 33) with a tissue and iso-propanol. Once the selected cylinder (MK-DIN 9 or MK-DIN 3) is installed, the first Hydrogel sample (25 mL) has been inserted in the corresponding tube (DIN 1 Tube or DIN 3 Tube); then, the tube has been put on the measuring head. After moving down the measuring head inside the EVA MS-DIN PLUS and waiting to reach the desired temperature (25 °C), it is possible to start the measurement. In order to analyze Hydrogel samples, the method "Viscosity" (Figure 38) has been used.

The “Viscosity” program has been set up in this way: after a preshearing time of 10 seconds with a shear rate of 10 s^{-1}, the analysis has been conducted with the use of a shear rate fixed at 50 s^{-1} for 60 seconds; in this time 100 points have been recorded.

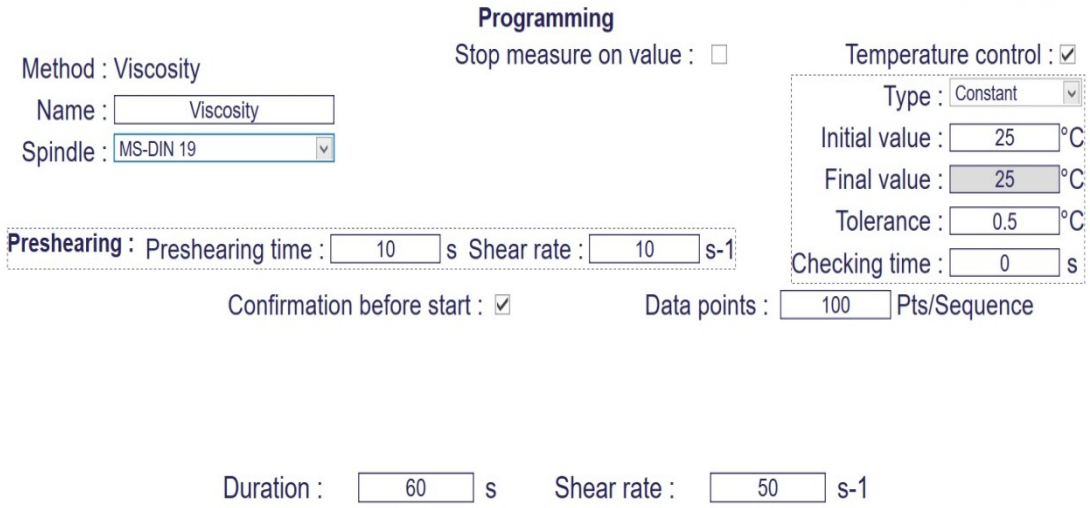

Figure 38. *“Viscosity” Program.*

The measurement system MS DIN 19 has been used for all the Not-Sterile samples. The analysis of the Sterile Hydrogels is not completely possible, due to the too high viscosity: thus, the analysis has been carried out only for HT 10 mM, HT 50 mM and HT 100 mM of the Phosphate Buffer-based Hydrogels and for HT 10 mM, HT 20 mM, HT 40 mM, HT 50 mM and HT 100 mM of the Citrate Buffer-based Hydrogels. The measurement system MS DIN 33 has been used for all the Sterile samples, except for the Citrate Buffer-based Hydrogel HT 100 mM, for which MS DIN 19 has been used.

The analysis has been carried out five times for each gel, in order to measure the minimum and maximum value, the mean, the median and the standard deviation (STD).

2.4 FT-IR Analysis

2.4.1 FT-IR Spectrometer

The FT-IR analysis has been done thanks to the FT-IR spectrometer Spectrum Two by Perkin Elmer (Figure 39) [62]. For accurate and repeatable measurements Spectrum Two employs an ultra-low maintenance optical system, while the proven interferometer design ensures reliability.

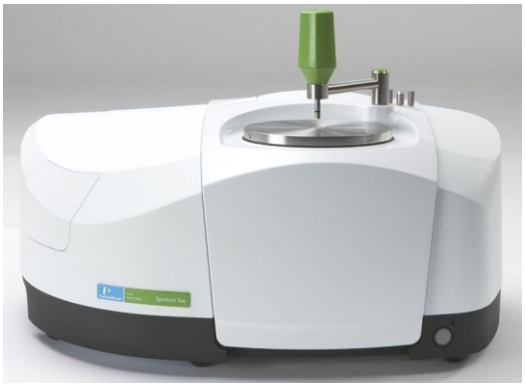

Figure 39. *FT-IR Spectrometer Spectrum Two (Perkin Elmer)* [62].

With a signal-to-noise ratio, advanced electronics and optimized sensitivity, Spectrum Two's consistent performance is guaranteed. The fixed mirror-pair interferometer design (Dynascan interferometer) does not require dynamic alignment to compensate for errors found in linear mirror movement systems; the field-proven interferometer incorporates a simple, non-critical bearing for unmatched longevity and reliability. An humidity shield design (OpticsGuar technology) protects Spectrum Two from environmental effects allowing it to be used in more challenging environments: the long life desiccant ensures maximum instrument uptime, regardless of where your analysis takes place. Atmospheric Vapor Compensation (AVC) features an advanced digital filtering algorithm designed to compensate for CO_2 and H_2O absorptions in real time; AVC effectively eliminates interference from these atmospheric components, removing the need for instrument purging, allowing laboratory to achieve more consistent results. In addition, Absolute Virtual Instrument (AVI) standardization using gas phase spectra ensures instruments are accurately calibrated. The instrument's wavenumber and line shape are standardized to a higher degree of accuracy than with conventional calibration methods: this unique standardization allows data to be transferred precisely between instruments, whether they are side-by-side or in remote locations.

Spectrum Two incorporates several features to enable infrared analysis to move out of the laboratory. Multiple power options allow Spectrum Two to be used with or without external mains power; once powered, a fast warm-up facilitates rapid measurement while optional wireless connectivity allows portable PC control. The comprehensive Spectrum 10 software suite (Figure 40) allows to focus on results; designed for busy industrial or academic laboratories, this comprehensive FT-IR software package facilitates data collection, processing and results generation.

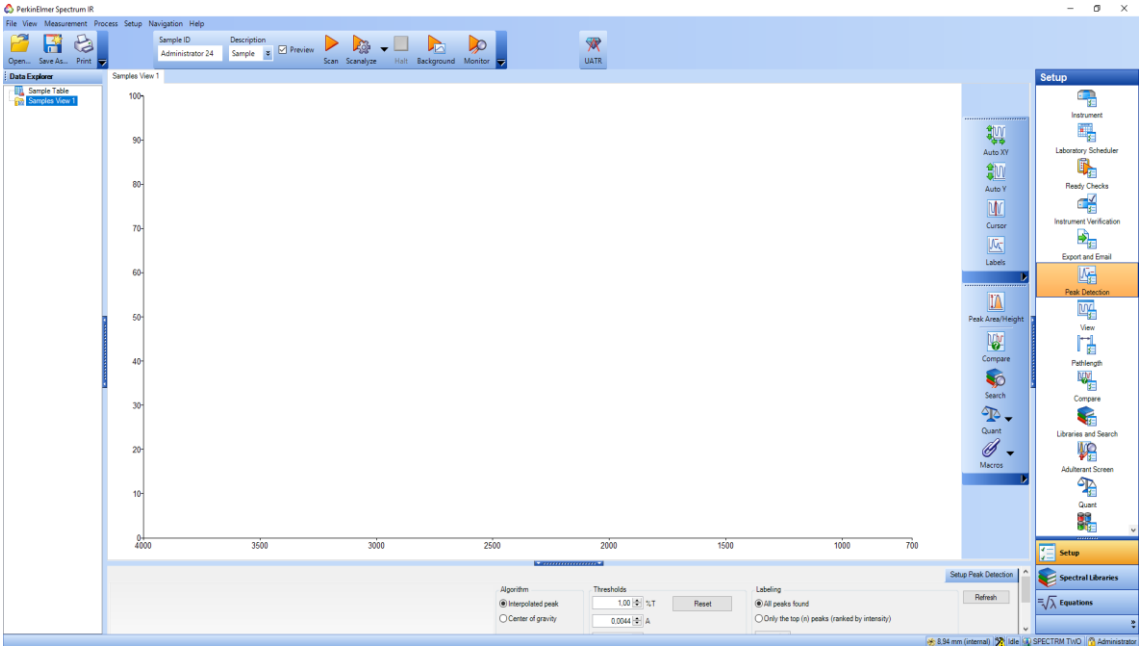

Figure 40. *Spectrum 10 Software Suite (Perkin Elmer)* [62].

Main technical data of Spectrum Two are summarized in Table XIV.

Table XIV. *Technical Data Spectrum Two, Perkin Elmer* [62]

TECHNICAL DATA SPECTRUM TWO	
Detector Type	$LiTaO_3$
Height	21.0 cm
Depth	30.0 cm
Width	45.0 cm
Weight	13.0 kg
Operating Range	5 – 45 °C
Wave Length	8
Wave Length Range	8300 – 350 cm^{-1}

2.4.2 Protocol of Analysis

In order to graphically display the main steps of FT-IR Analysis Protocol, a summary block diagram has been created (Figure 41).

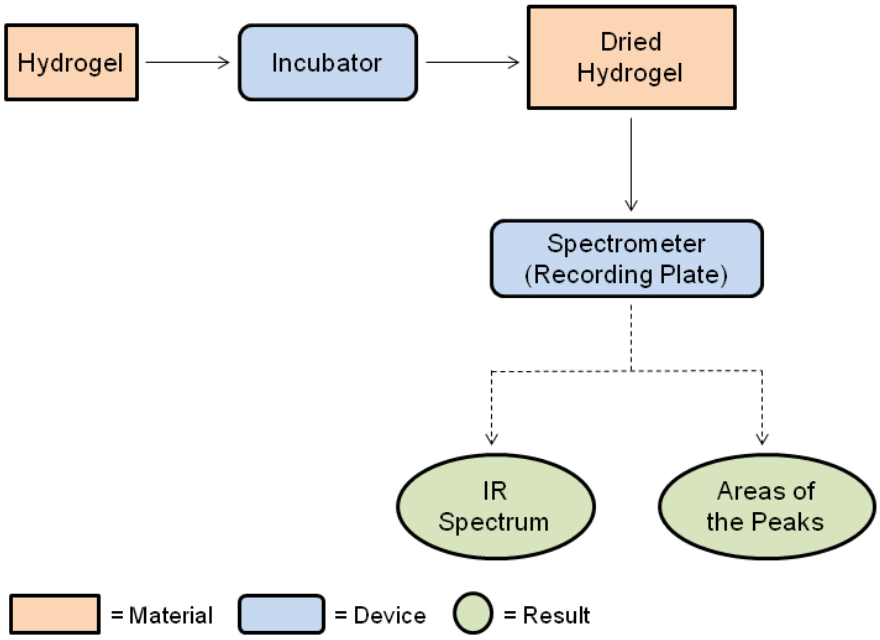

Figure 41. *FT-IR Analysis Block Diagram.*

In order to analyze Hydrogels' samples, aluminium plates have been prepared, dividing Phosphate Buffer-based Hydrogels from Citrate Buffer-based Hydrogels and Not-Sterile Hydrogels from Sterile Hydrogels; in each plate, a drop of each sample has been put (Figure 41 and Figure 42). Then, the plates have been positioned in the incubator (Incubator I, Memmert; Figure 43) [63] at 55 °C, in order to keep samples warm. Thanks to the finely-tuned control technology, critical temperature overshoots are completely ruled out, valuable loads are therefore warmed up particularly carefully in this highly precise microbiological incubator.

Figure 41. *Not-Sterile and Sterile Phosphate Buffer-based Hydrogels in Aluminium Plates before Incubation.*

Figure 42. *Not-Sterile and Sterile Citrate Buffer-based Hydrogels in Aluminium Plates before Incubation.*

Figure 43. *Incubator I (Memmert).*

After one day in incubator, samples of Hydrogels are ready for FT-IR Analysis (Figure 44 and Figure 45).

Figure 44. *Not-Sterile and Sterile Phosphate Buffer-based Hydrogels in Aluminium Plates after Incubation.*

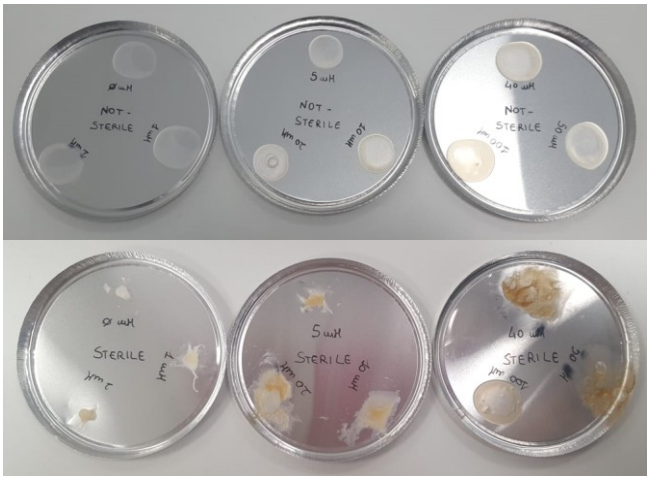

Figure 45. *Not-Sterile and Sterile Citrate Buffer-based Hydrogels in Aluminium Plates after Incubation.*

The FT-IR Analysis has been performed for all the Not-Sterile and Sterile Hydrogels. In addition, the Analysis has been conducted also for a solution previously prepared with PEO 4% and bi-distilled water with an high degree of purity, both Not-Sterile and Sterile. The analysis of this solution will allow, in fact, to understand which modifications are due to the polymerization of PEO and, therefore, in which way HT and different saline species (Phosphate or Citrate) affect the process.

Before using the spectrometer, it is important to check that the crystal is clean – eventually clean the plate with a tissue and iso-propanol – and that the arm is not over the crystal. The first phase is to record a background spectrum by clicking “Background”; now the spectrum of the compounds can be recorded. In order to cover completely the crystal, a small amount of the sample has been taken from the aluminium disk and has been added to the recording plate with a spatula. Then, the arm of the spectrometer has been moved so that it locks into place over the crystal; the green handle has been turned clockwise until the metal tip is close to the plate. By clicking “Scan”, it is possible to obtain a preview of the spectrum and pressure gauge; the handle has been twisted until the pressure gauge reads around 140 barg (relative pressure compared to the atmospheric pressure; ≈ 14 MPa). The final spectrum is obtained by clicking “Scan” again; in addition is possible to click “Labels” on the lateral toolbar to assign wave numbers to the major peaks, before printing the spectrum.

In order to proceed with the acquisition of the spectrum of another hydrogel sample, the green handle has been turned anticlockwise to raise the metal tip and the arm has

been returned to its original position; then, the plate and the metal tip have been cleaned with a tissue and iso-propanol.

Since FT-IR Analysis has been conducted in order to study chemical changes and to provide information on species crystallinity, an assessment of the areas of the selected peaks of interest has been carried out. Once the peak has been chosen, by clicking "Peak Area/Height" it is possible to obtain directly the measurement of the area under the peak; since this area is dimensionless, it corresponds to molar extinction coefficient.

2.5 Extraction HT and and HPLC Analysis

In order to graphically display the main steps of HT Extraction and HPLC Analysis Protocol, a summary block diagram has been created (Figure 46). The Protocol of Analysis will be described in the following paragraphs.

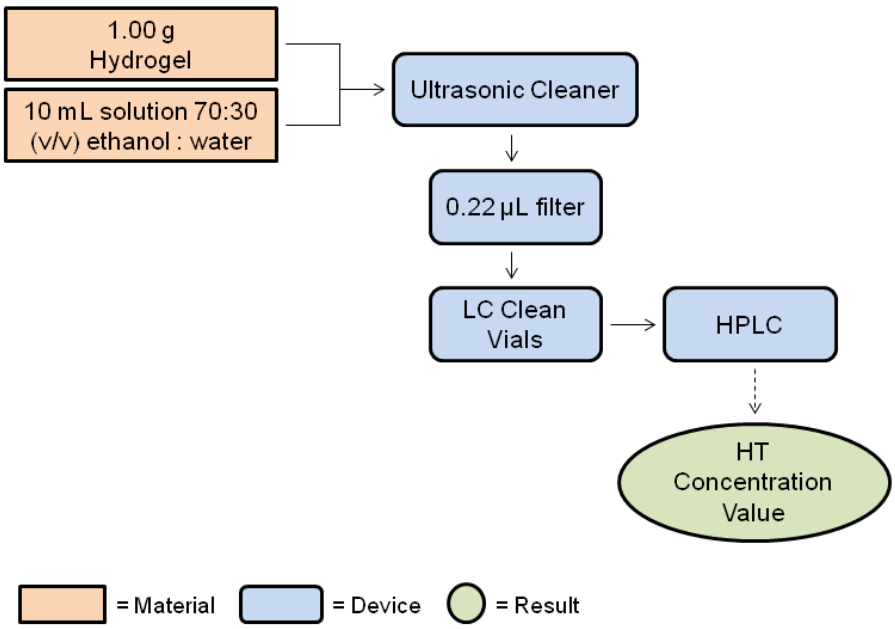

Figure 46. *HT Extraction and HPLC Analysis Block Diagram.*

2.5.1 Ethanol Sonication

The HT quantity inside the Hydrogel samples has been determined by the method described by Seker et al. [64], with some modifications.

An aqueous ethanol solvent extraction has been performed to isolate HT from Hydrogels. The compounds have been extracted at a solid to liquid ratio of 1:10 (w/v)

using 70:30 (v/v) ethanol; bi-distilled water with an high degree of purity has been used as the extraction solvent.

For each prepared gel, 1.00 g has been weighted and inserted in 15 mL Falcon tubes (tot. 28 tubes); then, for each sample, 10 mL of solution prepared with 70 mL of ethanol and 30 mL of water have been added (Figure 47 and Figure 48).

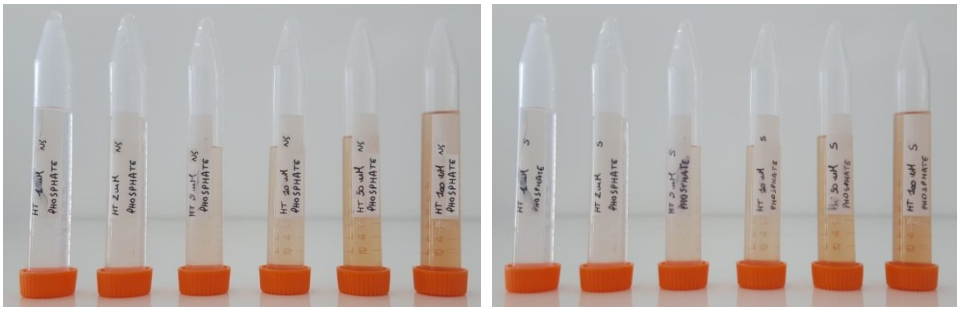

Figure 47. *Not-Sterile and Sterile Phosphate Buffer-based Hydrogels before Extraction.*

Figure 48. *Not-Sterile and Sterile Citrate Buffer-based Hydrogels before Extraction.*

The sonication has been performed for 30 minutes, thanks to the ultrasonic cleaner DK-80 by DK Sonic (Figure 49) [65]. Main technical data of DK-80 are summarized in Table XV.

Table XV. *Technical Data DK-80, DK Sonic* [65]

TECHNICAL DATA DK-80	
Tank Capacity	700 mL
Cleaning Time	18 Cleaning Times; 90 s to 30 min
Ultrasonic Frequency	42 kHz
Ultrasonic Power	35 W
Control Method	Digital Control
Tank Size	155 x 90 x 65 mm
Product Size	176 x 115 x 125 mm

Figure 49. *Ultrasonic Cleaner DK-80 (DK Sonic)* [65].

Then, the solutions have been prepared to perform the HPLC Analysis.

2.5.2 HPLC Analysis

2.5.2.1 Liquid Chromatograph

In order to perform HPLC analysis and to separate, identify, and quantify HT in every different Hydrogel sample, the liquid chromatograph Flexar LC by Perkin Elmer (conventional LC 6000 PSI; Figure 50) [66] has been used. The system provide a robust, trouble free-operation; it is composed by the following stackable, modular components:

- a Solvent Manager: it is an high-efficiency in-line module that removes dissolved gasses from HPLC solvents; with a 3-CH vacuum degasser or 5-CH vacuum degasser, it provides safe and convenient management of LC solvent bottles. The Flexar Solvent Manager vacuum degasser consists of a vacuum chamber, degassing tube, variable speed vacuum pump, microprocessor controller, sensor, and check valves. The solvent (mobile phase) flows into a degassing tube, which is inside a vacuum chamber; decreased pressure in the chamber causes the outward movement of gas dissolved in the mobile phase across the tube wall, in accordance to Henry's Law ($C = kP$ where C is the gas concentration in the solution, P is the pressure of the gas and k is a constant typical for each gas), thus degassing the mobile phase. The pressure in the vacuum chamber is established by the vacuum pump and monitored by the microprocessor through an integrated absolute pressure sensor. Degassed mobile phase exits the vacuum degasser and enters the pump;

- an LC Autosampler: it has an injection-to-injection precision and supports a wide variety of injection modes (Fixed Loop, Partial Fill and μL Pickup), autosampler trays and vials. The pressure limit is up to 6100 psi (428 bar); the injection volume varies depending to the injection modes (Fixed Loop mode: 2 μL to 500 μL, Partial Fill mode: 0.1 μL to 2.45 μL, μL Pickup mode: 1 μL to 977 μL);
- a Binary LC Pump: it has a pressure range between 0 and 6100 psi for the entire flow-rate range (form 0.01 to 10.0 mL/min). Flow-rate increments are of 0.01 from 0 to 0.99 mL/min and of 0.1 from 1.0 to 10 mL/min with a flow precision of 0.3% RSD (typical 0.1%) at 1 mL/min water and 1000 psi. Flow accuracy is ± 1% of setting at 1 mL/min and 1000 psi with water;
- an LC Column Oven: it has a large, easily accessible column compartment holds even 30 cm column format. The temperature range of 30 °C to 90 °C is controlled to within 0.2 °C throughout the entire range, with a temperature accuracy of ± 1 ˚C. The recommended flow range is up to 5 mL/min;
- a PDA Plus Detector: it is an advanced photo diode array detector (PDA) with an high sensitivity. The PDA Plus has a wide detection range, a very low baseline noise (spec. ≤ 8 μAU), an high wavelength accuracy (average error ≤0.5 nm) and an high data acquisition rate (up to 200 Hz).

Figure 50. *Flexar LC (Perkin Elmer)* [66].

Main technical data of Flexar LC are summarized in Table XVI.

Table XVI. *Technical Data Flexar LC, Perkin Elmer* [66]

TECHNICAL DATA FLEXAR LC	
Solvent Manager	
Channels	3-Channels or 5-Channels Version
Maximum Recommended Flow Rate	3.0 mL/min
Pressure Drop	1.37 mm Hg/mL/min
Degassing Capacity	~25% dissolved gases remaining in 60:40 MeOH/Water mixture at 1 mL/min
LC Autosampler	
Pressure Limits	Up to 6,100 psi (428 bar)
Injection Modes	Fixed Loop: 5x sample overfill; Partial Fill: Variable injection volumes; µL Pickup: Injections without any excess sample waste
Injection Volume	Fixed Loop mode: 2 µL to 500 µL, depending on loop volume; Partial Fill mode: 0.1 µL to 2.45 mL (up to half loop volume); µL Pickup mode (no sample waste): 1 µL to 977 µL, depending on loop volume
Binary LC Pump	
Flow-Rate Range	0.01 to 10.0 mL/min
Flow-Rate Increments	0.01 from 0 to 0.99 mL/min; 0.1 from 1.0 to 10 mL/min
Flow Precision	0.3% RSD (typical 0.1%) at 1 mL/min water and 1000 psi
Flow Accuracy	±1% of setting at 1 mL/min and 1000 psi with water
Compositional Range	0 to 100%, solvent A to B
PDA Plus Detector	
Wavelength Range	190 − 790 nm
Wavelength Accuracy	0.5 nm average absolute error
Optical Resolution	4 nm
Photodiodes	1024
Linearity Range	<3% at 2 AU
Baseline Noise	<8 µAU
Drift	<0.5 mAU/hr

Thanks to Chromera Software (Figure 51) it is possible to perform an efficient and effective speciation analysis. The software fully supports post-run review and data analysis: the “Post Run” environment displays the chromatograms and a scrolling list of results which updates after each sample is run.

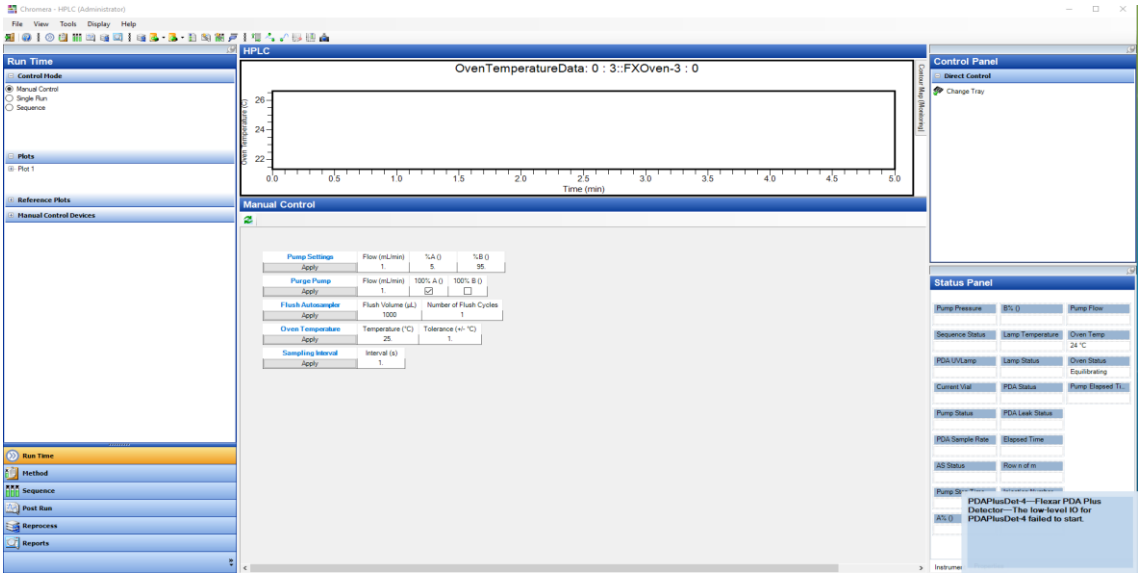

Figure 51. *Chromera Software (Perkin Elmer)* [66].

2.5.2.2 Protocol of Analysis

Solutions previously extracted have been prepared for HPLC Analysis. For each Hydrogel, 800 µL of solution 70:30 (v/v) and 200 µL of sonicated solution have been taken with a pipette P1000 (100 – 1000 µL) and inserted in an Eppendorf safe-lock tube. Each of these new solutions have been filtered with a 0.22 µL filter and inserted in LC Clean Vials (Figure 52 and Figure 53), made from Type 1 Borosilicate glass – which conforms to all USP, JP and EP requirements. The 50 mM and 100 mM solutions (both Not-Sterile and Sterile and both with Phosphate Buffer and Citrate Buffer) have been further diluted (1:10 with a solution prepared with 0.7 mL of ethanol and 0.3 mL of bi-distilled water) before being filtered and inserted in LC Clean Vials.

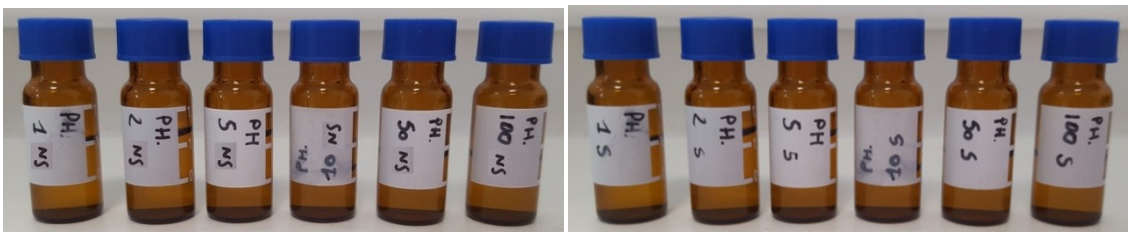

Figure 52. LC Clean Vials for Not-Sterile and Sterile Phosphate Buffer-based Hydrogels.

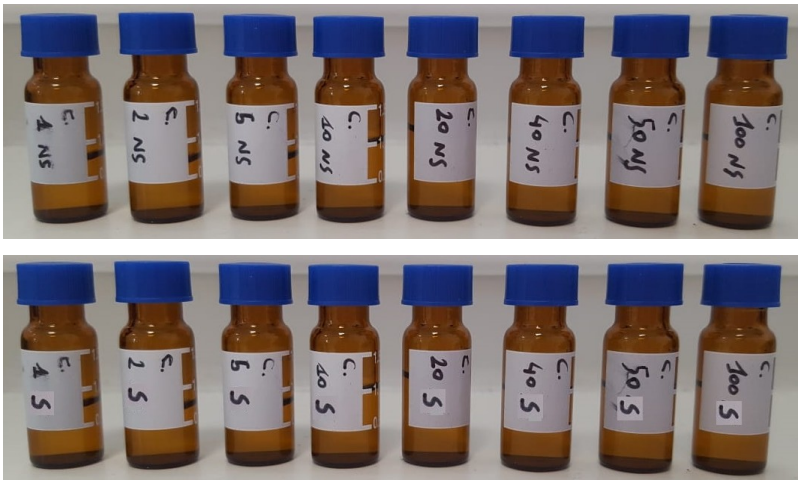

Figure 53. LC Clean Vials for Not-Sterile and Sterile Citrate Buffer-based Hydrogels.

In order to perform HPLC Analysis, the following protocol – inspired to the method of Gikas et al. [67] – has been used:

- Chromatographic conditions: isocratic 70% A, 30% B with A = 0.1% Acetic Acid and B = Acetonitrile (ACN);
- Temperature: 21 °C (± 1 °C);
- Flux and Runtime: 1.6 mL/min for 10.0 min;
- Absorbance: wavelength of 280 nm with an analytical bandwidth of 5 nm;
- Injection Volume: 1.0 μL;
- Column: HC-C18 Agilent 5 μm, 4.6 x 150 mm;
- Tarature: 1 mM, 2 mM.

After the preparation of a 50 mM stock solution (created with HT and 70:30 (v/v) solution), calibration samples (Figure 54) have been made as follow:

- 1 mM calibration sample (S1) prepared with 20 μL of stock solution and 980 μL of bi-distilled water;
- 2 mM calibration sample (S2) prepared with 40 μL of stock solution and 960 μL of bi-distilled water.

Figure 54. LC Clean Vials for Calibration Samples.

All the LC Clean Vials have been inserted in the LC Autosampler's grid. In order to create a calibration line, a new measurement code has been set up, thanks to Chromera Software: two "Calibration Replace" with standards S1 and S2 have been inserted and the HPLC analysis has been processed two times for each sample. After 20 minutes of analysis, the calibration line between absorbance and concentration has been created with the Least Mean Squares Algorithm.

Then, the same protocol has been applied to all the samples ("Sample"), but performing only one injection (tot. time = 280 min). Thus, the "Average Area" of the HT peak (retention time between 1.7 and 1.8 min) has been calculated for each sample by the software, in order to quantify the concentration of HT in each created Hydrogel. In fact, once determined the Absorbance [mAU], it is possible to obtain the related HT concentration [mM], considering dilution factors used. The following formula has been applied:

$$mM = \frac{[(Area/m) * 5\,] * 11}{154.16}$$

where $Area$ is the "Average Area" [dimensionless], m is the angular coefficient of the calibration line, 5 and 11 are coefficients due to dilution and 154.16 is the molecular weight [g/mol] of hydroxytyrosol. For HT 50 mM and HT 100 mM samples it is necessary an additional coefficient (10) due to 1:10 dilution.

3. Results

3.1 Production

Not-Sterile Phosphate Buffer-based Hydrogels are shown in Figure 54; Not-Sterile Citrate Buffer-based Hydrogels are shown in Figure 55.

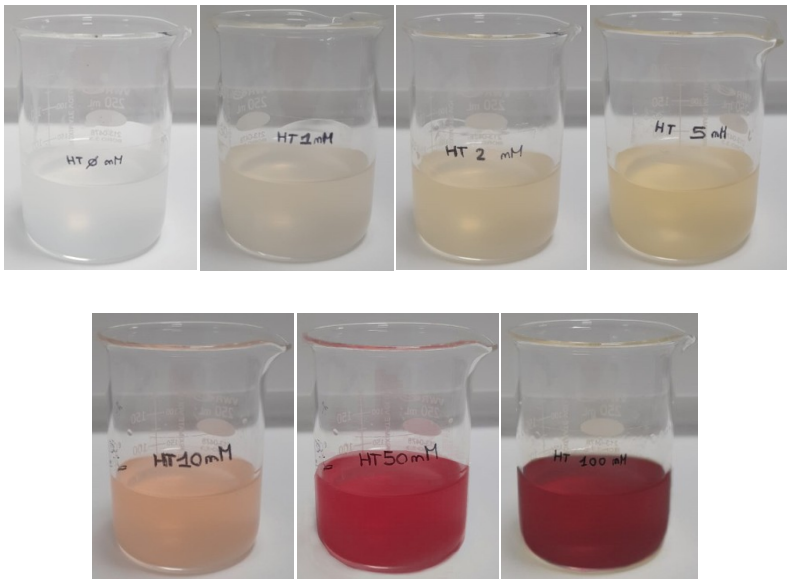

Figure 54. *Not-Sterile Phosphate Buffer-based Hydrogels. In the first line HT 0 mM, 1 mM, 2 mM and 5 mM; in the second line HT 10 mM, 50 mM and 100 mM.*

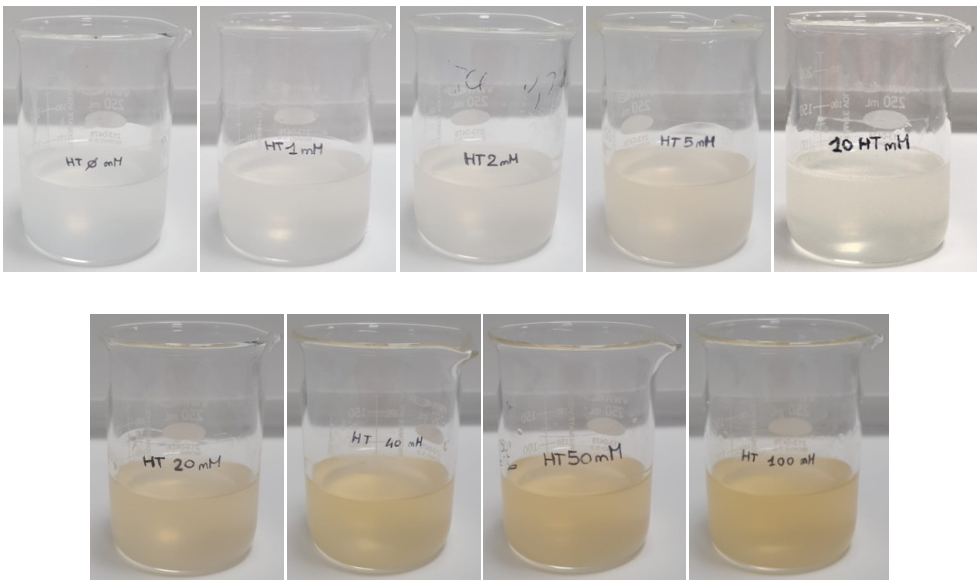

Figure 55. *Not-Sterile Citrate Buffer-based Hydrogels. In the first line HT 0 mM, 1 mM, 2 mM, 5 mM and 10 mM; in the second line HT 20 mM, 40 mM, 50 mM and 100 mM.*

The pH values obtained for Phosphate Buffer-based Hydrogels are reported in Table XVII; those ones obtained for Citrate Buffer-based Hydrogels are reported in Table XVIII. The pH trend of Not-Sterile samples is shown graphically in Figure 56.

Table XVII. *pH Values of Not-Sterile Phosphate Buffer-based Hydrogels*

pH VALUES OF NOT-STERILE PHOSPHATE BUFFER-BASED HYDROGELS				
HT [mM]	**min – max pH**	**median pH**	**mean pH**	**STD pH**
0	6.36 – 6.38	6.37	6.37	0.01
1	6.33 – 6.36	6.35	6.35	0.01
2	6.34 – 6.36	6.35	6.35	0.01
5	6.32 – 6.35	6.33	6.33	0.01
10	6.30 – 6.32	6.31	6.31	0.01
50	6.27 – 6.29	6.28	6.28	0.01
100	6.26 – 6.30	6.28	6.28	0.01

Table XVIII. *pH Values of Non-Sterile Citrate Buffer-based Hydrogels*

pH VALUES OF NOT-STERILE CITRATE BUFFER-BASED HYDROGELS				
HT [mM]	**min – max pH**	**median pH**	**mean pH**	**STD pH**
0	5.60 – 5.61	5.60	5.60	0.00
1	5.59 – 5.60	5.59	5.60	0.01
2	5.40 – 5.44	5.42	5.42	0.01
5	5.41 – 5.43	5.42	5.42	0.01
10	5.38 – 5.40	5.39	5.39	0.01
20	5.38 – 5.40	5.38	5.39	0.01
40	5.37 – 5.40	5.38	5.38	0.01
50	5.36 – 5.39	5.37	5.37	0.01
100	5.36 – 5.38	5.37	5.37	0.01

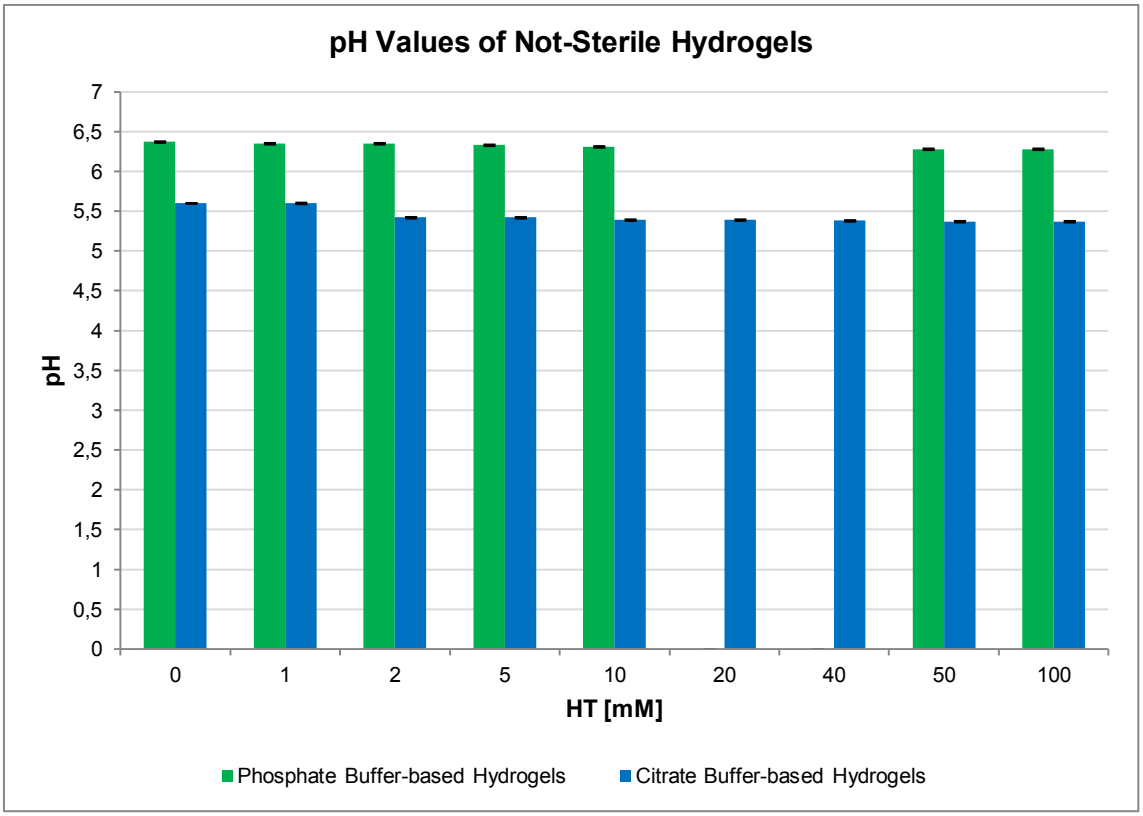

Figure 56. *pH Values of Not-Sterile Phosphate and Citrate Buffer-based Hydrogels.*

3.2 Sterilization

Sterile Phosphate Buffer-based Hydrogels are shown in Figure 57; Sterile Citrate Buffer-based Hydrogels are shown in Figure 58.

Figure 57. *Sterile Phosphate Buffer-based Hydrogels. From left to right the samples HT 0 mM, 1 mM, 2 mM, 5 mM, 10 mM, 50 mM and 100 mM.*

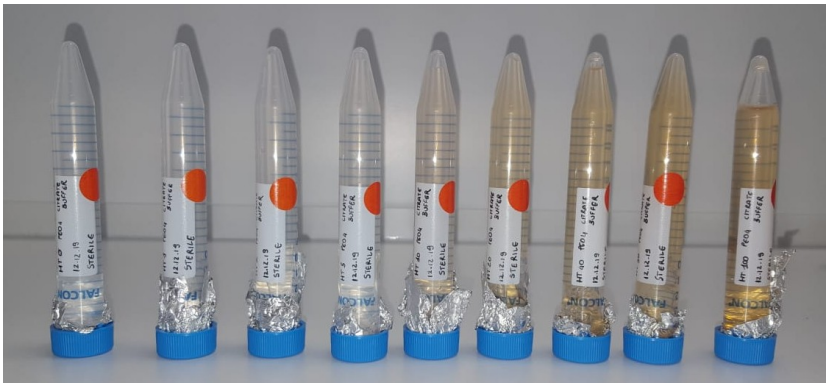

Figure 58. *Sterile Citrate Buffer-based Hydrogels. From left to right the samples HT 0 mM, 1 mM, 2 mM, 5 mM, 10 mM, 20 mM, 40 mM, 50 mM and 100 mM.*

The pH values obtained for each Sterile Hydrogel sample are reported in Table XIX and in Table XX. The pH trend of Sterile samples is shown graphically in Figure 59.

Table XIX. *pH Values of Sterile Phosphate Buffer-based Hydrogels*

pH VALUES OF STERILE PHOSPHATE BUFFER-BASED HYDROGELS				
HT [mM]	**min – max pH**	**median pH**	**mean pH**	**STD pH**
0	6.73 – 6.75	6.74	6.74	0.01
1	6.70 – 6.72	6.71	6.71	0.01
2	6.66 – 6.68	6.66	6.67	0.01
5	6.62 – 6.64	6.63	6.63	0.01
10	6.60 – 6.62	6.61	6.61	0.01
50	6.47 – 6.50	6.48	6.48	0.01
100	6.42 – 6.46	6.44	6.44	0.01

Table XX. *pH Values of Sterile Citrate Buffer-based Hydrogels*

pH VALUES OF STERILE CITRATE BUFFER-BASED HYDROGELS				
HT [mM]	**min – max pH**	**median pH**	**mean pH**	**STD pH**
0	5.80 – 5.82	5.81	5.81	0.01
1	5.69 – 5.72	5.70	5.70	0.01
2	5.67 – 5.70	5.68	5.69	0.01
5	5.67 – 5.69	5.68	5.68	0.01
10	5.64 – 5.66	5.65	5.65	0.01
20	5.60 – 5.62	5.61	5.61	0.01
40	5.60 – 5.62	5.60	5.61	0.01
50	5.59 – 5.61	5.60	5.60	0.01
100	5.58 – 5.60	5.59	5.59	0.01

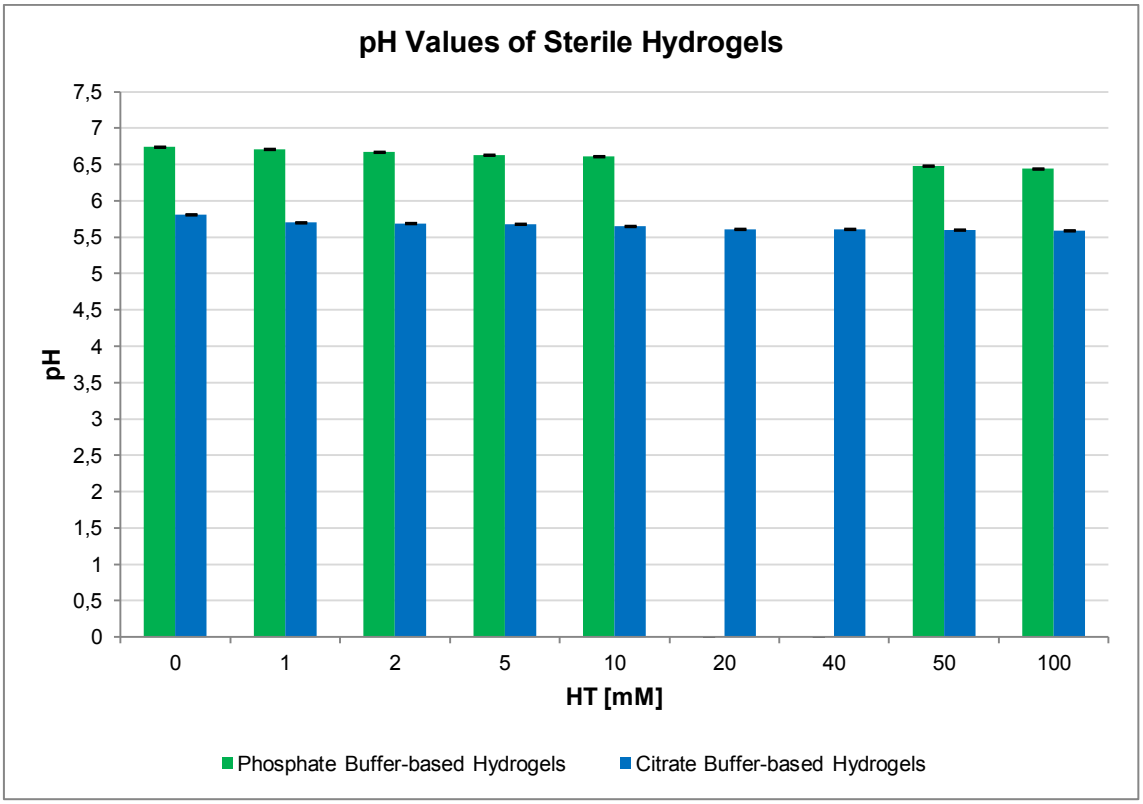

Figure 59. *pH Values of Sterile Phosphate and Citrate Buffer-based Hydrogels.*

3.3 Rheological Analysis

3.3.1 Not-Sterile Samples

Viscosity curves of Not-Sterile Phosphate Buffer-based Hydrogels is shown in the following figure (Figure 60).

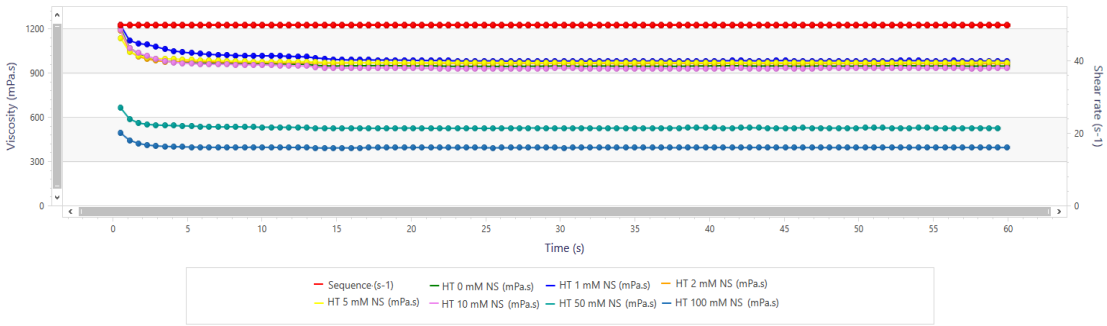

Figure 60. *Viscosities [mPas] of Not-Sterile Phosphate Buffer-based Hydrogels – HT 0 mM (in green), HT 1 mM (in electric blue), HT 2 mM (in orange), HT 5 mM (in yellow), HT 10 mM (in pink), HT 50 mM (in sea water) and HT 100 mM (in dark blue) – with the fixed shear rate [s^{-1}] (in red).*

A graph representing the HT [mM] related to Viscosity of Not-Sterile Phosphate Buffer-based Hydrogels at time t = 40.39 s is shown in Figure 61; Viscosity values (minimum and maximum, median, mean and standard deviation) are shown in Table XXI. The choice of the instant of time (t = 40.39 s) has been in made in order to have a constant viscosity.

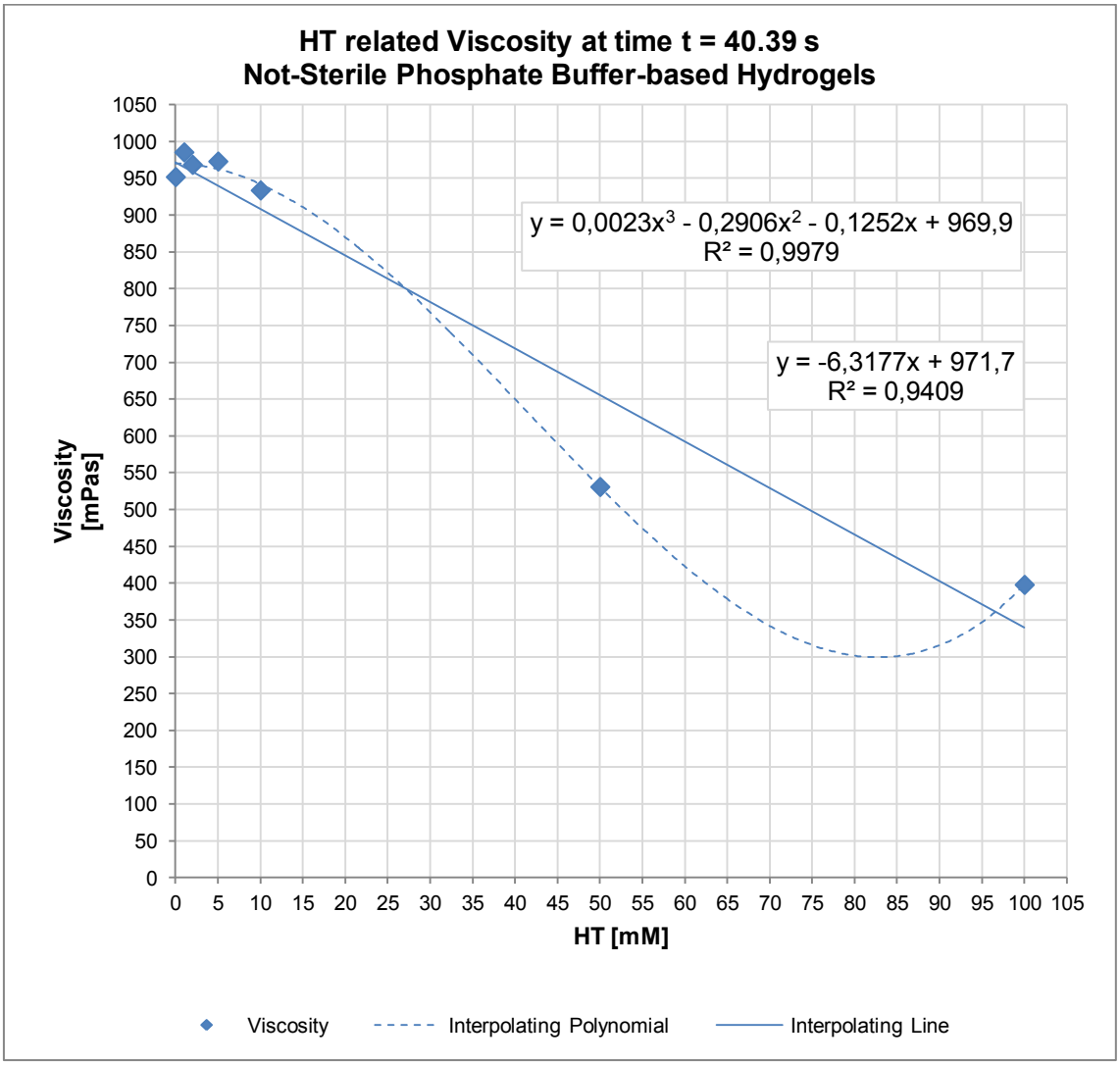

Figure 61. *HT concentration [mM] versus Viscosity [mPas] of Not-Sterile Phosphate Buffer-based Hydrogels, obtained with "Viscosity" Method at time t = 40.39 s. The interpolating third degree polynomial and the interpolating line are represented with their relative equation and R^2.*

Table XXI. *Viscosity Values of Not-Sterile Phosphate Buffer-based Hydrogels at t = 40.39 s*

VISCOSITY VALUES OF NOT-STERILE PHOSPHATE BUFFER-BASED HYDROGELS				
HT [mM]	**Viscosity Values at t = 40.39 s [mPas]**			
	min – max	**median**	**mean**	**STD**
0	945.42 957.95	951.87	951.75	5.12
1	979.14 990.37	986.34	985.28	4.65
2	962.57 974.76	967.52	968.28	5.01
5	966.54 977.59	974.52	972.88	4.66
10	926.83 937.99	935.92	933.58	4.85
50	526.25 536.04	530.52	530.84	4.01
100	393.98 402.67	396.88	397.88	3.60

Viscosity curves of Not-Sterile Citrate Buffer-based Hydrogels is shown in the following figure (Figure 62).

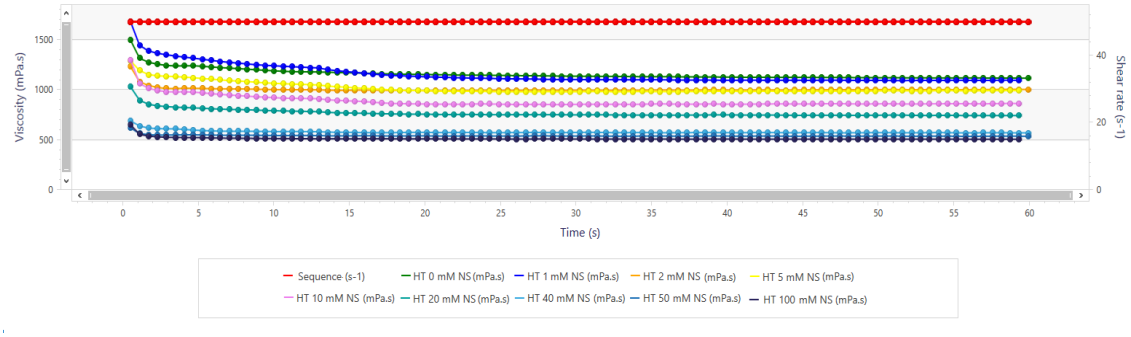

Figure 62. *Viscosities [mPas] of the Not-Sterile Citrate Buffer-based Hydrogels – HT 0 mM (in green), HT 1 mM (in electric blue), HT 2 mM (in orange), HT 5 mM (in yellow), HT 10 mM (in pink), HT 20 mM (in sea water), HT 40 mM (in light blue), HT 50 mM (in blue) and HT 100 mM (in dark blue) – with the fixed shear rate [s^{-1}] (in red).*

A graph representing the HT [mM] related Viscosity of Not-Sterile Citrate Buffer-based Hydrogels at time t = 40.39 s is shown in Figure 63; Viscosity values (minimum and maximum, median, mean and standard deviation) are shown in Table XXII.

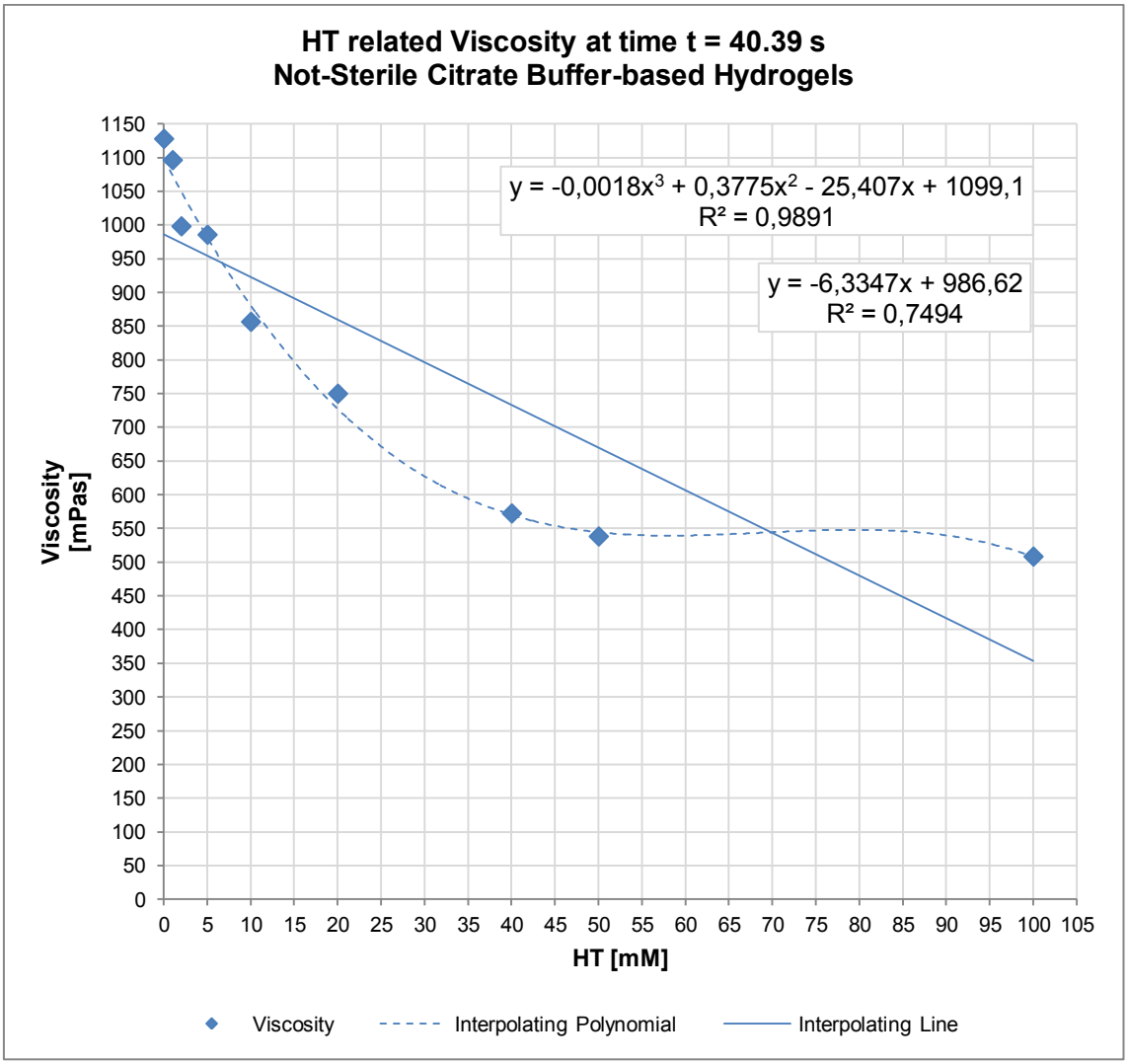

Figure 63. *HT concentration [mM] versus Viscosity [mPas] of Not-Sterile Citrate Buffer-based Hydrogels, obtained with "Viscosity" Method at time t = 40.39 s. The interpolating third degree polynomial and the interpolating line are represented with their relative equation and R^2.*

Table XXII. *Viscosity Values of Not-Sterile Citrate Buffer-based Hydrogels at t = 40.39 s*

VISCOSITY VALUES OF NOT-STERILE CITRATE BUFFER-BASED HYDROGELS				
HT [mM]	**Viscosity Values at t = 40.39 s [mPas]**			
	min – max	**median**	**mean**	**STD**
0	1121.24 1134.89	1127.95	1128.09	5.57
1	1090.74 1104.05	1097.02	1096.55	5.44

2	994.97 1004.67	997.86	998.37	5.15
5	980.28 991.89	984.71	985.88	5.01
10	849.98 861.17	857.13	856.70	4.99
20	745.23 755.47	749.74	750.12	4.82
40	568.45 577.13	573.15	572.55	4.31
50	532.65 543.42	537.81	538.43	3.89
100	503.63 513.56	507.71	508.57	3.59

The comparison of results obtained at time t = 40.39 s for the Not-Sterile Phosphate Buffer-based Hydrogel and the Not-Sterile Citrate Buffer-based Hydrogel is represented in the following histogram (Figure 64).

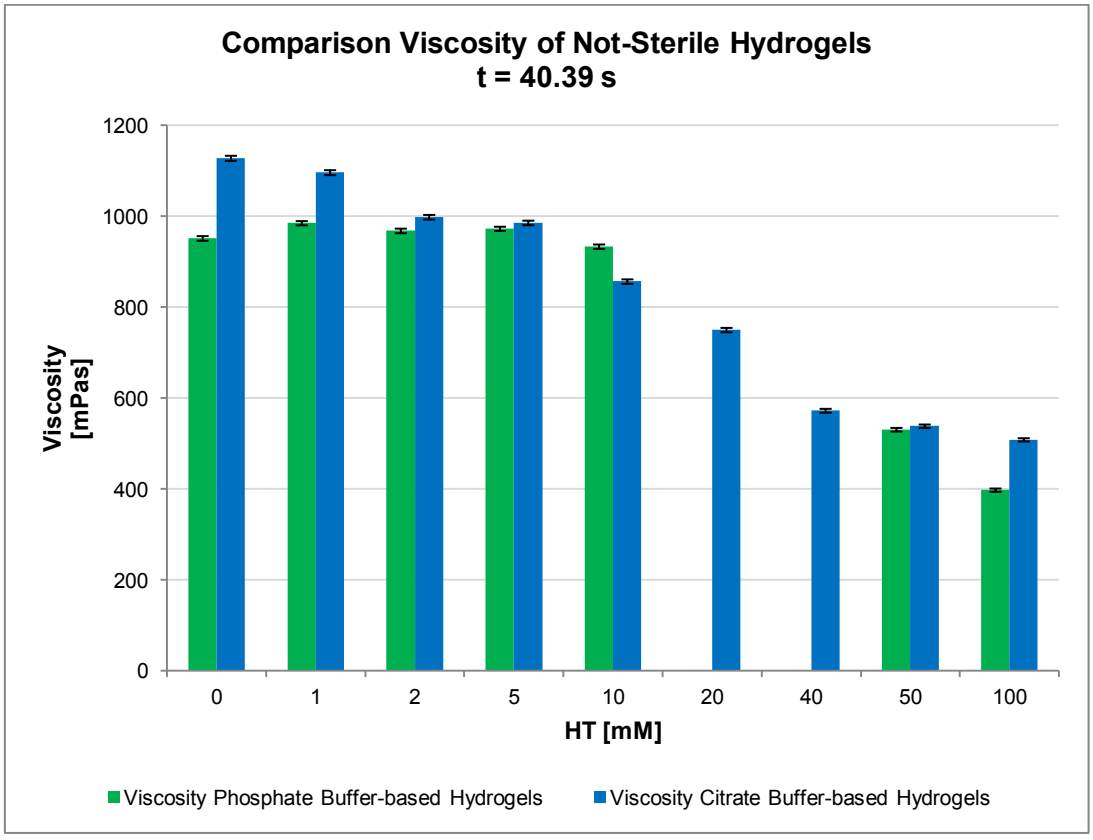

Figure 64. *HT [mM] dependent Viscosity [mPas] of Not-Sterile Phosphate Buffer-based Hydrogels and Not-Sterile Citrate Buffer-based Hydrogels, obtained with "Viscosity" Method at time t = 40.39 s.*

Considering HT 100 mM Hydrogel as a representative sample, the comparison between Not-Sterile Phosphate Buffer-based Hydrogel and the Not-Sterile Citrate Buffer-based Hydrogel is shown in the following figure (Figure 65).

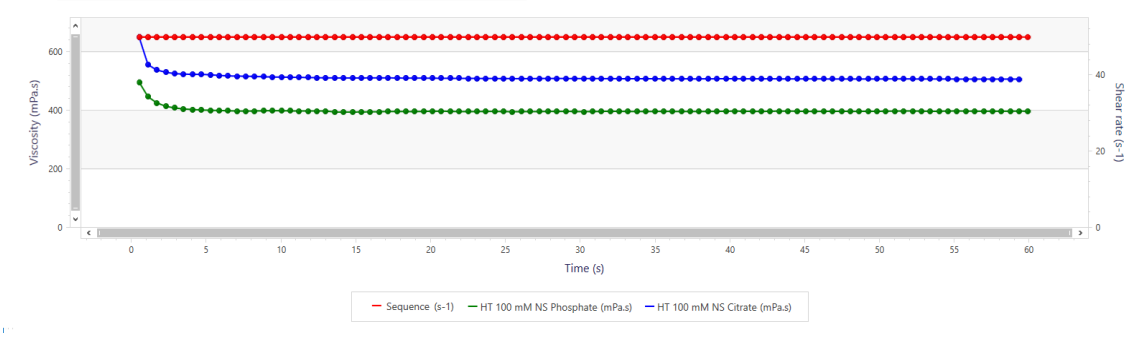

Figure 65. *Comparison between Viscosities [mPas] of the HT 100 mM Not-Sterile Phosphate Buffer-based Hydrogel (in green) and the HT 100 mM Not-Sterile Citrate Buffer-based Hydrogel (in electric blue) with a fixed shear rate [s^{-1}] (in red).*

3.3.2 Sterile Samples

Viscosities of Sterile Phosphate Buffer-based Hydrogels is shown in the following figure (Figure 66).

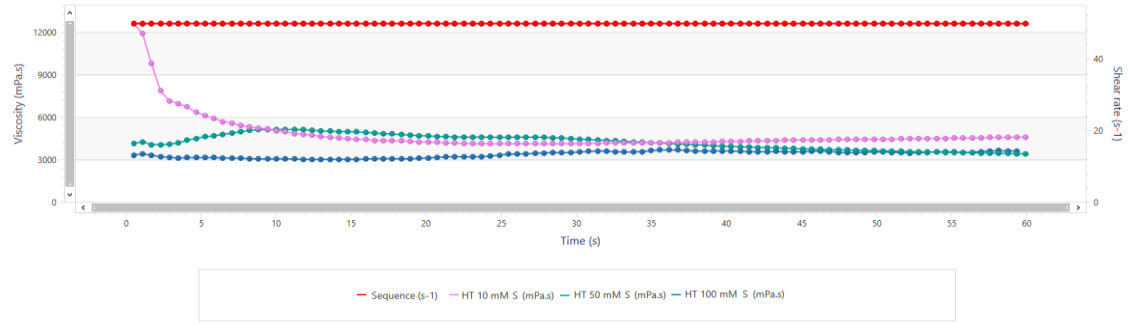

Figure 66. *Viscosities [mPas] of the Sterile Phosphate Buffer-based Hydrogels – HT 10 mM (in pink), HT 50 mM (in sea water) and HT 100 mM (in dark blue) – with the fixed shear rate [s^{-1}] (in red).*

A graph representing the HT [mM] related Viscosity of Sterile Phosphate Buffer-based Hydrogels at time t = 40.39 s is shown in Figure 67; Viscosity Values (minimum and maximum, median, mean and standard deviation) are shown in Table XXIII.

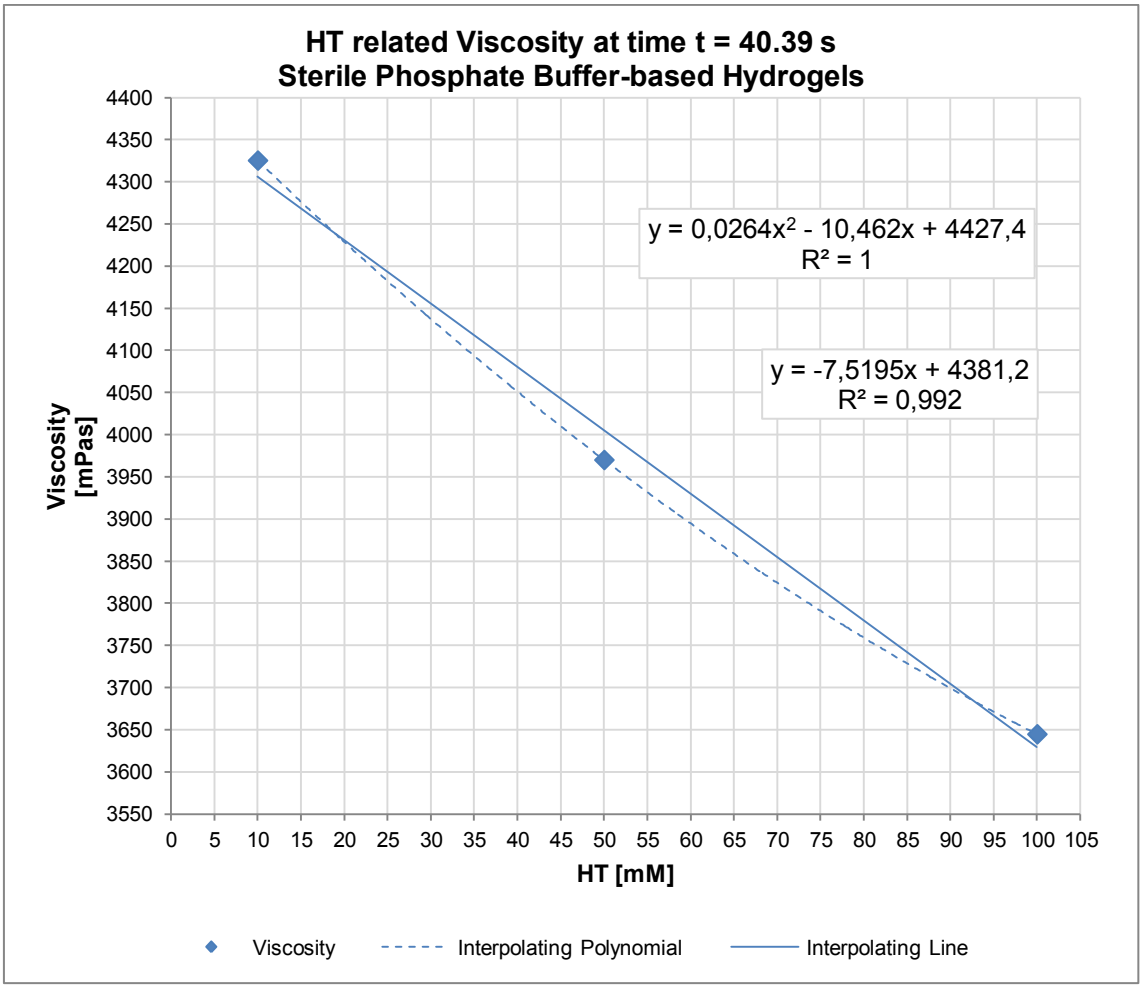

Figure 67. *HT concentration [mM] versus Viscosity [mPas] of Sterile Phosphate Buffer-based Hydrogels, obtained with "Viscosity" Method at time t = 40.39 s. The interpolating third degree polynomial and the interpolating line are represented with their relative equation and R^2.*

Table XXIII. *Viscosity Values of Sterile Phosphate Buffer-based Hydrogels at t = 40.39 s*

VISCOSITY VALUES OF STERILE PHOSPHATE BUFFER-BASED HYDROGELS				
HT [mM]	**Viscosity Values at t = 40.39 s [mPas]**			
	min – max	**median**	**mean**	**STD**
10	4316.54 4335.67	4320.98	4325.40	9.30
50	3959.96 3980.16	3969.18	3970.18	8.53
100	3636.42 3654.89	3645.66	3644.76	8.50

Viscosity curves of Sterile Citrate Buffer-based Hydrogels is shown in the following figure (Figure 68).

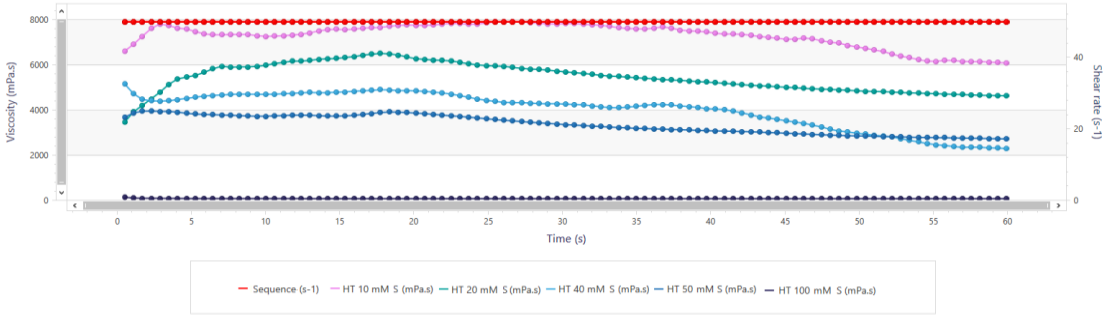

Figure 68. *Viscosities [mPas] of Sterile Citrate Buffer-based Hydrogels – HT 10 mM (in pink), HT 20 mM (in sea water), HT 40 mM (in light blue), HT 50 mM (in blue) and HT 100 mM (in dark blue) – with the fixed shear rate [s^{-1}] (in red).*

A graph representing the HT [mM] related Viscosity of Sterile Phosphate Buffer-based Hydrogels at time t = 40.39 s is shown in Figure 69; Viscosity Values (minimum and maximum, median, mean and standard deviation) are shown in Table XXIV.

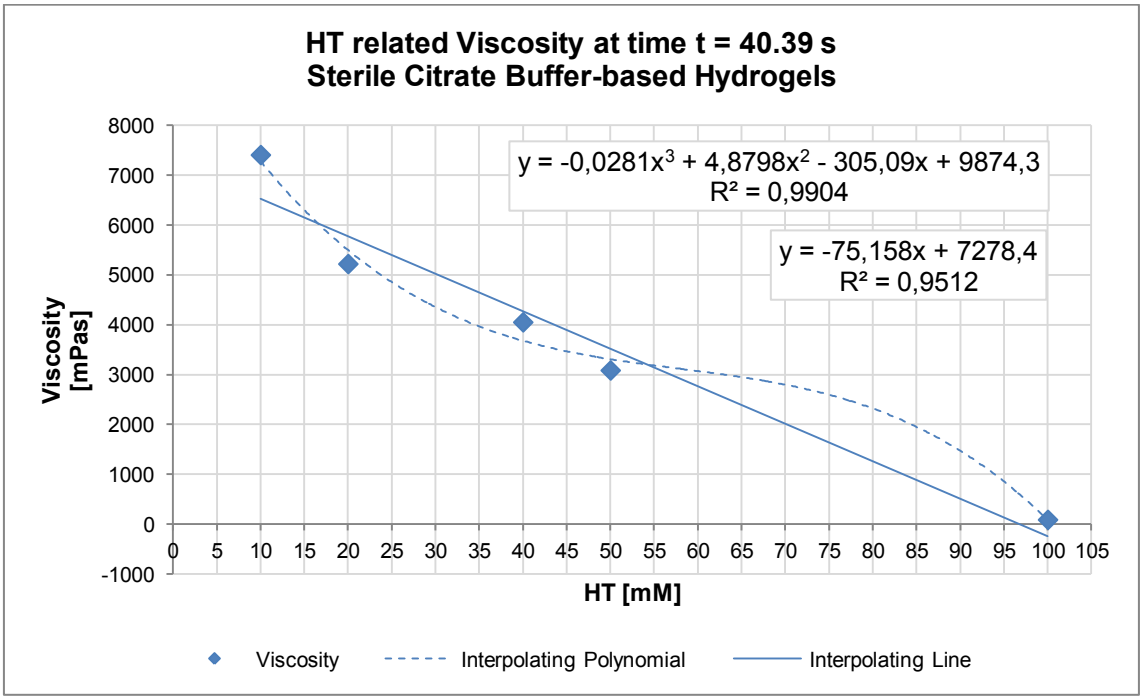

Figure 69. *HT concentration [mM] versus Viscosity [mPas] of Sterile Citrate Buffer-based Hydrogels, obtained with "Viscosity" Method at time t = 40.39 s. The interpolating third degree polynomial and the interpolating line are represented with their relative equation and R^2.*

Table XXIV. *Viscosity Values of Sterile Citrate Buffer-based Hydrogels at t = 40.39 s*

VISCOSITY VALUES OF STERILE CITRATE BUFFER-BASED HYDROGELS				
HT [mM]	**Viscosity Values at t = 40.39 s [mPas]**			
	min – max	**median**	**mean**	**STD**
10	7392.98 7419.97	7404.63	7406.99	10.97
20	5213.07 5230.01	5224.76	5221.28	9.26
40	4044.86 4062.07	4051.43	4052.35	8.95
50	3078.93 3093.72	3087.80	3086.48	7.87
100	89.91 90.12	89.15	90.41	1.78

The comparison of results obtained at time t = 40.39 s for the Not-Sterile Phosphate Buffer-based Hydrogel and the Not-Sterile Citrate Buffer-based Hydrogel is represented in the following histogram (Figure 70).

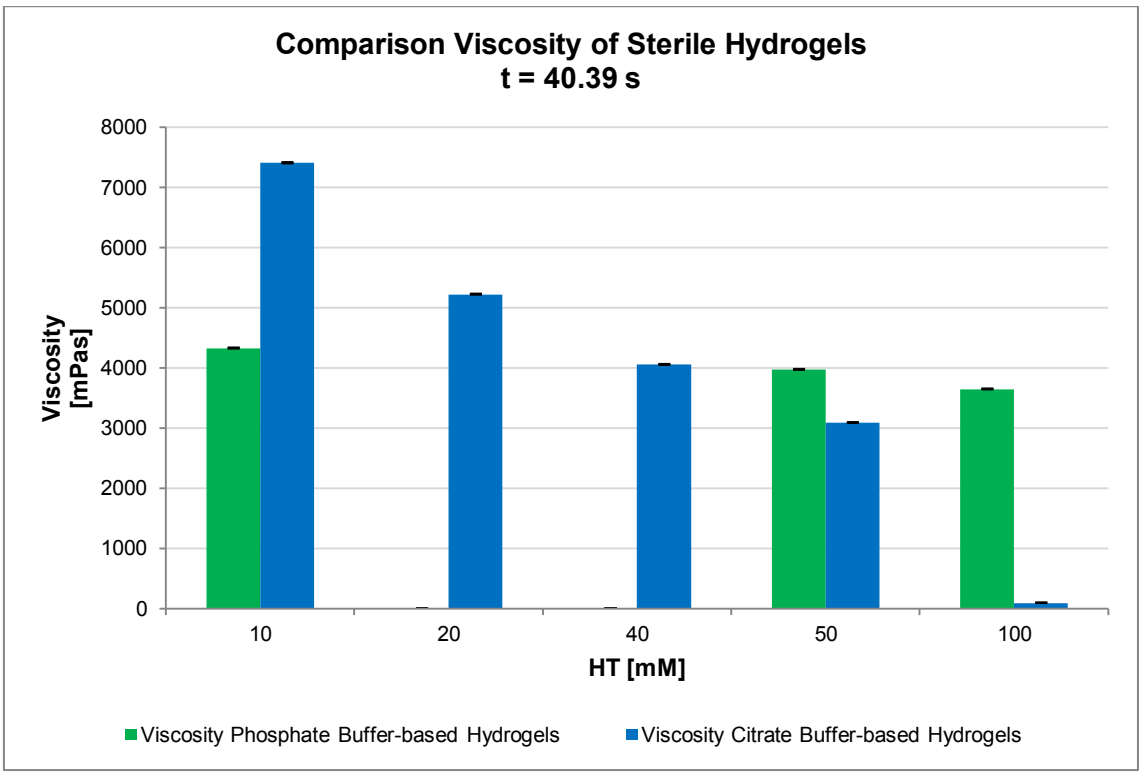

Figure 70. *HT [mM] dependent Viscosity [mPas] of Sterile Phosphate Buffer-based Hydrogels and Sterile Citrate Buffer-based Hydrogels, obtained with "Viscosity" Method at time t = 40.39 s.*

Considering HT 100 mM Hydrogel as a representative sample, the comparison between Sterile Phosphate Buffer-based Hydrogel and the Sterile Citrate Buffer-based Hydrogel is shown in the following figure (Figure 71).

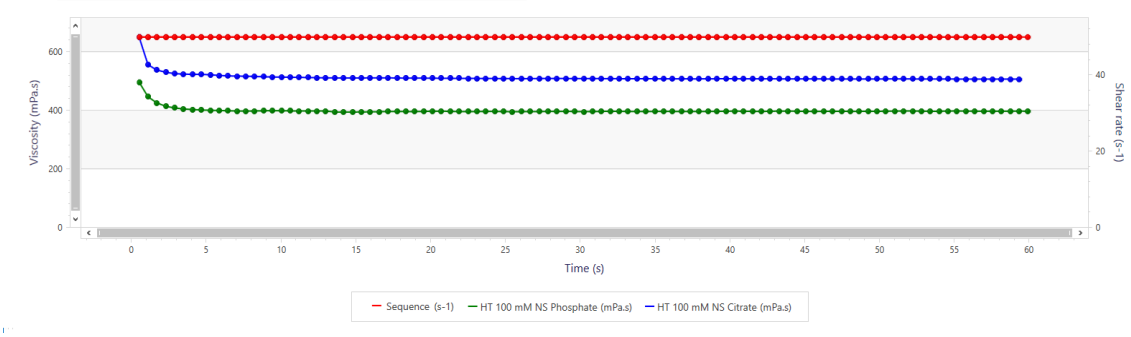

Figure 71. *Comparison between Viscosities [mPas] of the HT 100 mM Sterile Phosphate Buffer-based Hydrogel (in green) and the HT 100 mM Sterile Citrate Buffer-based Hydrogel (in electric blue) with the fixed shear rate [s^{-1}] (in red).*

3.3.3 Comparison of Not-Sterile and Sterile Samples

Considering HT 100 mM as a representative sample, the comparison between Not-Sterile Phosphate Buffer-based Hydrogel and the Sterile Phosphate Buffer-based Hydrogel is shown in Figure 72. Likewise, the comparison between Not-Sterile Citrate Buffer-based Hydrogel and the Sterile Citrate Buffer-based Hydrogel is shown in Figure 73.

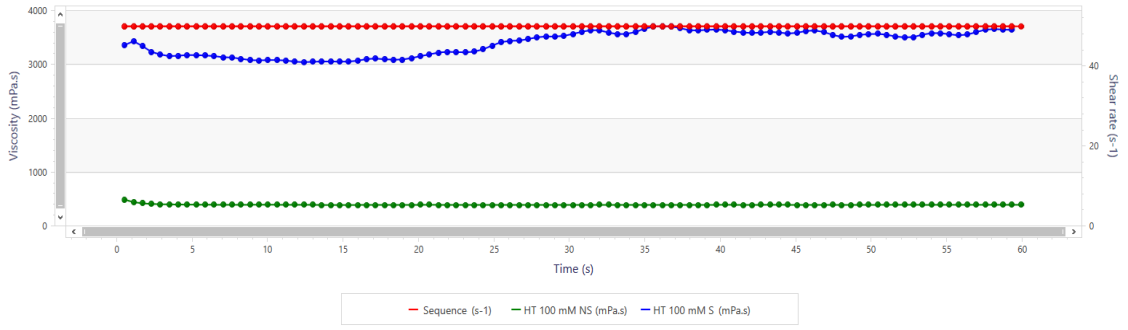

Figure 72. *Comparison between Viscosities [mPas] of the Not-Sterile Phosphate Buffer-based Hydrogel HT 100 mM (in green) and the Sterile Phosphate Buffer-based Hydrogel HT 100 mM (in electric blue) with the fixed shear rate [s^{-1}] (in red).*

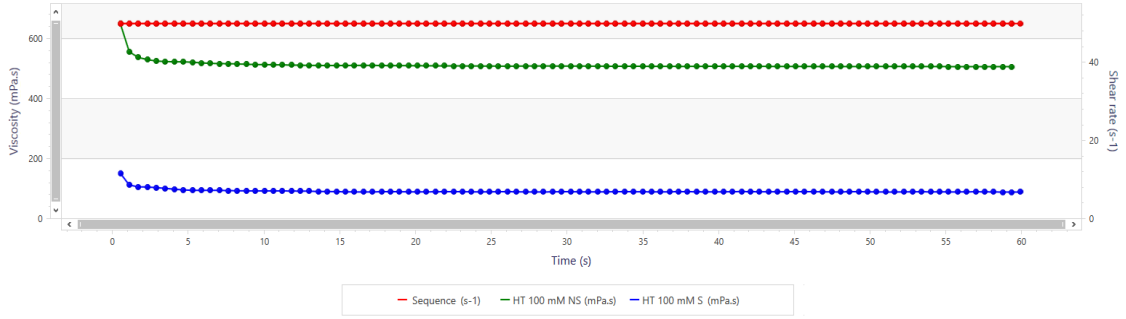

Figure 73. *Comparison between Viscosities [mPas] of the Not-Sterile Citrate Buffer-based Hydrogel HT 100 mM (in green) and the Sterile Citrate Buffer-based Hydrogel HT 100 mM (in electric blue) with the fixed shear rate [s^{-1}] (in red).*

3.4 FT-IR Analysis

IR spectra of Not-Sterile and Sterile samples with PEO 4% and bi-distilled water is shown in the following figure (Figure 74).

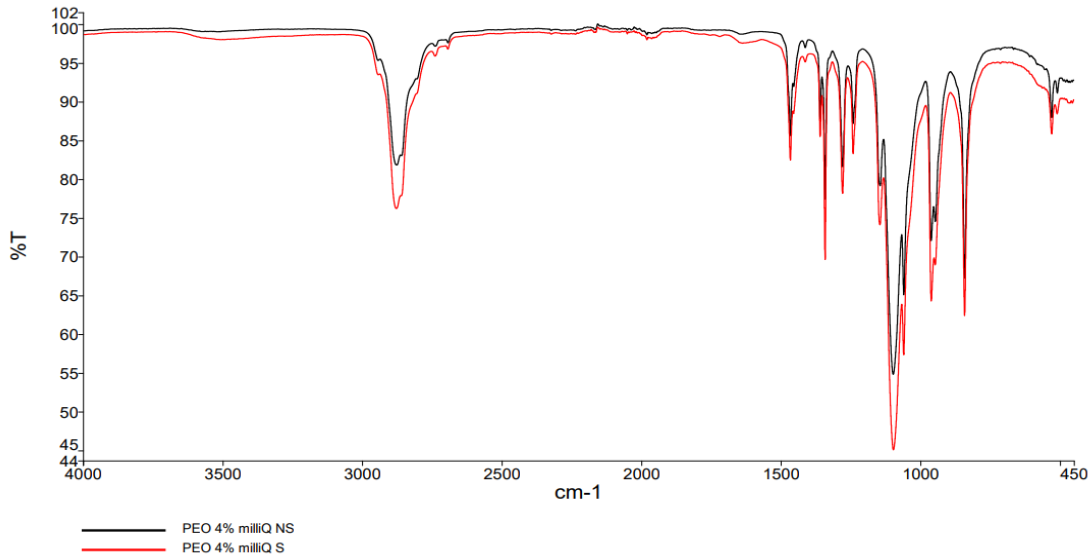

Figure 74. *Comparison between IR Spectra of Not-Sterile PEO 4% in bi-distilled water (in black) and Sterile PEO 4% in bi-distilled water (in red).*

The comparison between Not-Sterile HT 0 mM Phosphate Buffer-based Hydrogel and Sterile HT 0 mM Phosphate Buffer-based Hydrogel is shown in Figure 75 and in Figure 76.

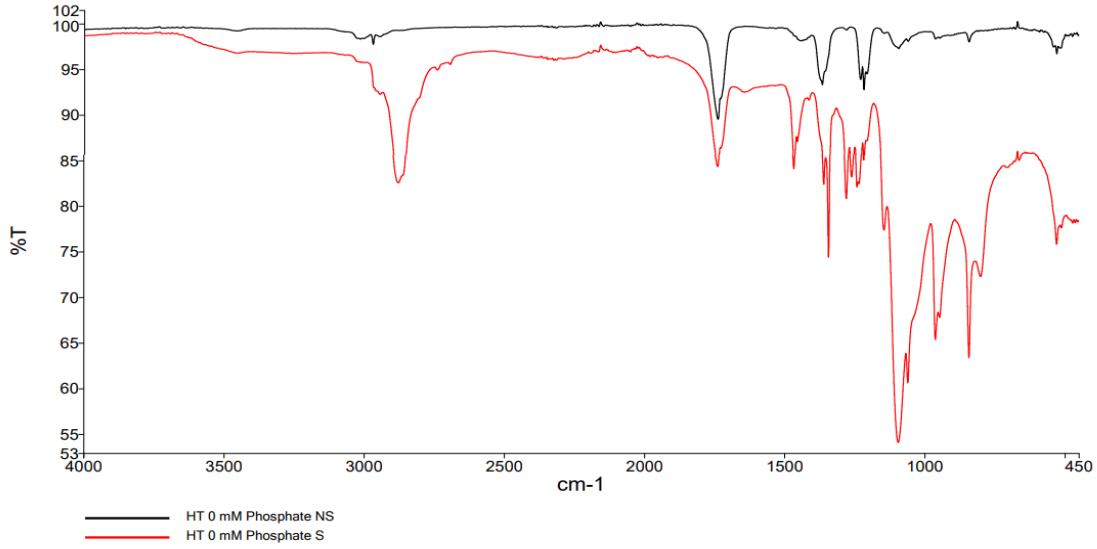

Figure 75. *Comparison between IR Spectra of Not-Sterile HT 0 mM Phosphate Buffer-based Hydrogel (in black) and Sterile HT 0 mM Phosphate Buffer-based Hydrogel (in red).*

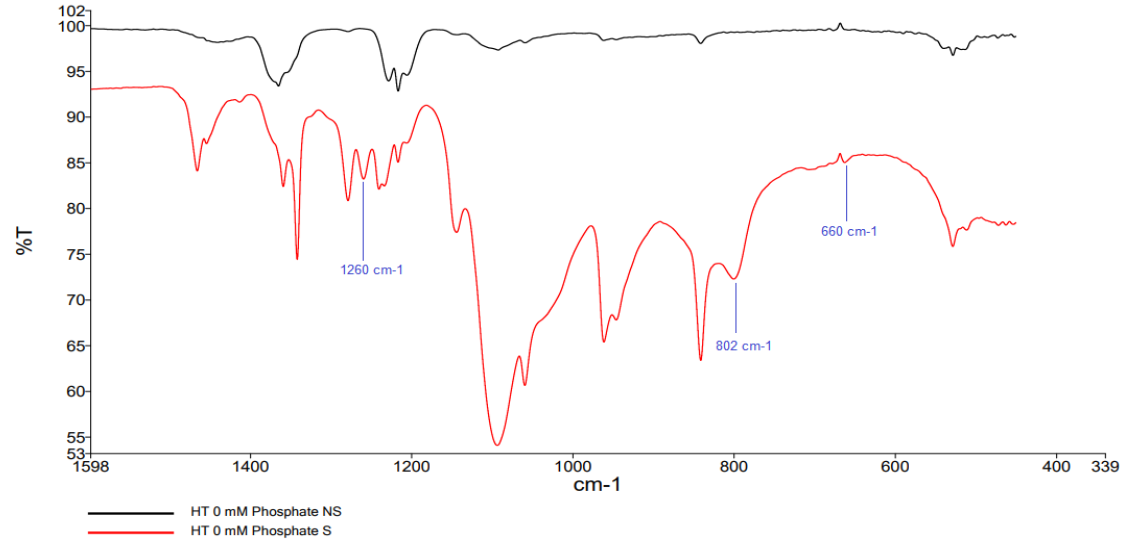

Figure 76. *Comparison between IR Spectra of Not-Sterile HT 0 mM Phosphate Buffer-based Hydrogel (in black) and Sterile HT 0 mM Phosphate Buffer-based Hydrogel (in red). In figure is represented only the fingerprint region; new peaks due to sterilization process have been highlighted.*

The comparison of all spectra obtained for Not-Sterile Phosphate Buffer-based Hydrogels is shown in Figure 77.

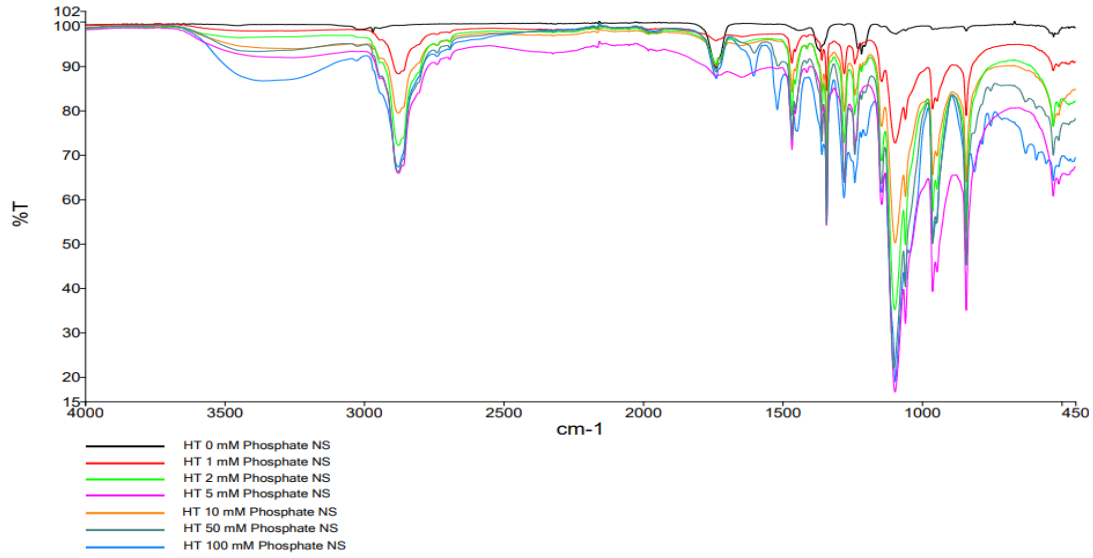

Figure 77. *Comparison of IR Spectra of Not-Sterile Phosphate Buffer-based Hydrogels: HT 0 mM (in black), HT 1 mM (in red), HT 2 mM (in green), HT 5 mM (in pink), HT 10 mM (in orange), HT 50 mM (in grey), HT 100 mM (in light blue).*

The comparison of all spectra obtained for Sterile Phosphate Buffer-based Hydrogels is shown in Figure 78.

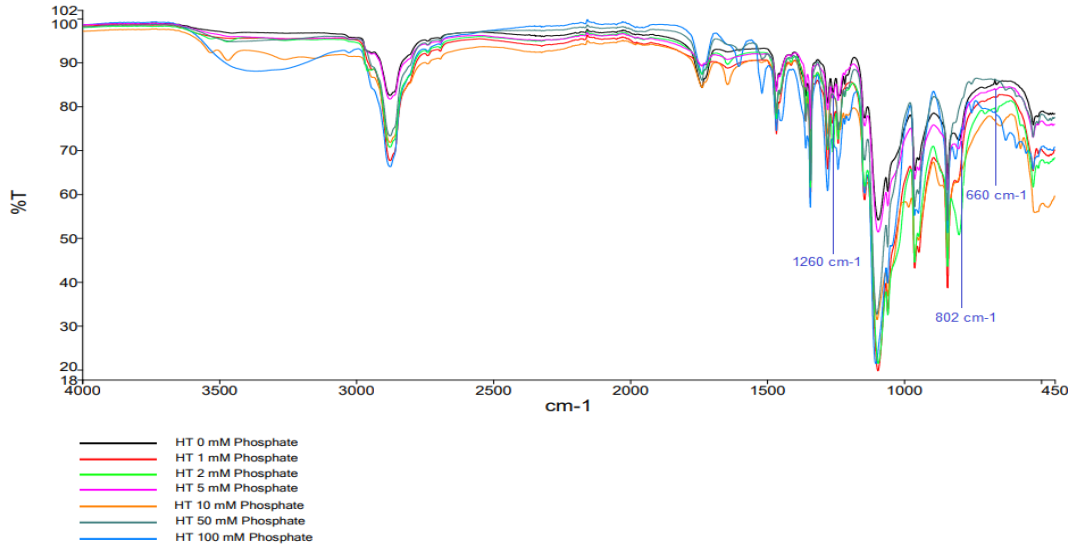

Figure 78. *Comparison of IR Spectra of Sterile Phosphate Buffer-based Hydrogels: HT 0 mM (in black), HT 1 mM (in red), HT 2 mM (in green), HT 5 mM (in pink), HT 10 mM (in orange), HT 50 mM (in grey), HT 100 mM (in light blue). New peaks due to sterilization process have been highlighted.*

The area [dimensionless] of the peaks of interest – highlighted in the previous figures – are reported in Table XXV. In addition, a graph representing the trend of the area of the selected peaks for Sterile Phosphate Buffer-based Hydrogels is shown in Figure 79.

Table XXV. *Area of the Peaks of Interest for Phosphate Buffer-based Hydrogels*

AREA OF PEAKS OF INTEREST PHOSPHATE BUFFER-BASED HYDROGELS			
1260 cm^{-1}			
HT 0 Not-Sterile	/	**HT 0 Sterile**	31.89
HT 1 Not-Sterile	/	**HT 1 Sterile**	27.55
HT 2 Not-Sterile	/	**HT 2 Sterile**	21.10
HT 5 Not-Sterile	/	**HT 5 Sterile**	20.02
HT 10 Not-Sterile	/	**HT 10 Sterile**	/
HT 50 Not-Sterile	/	**HT 50 Sterile**	/
HT 100 Not-Sterile	/	**HT 100 Sterile**	/
802 cm^{-1}			
HT 0 Not-Sterile	/	**HT 0 Sterile**	89.78
HT 1 Not-Sterile	/	**HT 1 Sterile**	61.98
HT 2 Not-Sterile	/	**HT 2 Sterile**	52.36
HT 5 Not-Sterile	/	**HT 5 Sterile**	32.06
HT 10 Not-Sterile	/	**HT 10 Sterile**	/
HT 50 Not-Sterile	/	**HT 50 Sterile**	/
HT 100 Not-Sterile	/	**HT 100 Sterile**	/
660 cm^{-1}			
HT 0 Not-Sterile	/	**HT 0 Sterile**	9.64
HT 1 Not-Sterile	/	**HT 1 Sterile**	9.50
HT 2 Not-Sterile	/	**HT 2 Sterile**	/
HT 5 Not-Sterile	/	**HT 5 Sterile**	/
HT 10 Not-Sterile	/	**HT 10 Sterile**	/
HT 50 Not-Sterile	/	**HT 50 Sterile**	/
HT 100 Not-Sterile	/	**HT 100 Sterile**	/

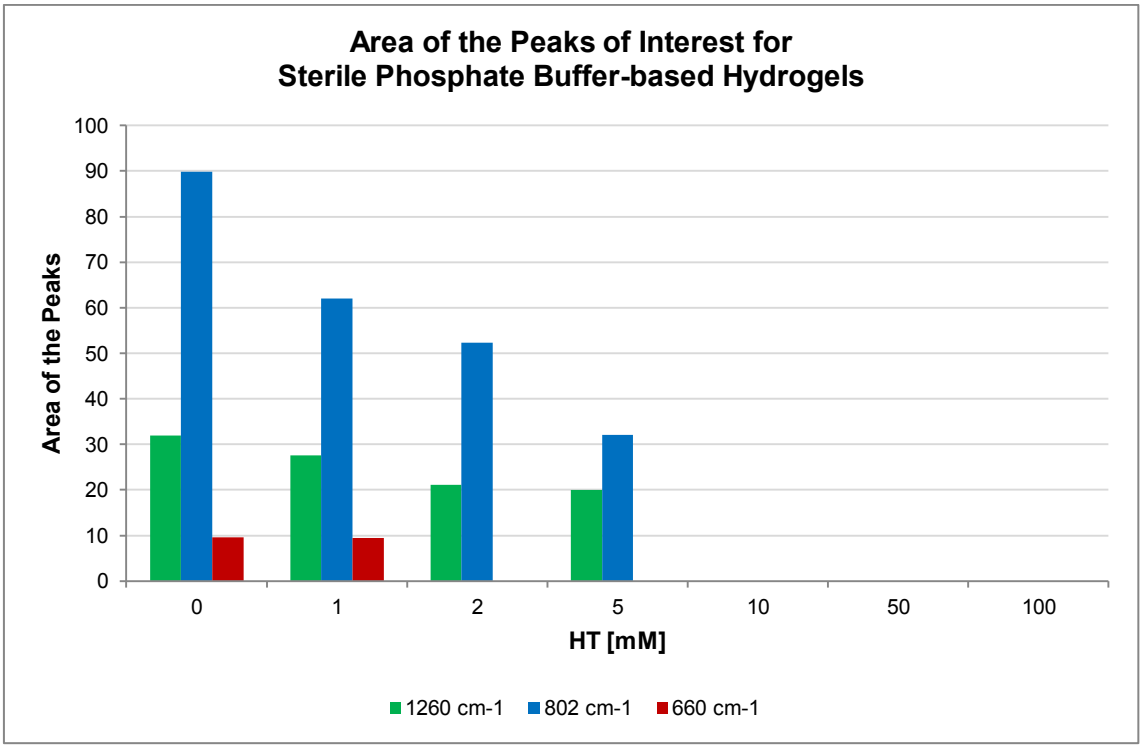

Figure 79. *Trend of the Area of the Peaks of Interest (1260 cm^{-1}, 802 cm^{-1} and 660 cm^{-1}) for Sterile Phosphate Buffer-based Hydrogels.*

The comparison of results obtained for Not-Sterile HT 0 mM Citrate Buffer-based Hydrogel and Sterile HT 0 mM Citrate Buffer-based Hydrogel is shown in Figure 80 and in Figure 81.

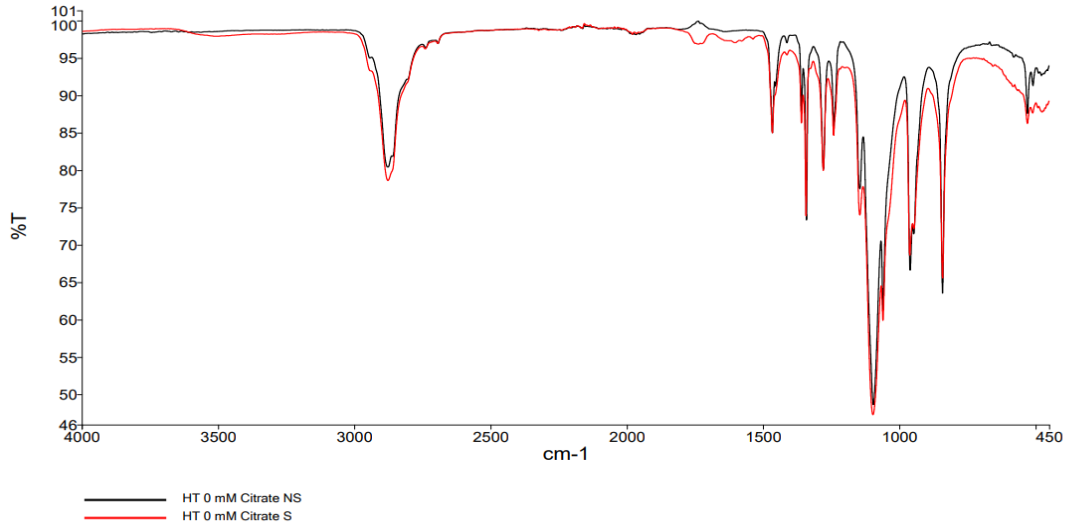

Figure 80. *Comparison of IR Spectra of Not-Sterile HT 0 mM Citrate Buffer-based Hydrogel (in black) and Sterile HT 0 mM Citrate Buffer-based Hydrogel (in red).*

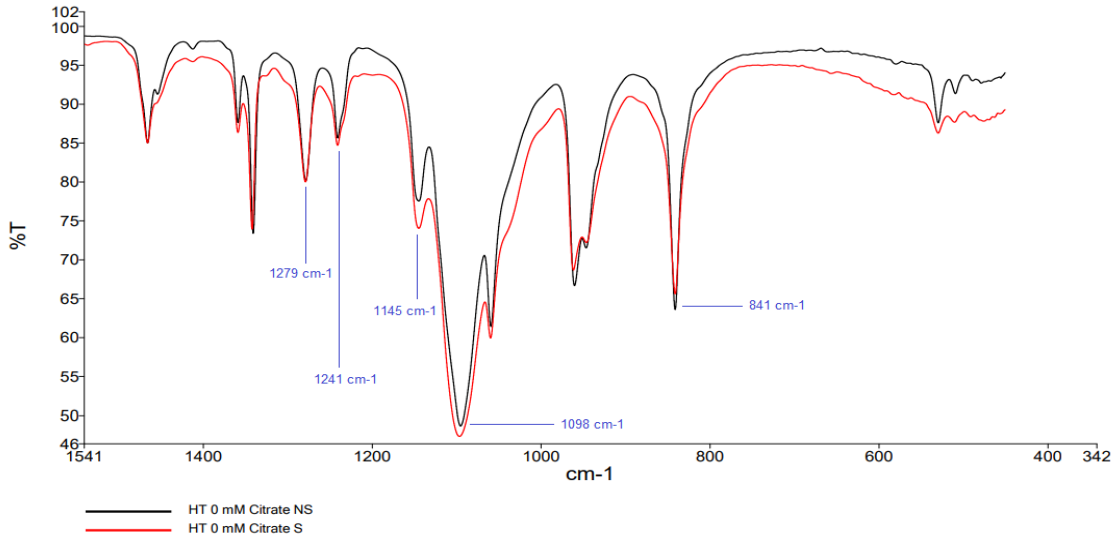

Figure 81. *Comparison of IR Spectra of Not-Sterile HT 0 mM Citrate Buffer-based Hydrogel (in black) and Sterile HT 0 mM Citrate Buffer-based Hydrogel (in red). In figure is represented only the fingerprint region; peaks of interest have been highlighted.*

The comparison of all spectra obtained for Not-Sterile Citrate Buffer-based Hydrogels is shown in Figure 82.

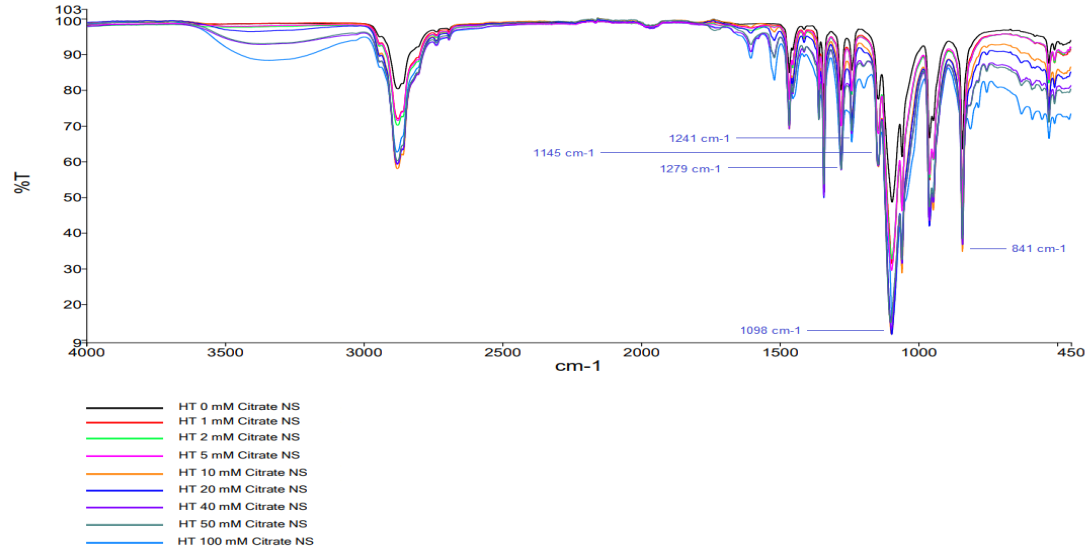

Figure 82. *Comparison of IR Spectra of Not-Sterile Citrate Buffer-based Hydrogels: HT 0 mM (in black), HT 1 mM (in red), HT 2 mM (in green), HT 5 mM (in pink), HT 10 mM (in orange), HT 20 (in electric blue), HT 40 mM (in purple), HT 50 mM (in grey), HT 100 mM (in light blue). Peaks of interest have been highlighted.*

The comparison of all the spectra obtained for Sterile Citrate Buffer-based Hydrogels is shown in Figure 83.

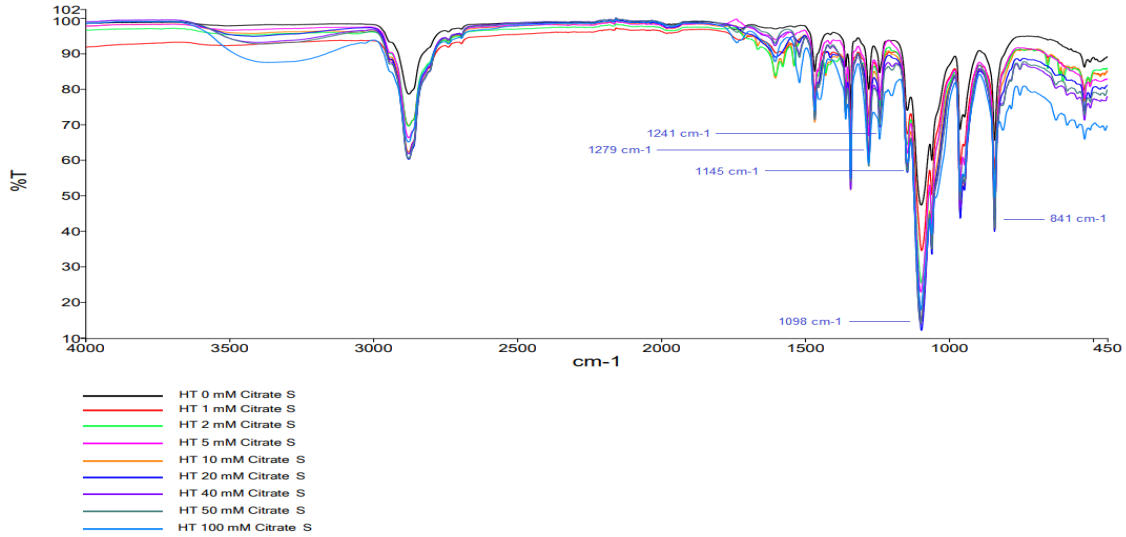

Figure 83. *Comparison of IR Spectra of Sterile Citrate Buffer-based Hydrogels: HT 0 mM (in black), HT 1 mM (in red), HT 2 mM (in green), HT 5 mM (in pink), HT 10 mM (in orange), HT 20 (in electric blue), HT 40 mM (in purple), HT 50 mM (in grey), HT 100 mM (in light blue). Peaks of interest have been highlighted.*

The area [dimensionless] of the peaks of interest – highlighted in the previous figures – are reported in Table XXVI. In addition, a graph representing the trend of the area of the selected peaks for Not-Sterile Citrate Buffer-based Hydrogels is shown in Figure 84; the same graph has been created also for Sterile Citrate Buffer-based Hydrogels and is shown in Figure 85.

Table XXVI. *Area of the Peaks of Interest for Citrate Buffer-based Hydrogels*

AREA OF PEAKS OF INTEREST CITRATE BUFFER-BASED HYDROGELS			
1279 cm^{-1}			
HT 0 Not-Sterile	232.45	**HT 0 Sterile**	205.87
HT 1 Not-Sterile	322.94	**HT 1 Sterile**	257.45
HT 2 Not-Sterile	342.20	**HT 2 Sterile**	298.24
HT 5 Not-Sterile	357.07	**HT 5 Sterile**	350.25
HT 10 Not-Sterile	491.56	**HT 10 Sterile**	408.25
HT 20 Not-Sterile	485.21	**HT 20 Sterile**	404.61
HT 40 Not-Sterile	474.03	**HT 40 Sterile**	400.59
HT 50 Not-Sterile	469.05	**HT 50 Sterile**	380.33
HT 100 Not-Sterile	380.62	**HT 100 Sterile**	357.57

1241 cm^{-1}			
HT 0 Not-Sterile	139.85	**HT 0 Sterile**	127.50
HT 1 Not-Sterile	206.61	**HT 1 Sterile**	192.90
HT 2 Not-Sterile	223.06	**HT 2 Sterile**	195.03
HT 5 Not-Sterile	242.89	**HT 5 Sterile**	226.49
HT 10 Not-Sterile	260.38	**HT 10 Sterile**	228.78
HT 20 Not-Sterile	192.73	**HT 20 Sterile**	183.02
HT 40 Not-Sterile	191.07	**HT 40 Sterile**	174.85
HT 50 Not-Sterile	189.35	**HT 50 Sterile**	164.91
HT 100 Not-Sterile	178.91	**HT 100 Sterile**	154.48
1145 cm^{-1}			
HT 0 Not-Sterile	115.46	**HT 0 Sterile**	96.34
HT 1 Not-Sterile	187.26	**HT 1 Sterile**	122.59
HT 2 Not-Sterile	202.43	**HT 2 Sterile**	136.49
HT 5 Not-Sterile	238.49	**HT 5 Sterile**	173.31
HT 10 Not-Sterile	245.21	**HT 10 Sterile**	190.49
HT 20 Not-Sterile	240.81	**HT 20 Sterile**	179.72
HT 40 Not-Sterile	209.90	**HT 40 Sterile**	169.10
HT 50 Not-Sterile	178.26	**HT 50 Sterile**	159.82
HT 100 Not-Sterile	164.41	**HT 100 Sterile**	151.86
1098 cm^{-1}			
HT 0 Not-Sterile	973.69	**HT 0 Sterile**	836.19
HT 1 Not-Sterile	1238.28	**HT 1 Sterile**	1119.18
HT 2 Not-Sterile	1255.55	**HT 2 Sterile**	1241.22
HT 5 Not-Sterile	1367.98	**HT 5 Sterile**	1345.25
HT 10 Not-Sterile	1621.95	**HT 10 Sterile**	1448.84
HT 20 Not-Sterile	1593.41	**HT 20 Sterile**	1444.75
HT 40 Not-Sterile	1571.48	**HT 40 Sterile**	1434.32
HT 50 Not-Sterile	1536.64	**HT 50 Sterile**	1354.02
HT 100 Not-Sterile	1265.38	**HT 100 Sterile**	1263.33
841 cm^{-1}			
HT 0 Not-Sterile	670.56	**HT 0 Sterile**	635.82
HT 1 Not-Sterile	876.01	**HT 1 Sterile**	783.25
HT 2 Not-Sterile	952.53	**HT 2 Sterile**	802.67
HT 5 Not-Sterile	1286.01	**HT 5 Sterile**	1080.02
HT 10 Not-Sterile	1299.11	**HT 10 Sterile**	1223.38
HT 20 Not-Sterile	1279.98	**HT 20 Sterile**	1177.45
HT 40 Not-Sterile	1224.68	**HT 40 Sterile**	1047.77
HT 50 Not-Sterile	925.22	**HT 50 Sterile**	853.27
HT 100 Not-Sterile	332.05	**HT 100 Sterile**	320.82

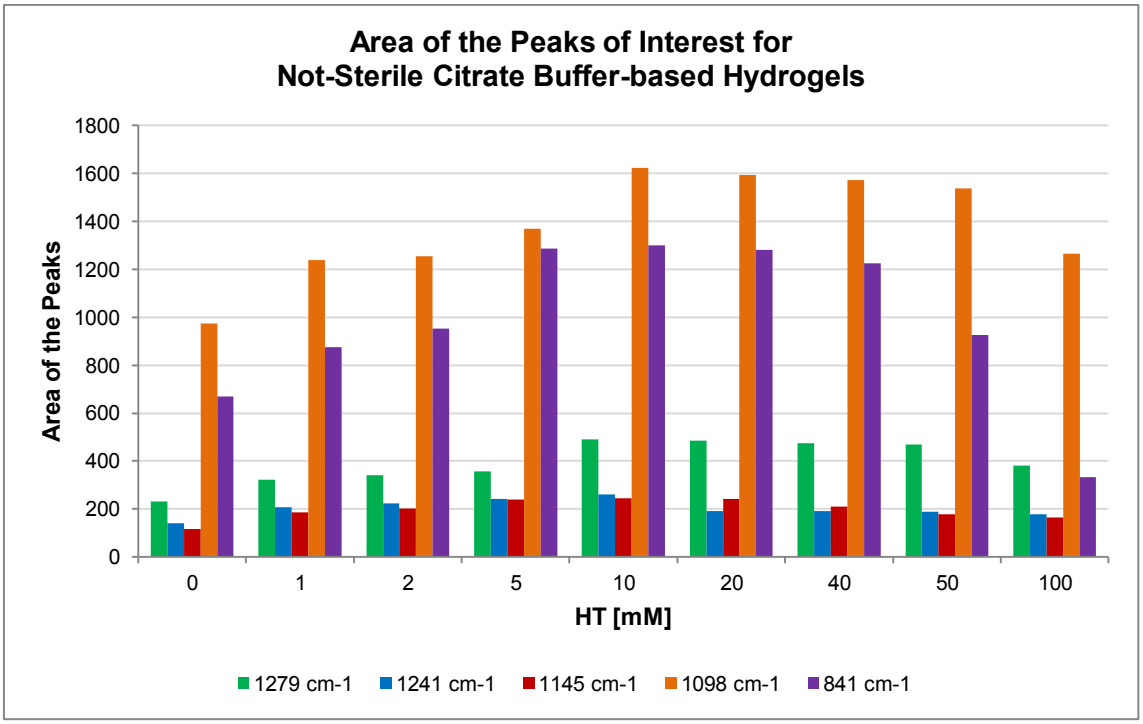

Figure 84. *Trend of the Area of the Peaks of Interest (1279 cm^{-1}, 1241 cm^{-1}, 1145 cm^{-1}, 1098 cm^{-1} and 841 cm^{-1}) for Not-Sterile Citrate Buffer-based Hydrogels.*

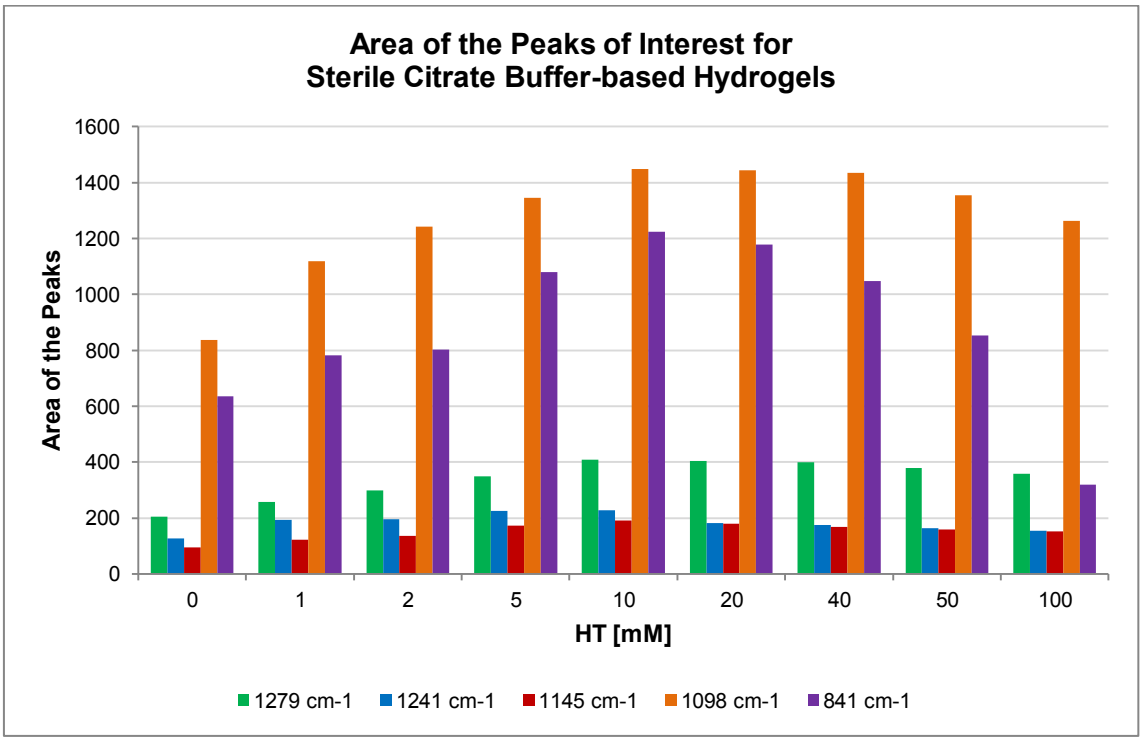

Figure 85. *Trend of the Area of the Peaks of Interest (1279 cm^{-1}, 1241 cm^{-1}, 1145 cm^{-1}, 1098 cm^{-1} and 841 cm^{-1}) for Sterile Citrate Buffer-based Hydrogels.*

3.5 HPLC Analysis

The calibration line, created automatically by Chromera software thanks to the HPLC Analysis of calibration samples, is shown in the following figure (Figure 86). Thanks to the software, the passage through the origin has been imposed.

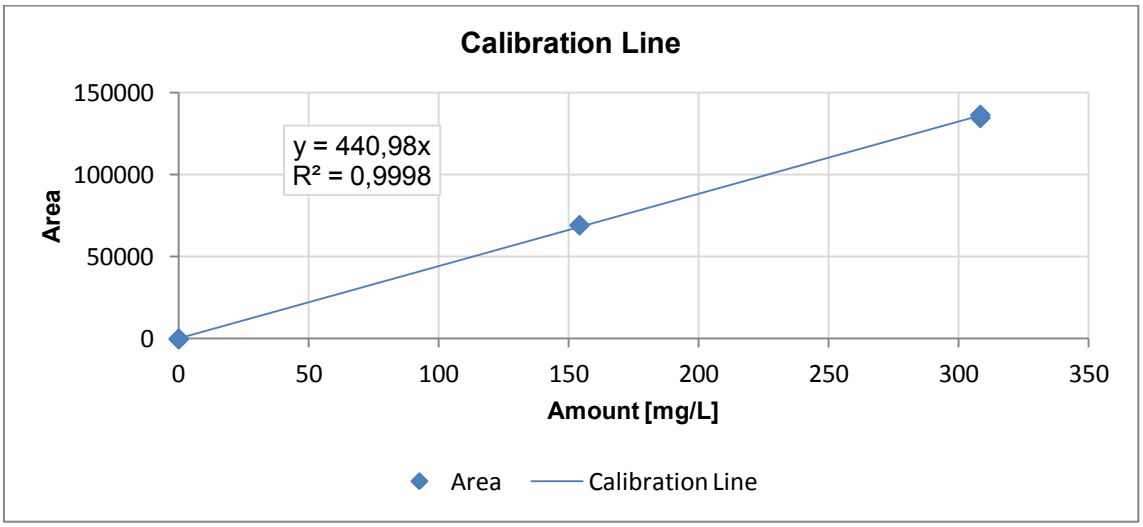

Figure 86. *Calibration Line used for HPLC Analysis.*

For each sample extracted and analyzed with chromatograph, the software has produced a graph Time [min] – Absorbance [mAU]. An example – representing Not-Sterile HT 5 mM Phosphate Buffer-based Hydrogel – is shown in Figure 87.

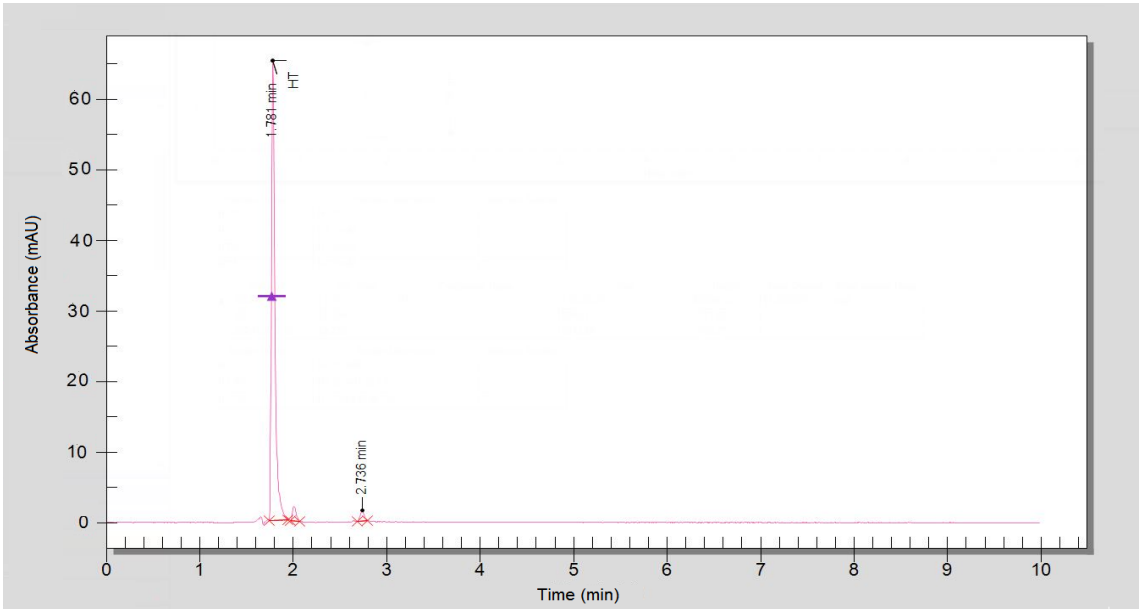

Figure 87. *HT peak for Not-Sterile HT 5 mM Phosphate Buffer-based Hydrogel.*

The area [dimensionless] of HT peaks and the corresponding amount of extracted HT [mM] are reported in Table XXVII for Phosphate Buffer-based Hydrogels.

Table XXVII. *Area of the HT Peaks (Phosphate Buffer-based Hydrogels) and Amount of Extracted HT [mM]*

AREA OF HT PEAKS AND CORRESPONDING AMOUNT OF EXTRACTED HT		
PHOSPHATE BUFFER-BASED HYDROGELS		
Sample	**Area [dimensionless]**	**Amount of Extracted HT [mM]**
Not-Sterile HT 1 mM	1049.78	0.84931828
Not-Sterile HT 2 mM	2143.42	1.73412319
Not-Sterile HT 5 mM	5913.82	4.78454155
Not-Sterile HT 10 mM	11016.53	8.9128562
Not-Sterile HT 50 mM	5297.48	42.858912
Not-Sterile HT 100 mM	11355.99	91.874912
Sterile HT 1 mM	/	/
Sterile HT 2 mM	/	/
Sterile HT 5 mM	/	/
Sterile HT 10 mM	7120.73	5.76098670
Sterile HT 50 mM	3468.12	28.05858830
Sterile HT 100 mM	6934.98	56.10703360

Table XXVIII. *Area of the HT Peaks (Citrate Buffer-based Hydrogels) and Amount of Extracted HT [mM]*

AREA OF HT PEAKS AND CORRESPONDING AMOUNT OF EXTRACTED HT		
CITRATE BUFFER-BASED HYDROGELS		
Sample	**Area [dimensionless]**	**Amount of Extracted HT [mM]**
Not-Sterile HT 1 mM	1234.44	0.99871753
Not-Sterile HT 2 mM	2253.05	1.82281520
Not-Sterile HT 5 mM	5976.38	4.83515023
Not-Sterile HT 10 mM	12195.90	9.86701835
Not-Sterile HT 20 mM	24538.16	19.85245230
Not-Sterile HT 40 mM	49233.74	39.83225520
Not-Sterile HT 50 mM	6171.00	49.92608640
Not-Sterile HT 100 mM	12350.10	99.91772270
Sterile HT 1 mM	/	/
Sterile HT 2 mM	/	/
Sterile HT 5 mM	5316.87	4.30158176
Sterile HT 10 mM	11632.13	9.41090763
Sterile HT 20 mM	24018.51	19.43203067

Sterile HT 40 mM	48539.70	39.27075150
Sterile HT 50 mM	6052.32	48.96595551
Sterile HT 100 mM	12236.48	98.99846190

A graph representing the trend of the amount of the extracted HT for Not-Sterile Phosphate and Citrate Buffer-based Hydrogels is shown in Figure 88; the comparison between the Sterile Phosphate and Citrate Buffer-based Hydrogels, instead, is shown in Figure 89.

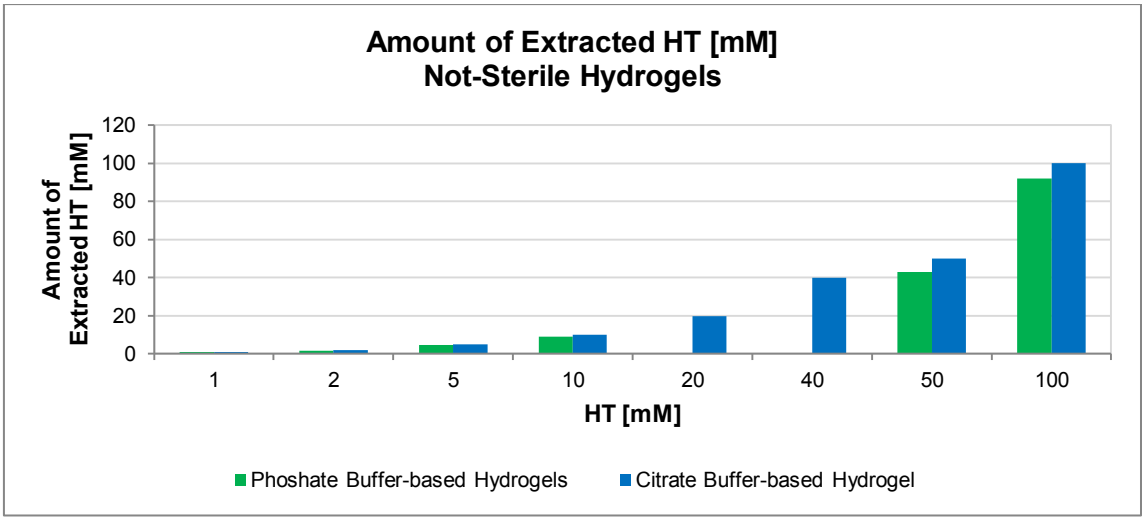

Figure 88. *Amount of Extracted HT [mM] for Not-Sterile Phosphate and Citrate Buffer-based Hydrogels.*

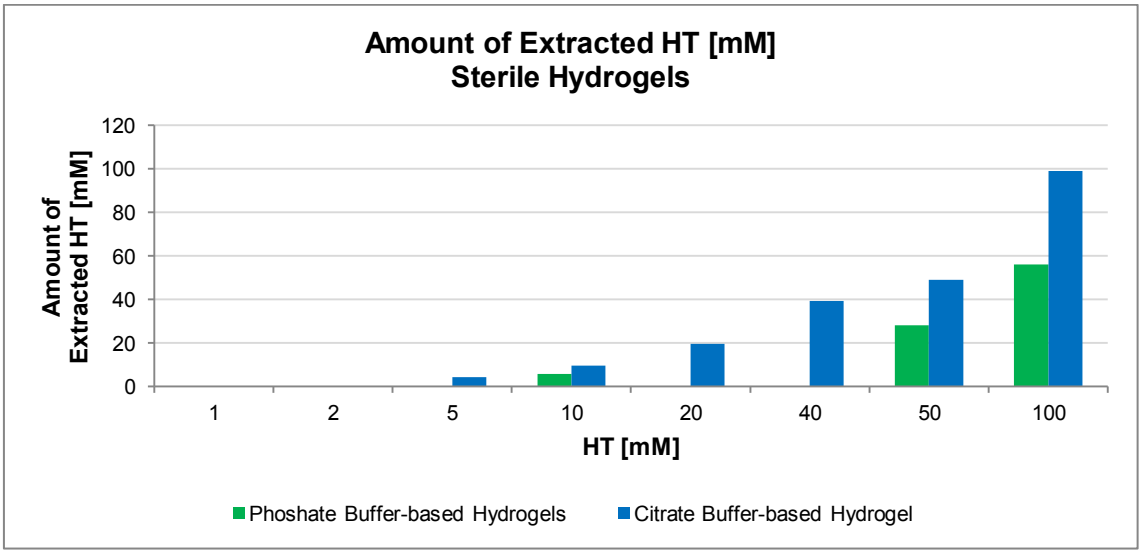

Figure 89. *Amount of Extracted HT [mM] for Sterile Phosphate and Citrate Buffer-based Hydrogels.*

4. Discussion

4.1 Production

As it is possible to see from Figure 54 and Figure 55 in Results, the Hydrogel samples show a progressively intense yellow colour; this is because the increasing amount of hydroxytyrosol (HT) added. Moreover, HT tends to be partially degrade in contact with atmospheric air: this process leads to a deprotonation of hydroxyls groups present on the aromatic ring of HT. The resulting resonance form is highly reactive on carbon 1, which loses the group hydroxyethyl- forming catechol; then, the catechol proceeds to oxidation, up to formation of orthoquinone (Figure 90), a toxic red compound, clearly visible in the more concentrated HT solutions. This is particularly evident in Phosphate Buffer-based Hydrogels, where the samples of HT 50 mM and 100 mM have an intense red colour.

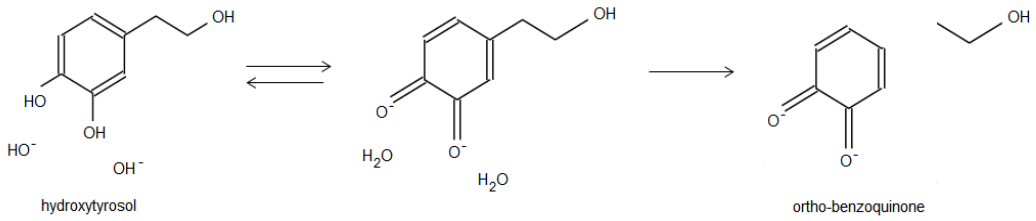

Figure 90. *Oxidation of Hydroxytyrosol and consequent formation of Orthoquinone.*

To support visual observation of the prepared Hydrogels, pH Values can be considered. As it is possible to observe from Table XVII and from Table XVIII, pH Values of Phosphate Buffer-based Hydrogels and Citrate Buffer-based Hydrogels are higher for samples with a lower concentration of HT and lower for samples with an higher concentration of HT. This data confirms the hypothesis that the carbon 1 of HT is easy attackable, since its resonance form that derives from deprotonation of the hydroxyl group of carbon 3 of the aromatic ring is possible only when the pH exceeds the acid dissociation constant of hydroxytyrosol. However, the increase in pH is not too high; this is because PEO and HT work in opposite directions: the first tends to alkalise (5.50 – 7.00 pH at 25 °C) and the second to acidify (pH acqueous solution: 3.50 – 4.50 pH). In addition, pH Values of Phosphate Buffer-based Hydrogels are around 6.00 pH and pH Values of Phosphate Buffer-based Hydrogels are around 5.00 pH (as it is also shown graphically in Figure 56): this is because Phosphate Buffer and Citrate Buffer alone has a mean pH Value of 6.00 and 5.00, respectively.

On the basis of this first analysis, the choice of the use of Citrate Buffer Solution seems to be more suitable in order to guarantee a better biocompatibility of Hydrogels; this choice might be supported also by a biochemical point of view. Indeed, Citric Acid – one of the components of the Citrate Buffer Solution – is involved in the Krebs Cycle (Figure 91), a metabolic cycle of fundamental importance in all cells that use oxygen in the process of cellular respiration. The Citric Acid Cycle, in fact, utilizes mitochondrial enzymes for final oxidation of carbohydrates, proteins and fats; moreover, the Krebs Cycle also produces intermediates which are important in gluconeogenesis, lipolysis, neurotransmitter synthesis, and other processes. Citric Acid is, thus, consumed and then regenerated by this sequence of reactions to complete the cycle [68].

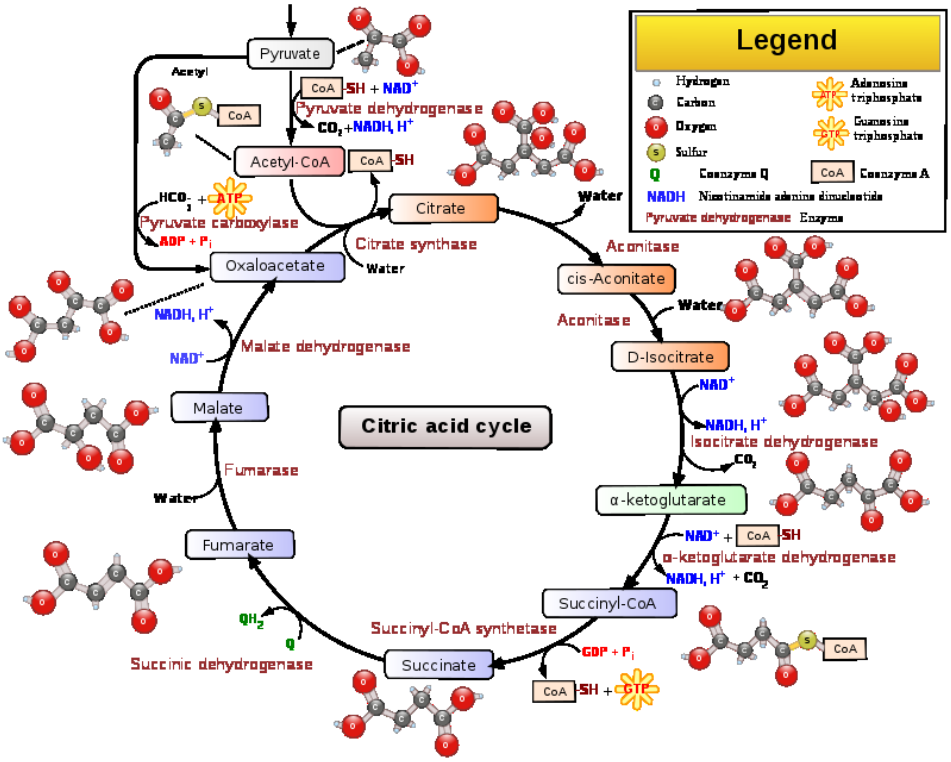

Figure 91. *Krebs Cycle* [68].

4.2 Sterilization

As it is possible to see from Figure 57 and Figure 58 in Results, in Sterile Hydrogel samples the degradation of HT is even more evident, especially in Phosphate Buffer's Hydrogels. This is due to Sterilization process: γ radiation, in fact, may induce some changes in chemical-physical of samples and increase rates of molecular degradation [20].

This is supported also by the results obtained for pH measurements. As it is possible to observe from Table XIX and from Table XX, pH Values of Sterile Hydrogels are higher than pH Values of Not-Sterile Hydrogels (Table XVII and Table XVIII). In addition, by observing Figure 59, it is clear that pH Values of Phosphate Buffer-based Hydrogels are around 6.00 pH and pH Values of Phosphate Buffer-based Hydrogels are around 5.00 pH. Also here, the relationship between pH and HT concentration – higher pH for lower concentrations and vice versa – is confirmed.

4.3 Rheological Analysis

By observing the results obtained for the Rheological Analysis of the Not-Sterile Phosphate Buffer-based Hydrogels, it is clear that the quantity of hydroxytyrosol influences the viscoelasticity of the gel. As it possible to see graphically in Figure 60, the viscosity [mPas] of Hydrogels with low HT concentration is higher than the viscosity of Hydrogels with high HT concentration. In addition, by looking also at Table XXI and Figure 61, it is possible to note that the significant change in viscosity occurs only for HT 50 mM (≈ 500 mPas) and HT 100 mM (≈ 400 mPas) Hydrogels. Conversely, the viscosity of the HT 0 mM to HT 10 mM Hydrogels remains barely unchanged (between 900 and 1000 mPas) and it is not possible to notice a fixed relationship between viscosity and quantity of HT for these samples. Figure 61 confirms that there is a negative correlation (correlation coefficient $R < 0$) between the amount of HT and the change in viscosity, thus, an increase in the amount of hydroxytyrosol corresponds to a decrease in viscosity. The correlation is quite strong ($R^2 = 0.9409$), as demonstrated by the value of R (-0.9700) and by the value of the angular coefficient; despite this, the lack of intermediate measurements makes the linear model unreliable. The interpolating third degree polynomial approximates the viscosity trend more correctly ($R^2 = 0.9979$), but it provides us complex – and, therefore, more difficult to interpret – solutions. In addition, the lack of samples with intermediate HT quantity means that the same output can be given by multiple inputs: this suggests caution in using the model for predicting values outside the experimental data range of the independent variable.

The results obtained for the rheological analysis of the Not-Sterile Citrate Buffer-based Hydrogels confirm that the quantity of hydroxytyrosol influences the viscoelasticity of the gel. By observing Figure 62, it is possible to see that, also in this case, the viscosity of Hydrogels with low HT concentration is higher than the viscosity of Hydrogels with high HT concentration. In addition, with the use of Citrate Buffer, as underlined also by

Table XXII and Figure 63, for every change – even minimal – in the amount of HT, there is a related change in viscosity: thus, in this case the linear negative correlation (correlation coefficient $R < 0$) between the amount of HT and the change in viscosity is respected also for hydrogels with low concentrations of HT. Figure 63 shows that the correlation is quite strong ($R^2 = 0.7494$); in fact, both the Pearson correlation coefficient R (-0.8657) and the angular coefficient have an high value. Also with the addition of intermediate measurements the linear model is unreliable: the interpolating third degree polynomial approximates the viscosity trend more correctly ($R^2 = 0.9891$). Therefore, also in this model the lack of more samples with intermediate HT quantity means that the same output can be given by multiple inputs.

On the basis of these considerations, it is noticeable that the behavior (summarized in Figure 64) of the two types of Hydrogels – Phosphate Buffer-based Hydrogels and Citrate Buffer-based Hydrogels – is due to the different degree of polymer hydration, in turn influenced by the different saline species. Furthermore, the different salinity of the buffers also affects the different degradation of HT, as seen also during the production phase; thus, the use of one buffer instead of another significantly influences the viscoelasticity of the gel.

For what concerns Sterile Hydrogels, the rheological analysis has not been performed for all the samples. In fact, gamma radiation induces structural changes and introduces crosslinking among polymer chains; as a consequence, these hydrogels undergo to viscosity increase [35]. Nevertheless, similar considerations can be made for Sterile Phosphate and Citrate Buffer-based Hydrogels: as for Not-Sterile samples, with an increase in the amount of HT, there is a decrease in viscosity (Figure 66 and Figure 68). The model, created to relate Viscosity [mPas] to HT [mM] for Sterile Phosphate Buffer-based Hydrogels (Figure 67), confirms that there is a strong negative correlation ($R^2 = 0.9920$) between the amount of HT and the change in viscosity; nevertheless, the interpolating third degree polynomial turns out to be the best model to represent the viscosity trend ($R^2 = 1$). Similarly, the third degree polynomial model ($R^2 = 0.9904$) created to relate Viscosity [mPas] to HT [mM] for Sterile Citrate Buffer-based Hydrogels (Figure 69), is more reliable and precise than the linear model ($R^2 = 0.9512$). These results are easily observable also from Table XXIII, Table XXIV and from Figure 70; particularly in this last one, it is possible to see graphically the comparison between the behavior of Sterile Phosphate and Citrate Buffer-based Hydrogels.

The HT 100 mM Citrate Buffer-based Hydrogel deserves particular attention: unlike other samples, for which the post-sterilization viscosity is higher than the pre-sterilization viscosity, HT 100 mM Hydrogel has a lower viscosity after sterilization. Gamma radiation, in fact, increases rates of degradation and , thus, induces an initial decrease in viscosity; the high concentration of hydroxytyrosol prevents polymeric chains crosslinking. In addition, this underlines that hydroxytyrosol is a very effective surfactant, as just demonstrated in literature [69]. This result is very important because confirms the hypothesis that HT can be used as a method for preventing polymeric crosslinking of injectable hydrogels and, thus, for limiting modifications of bio-mechanical properties (embrittlement, solidification, viscosity increase), while guaranteeing the product sterility.

4.4 FT-IR Analysis

By observing Figure 74, it is not possible to notice changes between IR spectra of Not-Sterile and Sterile solution of PEO 4% and bi-distilled water. This is because Polyethylene Oxide dissolved in bi-distilled water and subjected to gamma rays sterilization simply polymerizes and it does not induce the formation of new bonds.

Analyzing the IR spectrum obtained for Not-Sterile and Sterile HT 0 mM Phosphate Buffer-based Hydrogels (Figure 75 and Figure 76), the formation of new peaks in the fingerprint region is evident: these new bonds indicate that the phenomenon of crosslinking has occurred. Peaks of interest – as highlighted in Figure 76 and Figure 78 – are those at 1260 cm^{-1}, corresponding to the C-O-C stretching [71], and at 802 cm^{-1} and 660 cm^{-1}, both corresponding to the C-O-P stretching and scissoring [71]. What can be seen by observing Table XXV and Figure 77 is that, above a certain concentration of HT, the bonds are no longer visible: this is an important result because it supports the thesis that hydroxytyrosol acts as an anti-crosslinking agent for PEO.

For what concern the results obtained for Not-Sterile and Sterile HT 0 mM Citrate Buffer-based Hydrogels (Figure 80 and Figure 81), it is clear that there is not the formation of any new peak; thus, only a process of simple polymerization has occurred. Peaks of interest – highlighted in Figure 81, Figure 82 and Figure 83 – are present both in Not-Sterile and Sterile Hydrogels; therefore, the focus shifts to the analysis of how the selected peaks change after sterilization. The highlighted peaks are those at 1279 cm^{-1} (C-H twisting), 1241 cm^{-1} (C-O-C stretching), 1145 cm^{-1} (C-H rocking), 1098 cm^{-1} (C-O stretching) and 841 cm^{-1} (C-O-C stretching) [71]. By analyzing Table XXVI it is

possible to observe that the main difference between Not-Sterile and Sterile samples is given – for all the selected peaks – by the decrease of the Area, which indicate a stiffening of the polymer structure, due to the polymerization. In addition, as shown in Table XXVI, Figure 84 and Figure 85, as the HT concentration rises above 20 mM, there is a general decrease in the molar extinction coefficients, for Not-Sterile and Sterile, ascribable to the surfactant power of hydroxytyrosol [69], thus capable of sequestering polymer solvent, decreasing its vibrational capacity.

Therefore, the results obtained for FT-IR Analysis are perfectly in agreement with what observed for Rheological Analysis.

4.5 HPLC Analysis

HPLC Analysis has led to the desired result. In fact, thanks to the method of extraction that has been implemented based on method of Seker [64], the separation, identification and quantification of the active compound (hydroxytyrosol) has been possible for almost all the samples.

By observing Table XXVII, representing the Area of the HT peaks and the related amount of extracted HT [mM] for Phosphate Buffer-based Hydrogels, it is possible to notice a different result for Not-Sterile and Sterile samples. The amount of extracted HT for Not-Sterile Hydrogels, in fact, is almost equal to the quantity actually present in them; the samples HT 10 mM, HT 50 mM and HT 100 mM deviate, even if slightly, from the result obtained for the other Non-Sterile samples, probably due to a slight oxidation already in progress (as demonstrated also by the colour observation of the samples immediately after production, Figure 54). The results obtained for the Sterile Phosphate Buffer-based Hydrogels indicate an even more evident degradation after sterilization: gamma rays induce a change in the hydrogels structural properties with a consequent increase in the rate of degradation of HT and the inability to completely extract the active compound; the extracted quantity is, in fact, only about half of that actually present. The impossibility of extracting the active compound from the samples HT 1 mM, HT 2 mM and HT 5 mM is due, probably, to the low amount of HT present in them, to the very high viscosity of samples and to the degradation process (as demonstrated by the visual observation of the samples after sterilization, Figure 58).

Analyzing Table XXVIII, representing the Area of the HT peaks and the related amount of extracted HT [mM] for Citrate Buffer-based Hydrogels, it is immediately evident that

the amount of extracted HT for Not-Sterile Hydrogels is almost equal to the quantity actually present in them. In this case, in fact, there is no substantial change between extracted HT and real HT, even for samples from 10 mM to 100 mM. This result – interpolated to the visual observation (Figure 55) and pH data (Table XVIII) – allows to show that hydroxytyrosol is more preserved when formulated with Citrate Buffer. The results obtained from HPLC Analysis of Sterile Citrate Buffer-based Hydrogels show that, even after sterilization, these samples are less degraded than the corresponding samples produced with the Phosphate Buffer; this result – that allows the almost complete extraction of the active compound – is, like the previous ones, also supported by visual observation (Figure 58). The impossibility of extracting the active compound from the samples HT 1 mM and HT 2 mM is due, in this case, only to the low amount of HT present in them and the very high viscosity.

Figure 88 and Figure 89 can graphically explain what has been said by analyzing Table XXVII and Table XXVIII. The comparison between Not-Sterile Hydrogels shows that the Citrate Buffer allows to better separate, identify and quantify the active compound. This result is even more evident from the comparison between Sterile Phosphate and Citrate Buffer-based Hydrogels: in this case, in fact, the amount of active compound extracted from the samples formulated with Phosphate Buffer is about half the amount of extracted HT from the samples formulated with Citrate Buffer.

5. Concluding Remarks

Every year millions of patients experience the loss of or the damage to organs, tissues, or body parts [1]: for this reason, the development of therapies that can regenerate tissues and decrease reliance on transplantations has become of central importance [2]. Regenerative Medicine aims to the replacement or regeneration of human cells, tissues and organs, in order to re-establish normal functionality [3]; Tissue Engineering, involves the application of the principles and methods of engineering in order to develop biological substitutes to maintain or improve tissue function [4]. The field of Tissue Engineering and Regenerative Medicine (TERM) has significantly increased over the past decades, thanks to the use of porous, three-dimensional (3D) scaffolds to provide the appropriate environment for the regeneration of tissues [10].

Current strategies of scaffold synthesis involve the use of a wide variety of materials able to mimic the Extracellular Matrix (ECM), when native ECM is pathologically altered [11]. To achieve clinical tissue success, functional biomaterials research has been directed toward the development of improved scaffolds for Regenerative Medicine; the three main material types which have been investigated to be applied in developing scaffolds include natural polymers, synthetic polymers, and ceramics [1]. In particular, thanks to their properties, synthetic polymers are highly useful in biomedical field [12]: they are, in fact, highly versatile materials with physical and chemical properties that can be easily controlled and altered to produce a wide range of mechanical properties and degradation rates [11]. One of the main synthetic polymers used in tissue engineering is Polyethylene Oxide (PEO), that has mainly been employed in the form of hydrogels, a class of crosslinked polymeric materials which have been broadly used as matrices for scaffold applications [1]. Hydrogel-based systems, in fact, offer moderate-to-high physical, chemical and mechanical stability: the elastic behaviour and swelling capability resemble the natural ECM of many tissues, making hydrogels particularly suitable to scaffold production [5].

Biodegradable scaffolds have a potential to be infected by different types of microorganism, such as virus, bacteria, and fungi: sterilization is the process by which a product can be made free of contamination from living microorganisms [17]. Sterilization of hydrogels, however, may alter the characteristics of the scaffold, inducing some changes in material chemical properties, reducing compressive mechanical properties and molecular weights, and increasing rates of post-sterilization

degradation [20]. Gamma irradiation, for example, is one of the most used sterilization techniques; unfortunately, PVA, PVP and PEO based hydrogel formulations can be subjected to crosslinking reactions among polymer chains during irradiation processes [33], then leading to the formation of a three-dimensional polymer network complexity [34]. As a consequence, these hydrogels undergo to undesirable effects such as embrittlement, solidification, plasticization or viscosity increase [35].

The need for development of a method allowing to prevent or limit crosslinking phenomena of hydrogels [33] has become of fundamental importance in scientific research. The use of anti-crosslinking agents (that is, compounds with antioxidants and/or free-radical scavenger properties) has proven to be an effective way in preventing crosslinking of the hydrogel during irradiation [33]. Several studies have been so far performed using Vitamin C and Vitamin E as anti-crosslinking molecules; these vitamins are scientifically recognized as regenerating agents for oxidized and free radical species in the body [33].

Thanks to its antioxidant, anti-inflammatory and antimicrobial properties, hydroxytyrosol (HT) could been selected as a good alternative to Vitamin C and Vitamin E. In fact, HT has an oxygen radical absorption capacity ten times higher than green tea and two times higher than that of coenzyme Q-10 [53]; in addition, according to the study of Fruhwirth et al. [54] hydroxytyrosol has an antioxidant capacity significantly higher than Vitamin C.

Based on these considerations, the hypothesis behind this study is that radiation-induced cross-linking of PEO-based hydrogels could be either prevented or limited by tailoring the concentration of hydroxytyrosol introduced as an anti-crosslinking agent. In addition, this work aims to evaluate how the use of a specific kind of buffer saline solution can affect the final characteristics of the optimized hydrogel.

Thus, in order to verify the above mentioned assumptions, the study has been performed by producing gels with PEO, HT and two different buffer solutions (such as, Phosphate Buffer Solution, PBS and Citrate Buffer Solution, CBS).

The samples characterization (pre- and post- sterilization) has been carried out – in addition to a simple visual observation and pH measurement of the prepared hydrogels – on two analytical levels: the rheological and the chemical one.

Rheology is the study of flow behaviour, either simply in terms of viscosity or also relative to various viscoelastic properties [42]. For this reason, the Rheological Analysis has been conducted in order to evaluate the hydrogel viscoelasticity changes depending on a variation of HT concentration (both in Not-Sterile and Sterile condition). To do this, the "Viscosity" method has been programmed with constant shear rate to follow evolution of viscosity as a function of time.

The chemical characterization has been conducted through both Fourier-Transform Infrared Spectroscopy (FTIR) and High Performance Liquid Chromatography (HPLC).

FT-IR Analysis has been performed for all the Not-Sterile and Sterile Hydrogels; in addition, it has been performed also for a solution prepared with only PEO 4% and bi-distilled water in order to understand which modifications are due to the polymerization of PEO and, therefore, how much hydroxytyrosol and different saline species (Phosphate or Citrate) can affect the process. Since FT-IR Analysis has been done in order to study chemical changes and to provide information on species crystallinity, an assessment of the areas of the peaks of interest has been carried out.

After an aqueous ethanol solvent extraction, performed to isolate HT from hydrogels, HPLC has been used to separate, identify and quantify the active compound (hydroxytyrosol, HT) detectable inside hydrogels. Once all the samples have been acquired, the “Average Area” of the HT peaks has been calculated by the software: once determined the Absorbance [mAU], it is possible to obtain the related HT concentration [mM], considering dilution factors used.

As it is possible to observe already from the production phase, Hydrogel samples have a progressively intense yellow colour: this is due to both an increase of HT amount in solution and to its tendency to be partially degradated in contact with atmospheric air. This process leads to the formation of orthoquinone, a toxic red compound, clearly visible in the most concentrated HT solutions, particularly in Phosphate Buffer-based Hydrogels. By interpolating the visual observation and pH data, it is possible to notice how HT remains more preserved when added in Citrate Buffer, where the pH is always less than 6: this data confirms the hypothesis that the carbon 1 of HT is easy attackable, since its resonance form that derives from deprotonation of the hydroxyl group of carbon 3 is possible only when the pH exceeds the acid dissociation constant of hydroxytyrosol. Degradation is even more evident after sterilization, since gamma rays induce a change in the structural properties of the gels with the consequent

increase of the degradation rate of HT. Based on this first analysis, the use of Citrate Buffer Solution appears to be the most convenient in order to guarantee the greatest biocompatibility of the Hydrogels.

By observing the results of the Rheological Analysis of Not-Sterile Hydrogels, it is clear that the quantity of hydroxytyrosol influences the viscoelasticity of the gel: the viscosity [mPas] of Hydrogels with low HT concentration is higher than the viscosity of Hydrogels with high HT concentration. This is evident both for Phosphate and Citrate Buffer-based Hydrogels, also if the correlation between the amount of HT and the change in viscosity is respected also for hydrogels with low concentrations of HT only by hydrogels formulated with Citrate Buffer. Analyzing the third degree polynomial models it is clear that the behavior of the two types of Hydrogels is correlated to the different degree of polymer hydration, in turn influenced by the different saline species. Furthermore, the different salinity of the buffers also affects the different degradation of HT, as seen also during the production phase; thus, the use of one buffer instead of another significantly influences the viscoelasticity of the gel. This is confirmed by observing the results obtained for Sterile Hydrogels, although the Rheological Analysis has not been performed for all the samples, because of an increase of viscosity due to gamma radiation. The HT 100 mM Citrate Buffer-based Hydrogel deserves particular attention, because, unlike other samples, it has a lower viscosity after sterilization: this is probably due to the action of the HT which reduces the polymerization and acts as a surfactant, as well. This result is very important because strengthens the hypothesis that HT can be used as a biomolecule for preventing crosslinking of injectable hydrogels and, thus, for limiting related modifications in mechanical behaviour (embrittlement, solidification, viscosity increase) during gamma ray sterilization process.

Analyzing the IR spectrum obtained for Not-Sterile and Sterile HT 0 mM Phosphate Buffer-based Hydrogels, the formation of new peaks in the fingerprint region is evident: these new bonds indicate that the phenomenon of crosslinking has occurred. In addition, above a certain concentration of HT, the bonds are no longer visible: this is an important result because it supports the thesis that hydroxytyrosol acts as an anti-crosslinking agent for PEO polymeric chains. For what concern the results obtained for Not-Sterile and Sterile HT 0 mM Citrate Buffer-based Hydrogels, it is clear that there is not the formation of any new peak; thus, only a process of simple polymerization has occurred. The main difference between Not-Sterile and Sterile samples is given by the

Area decrease, which indicates a stiffening of the polymer structure, due to the polymerization. In addition, as the HT concentration rises above 20 mM, there is a general decrease in the molar extinction coefficients, both for Not-Sterile and Sterile samples, ascribable to the surfactant power of hydroxytyrosol, therefore capable of sequestering polymer solvent, then decreasing its vibrational capacity. These results clearly match to the results of Rheological Analysis: the different salinity of the buffers influences not only the viscoelasticity of the gel, but also the formation of bonds after gamma radiation sterilization.

Thanks to the method of extraction implemented, the separation, identification and quantification of the active compound (hydroxytyrosol) has been possible for almost all the hydrogel samples. For Phosphate Buffer-based Hydrogels, it is possible to notice a different result for Not-Sterile and Sterile samples: the amount of extracted HT for Not-Sterile Hydrogels, in fact, is almost equal to the quantity actually present in them; the samples HT 10 mM, HT 50 mM and HT 100 mM deviate, even if slightly, from the result obtained for the other Non-Sterile samples, probably due to a minimum oxidation already in progress. The results obtained for the Sterile Phosphate Buffer-based Hydrogels indicate an even more evident degradation after sterilization: the extracted quantity is, in fact, only about half of that actually present. For what concerns the results of Citrate Buffer-based Hydrogels, it is immediately evident that the amount of extracted HT for Not-Sterile Hydrogels is almost equal to the quantity actually added in solution: in this case, in fact, there is no substantial change between extracted HT and real HT, even for samples from 10 mM to 100 mM. In addition, even after sterilization, samples formulated with Citrate Buffer are less degraded than those ones containing the Phosphate Buffer: this allows the almost complete extraction of the active compound. The comparison between Phosphate and Citrate Buffer-based Hydrogels shows that hydroxytyrosol is more preserved when formulated in Citrate Buffer and, thus, that the second formulation allows to better separate, identify and quantify the active compound.

In conclusion, considering all the performed analyses, it is possible to affirm that:

- hydroxytyrosol (HT) represents a good alternative to Vitamin C and Vitamin E: in fact, it has been demonstrated that radiation-induced cross-linking of PEO-based hydrogels could be either prevented or limited by tailoring the concentration of hydroxytyrosol introduced as an anti-crosslinking agent;

- the specific kind of buffer saline solution affects the final characteristics of the optimized hydrogel; the different salinity of the buffers influences, in fact, both the viscoelasticity of the gel and the formation of bonds after gamma radiation sterilization. In addition, since hydroxytyrosol results to be more preserved when formulated in Citrate Buffer Solution, the choice of the use of CBS is the most convenient in order to increase the biocompatibility of the final Sterile Hydrogels.

6. Future Perspectives

On the basis of the initial hypothesis and the obtained results, it is possible to affirm that hydroxytyrosol can be introduced in Hydrogels formulations as an anti-crosslinking agent, as a valid substitute of Vitamin C and Vitamin E. The result obtained with this study is of great importance in the application field of Regenerative Medicine: thanks to its high antioxidant, anti-inflammatory and antimicrobial properties, HT allows to prevent or limit the radiation-induced cross-linking of PEO-based hydrogels. In this way, the characteristics of the biodegradable scaffolds are not altered and, therefore, the formation of a three-dimensional polymer network complexity and the consequent undesirable effects such as embrittlement, solidification, plasticization or viscosity increase do not occur.

In addition, the discovery of that the specific kind of buffer saline solution affects the final characteristics of the optimized hydrogel and that the choice of the use of Citrate Buffer Solution is the most convenient in order to obtain the greatest biocompatibility is of great scientific relevance. In fact, until now, Phosphate Buffer Solution has been the most used in scientific studies present in literature.

The impossibility to perform the Rheological Analysis for all the Sterile samples – due to a viscosity increase induced by gamma radiation – and the lack of samples with intermediate HT quantity – due to the long production process of the gels – make it essential to carry out new studies. Only after an exhaustive physical-chemical characterization of Hydrogels with Citrate Buffer will be possible to formulate Hydrogels with bone powder and/or granules substitutes and subject them to biocompatibility assessments, according to ISO 10993. This last step will lead to the creation of a new biomedical device to be used as a scaffold for Regenerative Medicine and Tissue Engineering applications.

References

[1] Kim MS, Kim JH, Min BH, Chun HJ, Han DK, Lee HB. Polymeric scaffolds for regenerative medicine. Polymer Reviews 2011; 50(1): 23-52.

[2] Mao AS, and Mooney DJ. Regenerative medicine: current therapies and future directions. Proceedings of the National Academy of Sciences 2015; 112(47): 14452-14459.

[3] Reis RL. Encyclopedia of Tissue Engineering and Regenerative Medicine. Academic Press; 2019.

[4] Pignatello R. Biomaterials science and engineering. BoD–Books on Demand; 2011.

[5] Pina S, Ribeiro VP, Marques CF, Maia FR, Silva TH, Reis RL, Oliveira JM. Scaffolding Strategies for Tissue Engineering and Regenerative Medicine Applications. Materials 2019; 12(11): 1824.

[6] Ratner BD, Hoffman AS, Schoen FJ, Lemons JE. An introduction to materials in medicine. Biomaterials science 1996: 484.

[7] Lanza R, Langer R, Vacanti JP. Principles of tissue engineering. Academic press; 2011.

[8] Giannoudis PV, Einhorn TA, Schmidmaier G, Marsh D. The diamond concept–open questions. Injury 2008; 39: S5-S8.

[9] Langer Robert, Vacanti JP. Tissue engineering. Science 1993: 920-6.

[10] Mazzoli A, Ferretti C, Gigante A, Salvolini E, Mattioli-Belmonte M. Selective laser sintering manufacturing of polycaprolactone bone scaffolds for applications in bone tissue engineering. Rapid prototyping journal 2015; 21(4): 386-392.

[11] Naahidi S, Jafari M, Logan M, Wang Y, Yuan Y, Bae H, Chen P. Biocompatibility of hydrogel-based scaffolds for tissue engineering applications. Biotechnology advances 2017; 35(5): 530-544.

[12] Dhandayuthapani B, Yoshida Y, Maekawa T, Kumar DS. Polymeric scaffolds in tissue engineering application: a review. International journal of polymer science 2011.

[13] Bruder SP, Caplan AI. Bone regeneration through cellular engineering. Principles of tissue engineering 2000; 2: 683-696.

[14] Liu H, Ding X, Zhou G, Li P, Wei X, Fan Y. Electrospinning of nanofibers for tissue engineering applications. Journal of Nanomaterials 2013; 3.

[15] Chen Q, Roether JA, Boccaccini AR. Tissue engineering scaffolds from bioactive glass and composite materials. Topics in tissue engineering 2008; 4(6): 1-27.

[16] Subramanian UM, Kumar SV, Nagiah N, Sivagnanam UT. Fabrication of polyvinyl alcohol-polyvinylpyrrolidone blend scaffolds via electrospinning for tissue engineering applications. International Journal of Polymeric Materials and Polymeric Biomaterials 2014; 63(9): 476-485.

[17] Pal K, Banthia AK, Majumdar DK. Polymeric hydrogels: characterization and biomedical applications. Designed monomers and polymers 2009; 12(3): 197-220.

[18] Gibbs DM, Black CR, Dawson JI, Oreffo RO. A review of hydrogel use in fracture healing and bone regeneration. Journal of tissue engineering and regenerative medicine 2016; 10(3): 187-198.

[19] Peppas NA. Biomedical applications of hydrogels handbook. Springer Science & Business Media; 2010.

[20] Dai Z, Ronholm J, Tian Y, Sethi B, Cao X. Sterilization techniques for biodegradable scaffolds in tissue engineering applications. Journal of tissue engineering 2016; 7: 2041731416648810.

[21] Perni S. Microbial control and safety in inhalation devices. Inhaler Devices. Woodhead Publishing 2013: 51-74.

[22] Lerouge S. Sterilization and cleaning of metallic biomaterials. Metals for Biomedical Devices. Woodhead Publishing 2019: 405-428.

[23] Martin S, Duncan E. Sterilisation considerations for implantable sensor systems. Implantable Sensor Systems for Medical Applications. Woodhead Publishing 2013: 253-278.

[24] Tekade RK. Dosage Form Design Parameters. Vol. 2. Academic Press; 2018.

[25] Rozema FR, Bos RRM, Boering G, Van Asten JAAM, Nijenhuis AJ, Pennings AJ. The effects of different steam-sterilization programs on material properties of poly (l-lactide). Journal of applied biomaterials 1991; 2(1): 23-28.

[26] Lambert B, Martin J. Sterilization of implants and devices. Biomaterials Science. Academic Press 2013: 1339-1353.

[27] Moore MA, Samsell B, McLean J. Allograft tissue safety and technology. 1 ed. Biologics in Orthopaedic Surgery. Elsevier; 2018.

[28] Seto AU. Stabilization of irradiated allografts via crosslinking and free radical scavenging [PhD Thesis]. Rutgers University-Graduate School-New Brunswick, 2007.

[29] Massey LK. Introduction to sterilization methods. The effect of sterilization methods on plastics and elastomers. Norwich, NY: William Andrew Publishing; 2005.

[30] Mendes GCC, Brandao TRS, Silva CLM. Ethylene oxide sterilization of medical devices: a review. American journal of infection control 2007; 35(9): 574-581.

[31] Sastri VR. Material Requirements for Plastics used in Medical Devices. Plastics in Medical Devices: Properties, Requirementes and Applications. Pennsylvania: William Andrew; 2014.

[32] Rogers WJ. The effects of sterilization on medical materials and welded devices. Joining and Assembly of Medical Materials and Devices. Woodhead Publishing; 2013.

[33] Muratoglu OK, Oral E, Bodugoz-Senturk H, inventors. Anti-cross-linking agents and methods for inhibiting cross-linking of injectable hydrogel formulations. International patent WO 2007140312A3. 2007 December 6.

[34] Pucić I, Jurkin T. FTIR assessment of poly (ethylene oxide) irradiated in solid state, melt and aqeuous solution. Radiation Physics and Chemistry 2012; 81(9): 1426-1429.

[35] Oral E, Bodugoz-Senturk H, Macias C, Muratoglu OK. Vitamin C hinders radiation cross-linking in aqueous poly (vinyl alcohol) solutions. Nuclear Instruments and Methods in Physics Research Section B: Beam Interactions with Materials and Atoms 2017; 265(1): 92-97.

[36] Fernández-Bolaños JG, López Ó, López-García MÁ, Marset A. Biological properties of hydroxytyrosol and its derivatives. Olive oil-constituents, quality, health properties and bioconversions. IntechOpen 2012.

[37] Aydar AY, Öncü B, Öner OT, Ücok EF. Effects of Hydroxytyrosol on Human Health. EC Nutrition 2017; 11(4): 147-157.

[38] Robles-Almazan M, Pulido-Moran M, Moreno-Fernandez J, Ramirez-Tortosa C, Rodriguez-Garcia C, Quiles JL, Ramirez-Tortosa M. Hydroxytyrosol: Bioavailability, toxicity, and clinical applications. Food Research International 2018; 105: 654-667.

[39] Granados-Principal S, Quiles JL, Ramirez-Tortosa CL, Sanchez-Rovira P, Ramirez-Tortosa MC. Hydroxytyrosol: from laboratory investigations to future clinical trials. Nutrition reviews 2010; 68(4): 191-206.

[40] Martínez L, Ros G, Nieto G. Hydroxytyrosol: Health benefits and use as functional ingredient in meat. Medicines 2018; 5(1): 13.

[41] Ramachandran VS, Beaudoin JJ. Handbook of analytical techniques in concrete science and technology: principles, techniques and applications. Elsevier; 2000.

[42] Petsev DN. Emulsions: structure, stability and interactions. Vol. 4. Elsevier; 2004.

[43] Dukhin AS, Goetz PJ. Fundamentals of interface and colloid science. Studies in Interface Science. Vol. 24. Elsevier; 2010.

[44] Speight JG. Environmental organic chemistry for engineers. Butterworth-Heinemann; 2016.

[45] Stuart B. Infrared spectroscopy. Kirk-Othmer Encyclopedia of Chemical Technology 2000: 1-18.

[46] Lindon JC, Tranter GE, Koppenaal D. Encyclopedia of spectroscopy and spectrometry. Academic Press; 2016.

[47] Percec V, Pugh C. Comprehensive Polymer Science and Supplements. Elsevier; 1989.

[48] Baker M, Hollywood KA, Hughes C. Biophotonics: Vibrational Spectroscopic Diagnostics. Morgan & Claypool Publishers; 2016.

[49] Bergaya F, Lagaly G. Handbook of clay science. Vol. 5. Newnes; 2013.

[50] Malviya R, Bansal V, Pal OP, Sharma PK. High performance liquid chromatography: A short review. Journal of Global Pharma Technology 2010; 2(5): 22-26.

[51] World Health Organization. The International Pharmacopoeia. 9 ed. Columbia University Press; 2019.

[52] Oral E, Ghali BW, Rowell SL, Micheli BR, Lozynsky AJ, Muratoglu OK. A surface crosslinked UHMWPE stabilized by vitamin E with low wear and high fatigue strength. Biomaterials 2010; 31(27): 7051-7060.

[53] Tuck KL, Hayball PJ. Major phenolic compounds in olive oil: metabolism and health effects. The Journal of nutritional biochemistry 2002; 13(11): 636-644.

[54] Fruhwirth GO, Wagner FS, Hermetter A. The αPROX assay: fluorescence screening of the inhibitory effects of hydrophilic antioxidants on protein oxidation. Analytical and bioanalytical chemistry 2006; 384(3): 703-712.

[55] Ohaus, Adventurer AX Data Sheet, 88774756_A.

[56] Ohaus, Scout STX Data Sheet,80775008_C.

[57] BIPEE, Joan-SH-2 Laboratory Magnetic Stirrer.

[58] ArgoLab, Rod Stirrers, 2015.

[59] Hanna Instrument, HALO HI13302 Data Sheet, QR13302IT, 2018.

[60] Lamy Rheology, Using Manual RM 200 PLUS, 2019.

[61] Lamy Rheology, Temperature Control EVA MS-DIN PLUS, 2019.

[62] Perkin Elmer, Spectrum Two FT-IR Spectroscopy, 009430_01, 2011.

[63] Memmert, Incubator I, D13644.

[64] Seker A, Arslan B, Chen S. Recovery of Polyphenols from Grape Pomace Using Polyethylene Glycol (PEG)-Grafted Silica Particles and PEG-Assisted Cosolvent Elution. Molecules 2019; 24(12): 2199.

[65] DK Sonic, Ultrasonic Cleaner DK-80 Data Sheet.

[66] Perkin Elmer, Flexar LC Systems, 008523D_01, 2017.

[67] Gikas E, Papadopoulos N, Tsarbopoulos A. Kinetic study of the acidic hydrolysis of oleuropein, the major bioactive metabolite of olive oil. Journal of liquid chromatography & related technologies 2006; 29(4): 497-508.

[68] Kumari A. Sweet Biochemistry: Remembering Structures, Cycles, and Pathways by Mnemonics. Academic Press; 2017.

[69] Lucas R, Comelles F, Alcantara D, Maldonado OS, Curcuroze M, Parra JL, Morales JC. Surface-active properties of lipophilic antioxidants tyrosol and hydroxytyrosol fatty acid esters: a potential explanation for the nonlinear hypothesis of the antioxidant activity in oil-in-water emulsions. Journal of agricultural and food chemistry 2010; 58(13): 8021-8026.

[70] Larkin P. Infrared and Raman spectroscopy: principles and spectral interpretation. Elsevier; 2017.